Doctoral Dissertation

博士学位論文

A Study on Nonlinear Distortion Suppression Scheme Employing Transmit Power Control in OFDM Transmission

OFDM伝送における送信電力制御を用いた非線形ひずみ抑圧法に関する研究

February 2015

Waseda University

Graduate School of Fundamental Science and Engineering
Department of Computer Science and Engineering
Research on Wireless Signal Processing

Shoya TAKEBUCHI

竹渕 翔矢

Contents

Acknowledgment

First of all, I would like to express my sincere gratitude to Professor Fumiaki Maehara of Waseda University for his continuous support, guidance and encouragement on research work toward my Ph.D. His great foresight and sagacity guide me throughout my research work.

I also would like to appreciate Professor Fumio Takahata and Professor Jiro Katto of Waseda University, and Associate Professor Akinori Taira of Tohoku University for their patient teaching and inspiring advice on my research, and for their valuable comments on my dissertation.

I would like to thank Mr. Gen Osada and Mr. Tomoki Maruko for their valuable discussions on the topic of the nonlinear distortion problems in OFDM transmission. Specially, I would like to thank Mr. Gen Osada for giving me support on the extension of the proposed method. I also would like to thank all the members of Professor Maehara's laboratory for bringing me so much fun during my Ph.D. program.

Moreover, this research was partly supported by "Support foundations for improvement of prominent graduate school, Waseda University" of the Ministry of Education, Culture, Sports, Science and Technology, Japan. I would like to thank heartily for this support.

Finally, I would like to extend my heartfelt thanks to grateful support and care of my family.

1 Introduction

In recent years, high-speed and high-reliability transmission is required in wireless communication systems with the advances in digital processing technologies and the rapid spread of the Internet and the mobile phone [1]-[3]. To realize high-speed and high-reliability wireless communication, it is essential to overcome a problem of the degradation of the transmission performance due to multipath fading [4]-[7].

Orthogonal frequency division multiplexing (OFDM) [8]-[12] has become one of the most promising techniques to overcome this problem, and it has already been adopted in broadcasting [13], mobile communications, wireless LAN [14], and so on [15]. OFDM is a kind of multi-carrier technique for achieving simultaneous transmission of the modulated symbols. Moreover, OFDM can effectively combat the inter-symbol interference (ISI) which is caused by multipath fading by means of the guard interval (GI) insertion.

However, OFDM has an inherent drawback that the time domain waveform suffers from an extremely high peak-to-average power ratio (PAPR) because its transmission is performed by employing a number of sub-carriers [10]-[12], [16], [17]. This large envelope variation due to high PAPR causes the nonlinear distortion when passing through the high-power amplifier (HPA), which leads to the out-of-band radiation as well as the BER degradation. Especially, the out-of-band radiation becomes the critical factor of the adjacent channel interference, which leads to decreasing the spectrum utilization efficiency. In this context, it can be said that the nonlinear distortion suppression is a crucial issue in the field of broadband wireless communications employing OFDM transmission.

In order to suppress the nonlinear distortion, a number of techniques have been proposed [18]. More specifically, clipping and filtering (CAF) [19]-[22], partial transmit sequence [23]-[25], coding [26], [27], and predistortion [28]-[30] can be seen as well-known techniques. Among these techniques, partial transmit sequence and coding are effective to combat the nonlinear distortion,

but both techniques require heavy transmission overhead and computational complexity. Predistorion is also an effective approach but the peak power level has to be suppressed below the saturation level, which implies that the relatively high input back-off (IBO) is required in a realistic scenario.

From a practical point of view, clipping and filtering can be seen as an attractive technique because there are no constraints of the overhead, the computational complexity, and the IBO margin. However, clipping and filtering has a critical problem of the significant BER degradation because clipping significantly destroys OFDM time domain waveform while suppressing the out-of-band radiation. Therefore, there are existing some effective approaches to overcome the BER degradation of clipping and filtering. For example, as for the transmitter side, the peak power reduction method employing peak reduction sub-carrier signals [31], [32] and the method to control the optimum clipping level considering the peak power regrowth due to the filtering process after the clipping process [33] have been proposed. On the other hand, as for the receiver side, the method to improve the BER by estimating and removing the nonlinear distortion component [34], [35] has been also proposed. Although these methods can effectively overcome the BER degradation of clipping and filtering at the transmitter or the receiver side, these methods unfortunately require iterative processes, which consequently increases computational complexity.

Considering the background described above, we propose a deterministic transmit power control method for OFDM clipping and filtering. The feature of the proposed approach is to derive the transmit power level with the maximum signal-to-noise-plus-distortion power ratio (SNDR) by using the simple theoretical mathematical formula [36]. The effectiveness of the proposed method is demonstrated by means of computer simulations in comparison with the traditional clipping and filtering method [37]-[39].

In addition, multiple antenna systems such as single user-MIMO (SU-MIMO) [40], [41] and multi user-MIMO (MU-MIMO) [42]-[44] have recently received increased attention due to the ability to enhance the channel capacity of wire-

less systems. In application of OFDM to MIMO, the space diversity benefit is decreased in the presence of the nonlinear distortion [45]. Therefore, the transmission performance is firstly evaluated in SU-MIMO-OFDM systems [46]-[50]. Next, it is demonstrated how much the proposed method can recover the space diversity benefit which is decreased by the traditional clipping and filtering method. Furthermore, in application of clipping and filtering to MU-MIMO which is an essential technique to realize the fifth-generation (5G) mobile communications systems, the influence of the nonlinear distortion becomes severe with increase in the number of transmit antennas, which leads to the BER degradation [51], [52]. Thus, the problem statement in application of the proposed method to MU-MIMO-OFDM [53]-[55] is described and its effectiveness is demonstrated in comparison with the traditional clipping and filtering [51], [52].

This dissertation contains this chapter and the following 5 chapters.

Chapter 2 presents the basic knowledge to help us to understand the principle of OFDM, the effect of the nonlinear distortion on OFDM, and the transmission performance of OFDM in the presence of the nonlinear distortion. The performance evaluation is carried out over not only AWGN but also multipath fading channels. Moreover, the nonlinear distortion causes the out-of-band radiation and therefore it is mentioned that oversampling is required to evaluate the effect of the nonlinear distortion.

Chapter 3 presents the nonlinear suppression scheme employing the transmit power control in OFDM transmission which is the main issue of this dissertation. Firstly, the concept and the operating principle of the traditional clipping and filtering are introduced and its performance evaluation is carried out. In particular, it is clarified how much the BER is degraded due to the clipping process. Next, the proposed nonlinear distortion suppression scheme employing the transmit power control is introduced and its effectiveness is verified in comparison with the traditional clipping and filtering by means of computer simulations. Here, it should be noted that the performance evaluation is carried out in terms of the frequency spectrum and the BER. From this evaluation, it

is clarified that the proposed method can determine the transmit power level to satisfy the maximum SNDR by means of the simple theoretical formula which represents the relationship between the SNDR and the input signal level. Moreover, it is demonstrated that the proposed method can dramatically improve the BER performance because the input signal level is successfully controlled in order to satisfy the maximum SNDR.

Chapter 4 presents the application of the proposed clipping and filtering method to SU-MIMO which is a promising technique to realize high-speed wireless communications systems. In this chapter, zero-forcing (ZF), minimum mean square error (MMSE), and maximum likelihood detection (MLD) are considered as the signal detection technique for MIMO systems. Firstly, it is pointed out that the BER degradation becomes significant in the traditional clipping and filtering. This is because the effect of the nonlinear distortion caused by the clipping process accumulates in each stream with increase in the number of streams, which indicates that the space diversity gain is significantly reduced especially in use of MLD. On the other hand, it is demonstrated that the proposed method can suppress the effect of the nonlinear distortion and improve the BER performance in comparison with the traditional clipping and filtering and that the significant improvement can be found in use of MLD.

Chapter 5 presents the application of the proposed clipping and filtering method to MU-MIMO which is an essential technique to realize the fifth-generation (5G) mobile communications systems. Firstly, it is pointed out that the BER degradation becomes significant in the traditional clipping and filtering with increase in the number of transmit antennas. This is because the effect of the nonlinear distortion caused at each transmit antenna is accumulated at a mobile station. To cope with this problem, the proposed method controls the transmit power level to satisfy the maximum SNDR. Here, it should be noted that the transmit power level has to be the same among the transmit antennas because the different transmit power levels destroy the space orthogonality. From performance evaluations, it is demonstrated that the proposed method can improve

the BER performance in comparison with the traditional clipping and filtering regardless of the number of transmit antennas.

Finally, Chapter 6 concludes the contribution of this dissertation and discusses my future work.

2 Orthogonal Frequency Division Multiplexing (OFDM)

Orthogonal frequency division multiplexing (OFDM) has become one of the most promising techniques in broadband wireless systems because of its high bandwidth efficiency as well as its robustness against severe frequency selective fading [8]-[12]. Therefore, OFDM is of great interest by a lot of researchers in universities and research laboratories all over the world. Actually, OFDM has already been widely adopted in broadcasting [13], mobile communications, wireless LAN [14], and so on [15]. Moreover, OFDM can also be regarded as one of the highly efficient modulation schemes because multiple symbols modulated by PSK and QAM are transmitted at the same time with minimum frequency separation.

2.1 Principle of OFDM Modulation

Figure 2.1 shows the concept of the time domain waveform and the frequency spectrum in the baseband of single carrier modulation, multi-carrier modulation, and OFDM. Fig. 2.1(a) shows an example of the single carrier signals with BPSK, where the amplitude envelope, the symbol period, and the transmission bandwidth are defined as A (the power is A^2), T_s, and $2/T_s$, respectively. Here, assuming that four symbols are simultaneously transmitted by means of multi-carrier modulation under the same bandwidth, the amplitude envelope and the transmission bandwidth of each sub-carrier become $A/\sqrt{4}$ and $2/(4T_s) = 1/(2T_s)$, respectively. It indicates that the symbol period is four times as long as that of single carrier scheme.

In Fig. 2.1(b), we can see that rectangular pulse has a zero-crossing at intervals of $1/T_s$, which implies that adjacent sub-carriers can be overlapped at intervals of $1/T_s$. OFDM is a modulation scheme to makes use of this property, which make it possible to reduce the bandwidth as shown in Fig. 2.1(c). In the case of a large number of sub-carriers, the bandwidth can be reduced to one-half in comparison with signal carrier modulation and traditional multi-carrier

modulation, which is a reason why OFDM is regarded as a highly efficient modulation scheme.

Figure 2.2 shows the frequency spectrum of adjacent sub-carriers in OFDM. As shown in Fig. 2.2, the sub-carrier signals of $Z_0(f)$ and $Z_1(f)$ are orthogonal to each other thanks to the property of zero-crossing in a rectangular pulse.

Transmit baseband signal of the n-th sub-carrier $s_n(t)$ is represented as

$$s_n(t) = A_{In} + jA_{Qn}, \tag{2.1}$$

where A_{In} is the in-phase component, A_{Qn} is the quadrature component, respec-

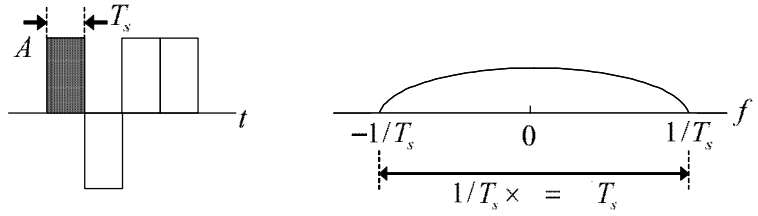

(a) Single carrier scheme

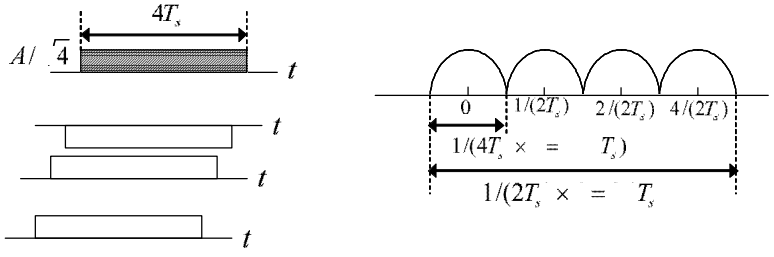

(b) Multi-carrier scheme

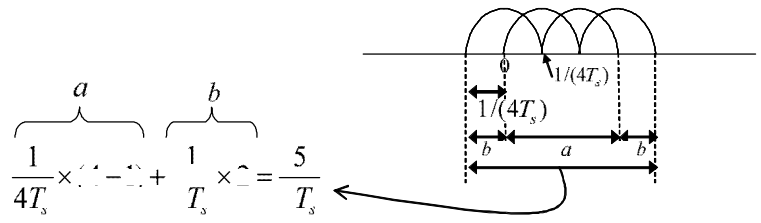

(c) OFDM scheme

Figure 2.1: Time waveform and frequency spectrum of each modulation scheme.

tively. If the symbol period of the OFDM signal is defined as T_s, the transmit signal $z_n(t)$ can be represented as

$$z_n(t) = (A_{In} + jA_{Qn})\, e^{j2\pi \frac{n}{T_s} t}. \tag{2.2}$$

From Eq. (2.2), the baseband OFDM signal $z_F(t)$ is represented as

$$\begin{aligned} z_F &= \sum_{n=0}^{N-1} z_n(t) \\ &= \sum_{n=0}^{N-1} \left\{ A_{c_n} \cos\left(2\pi \frac{n}{T_F} t\right) - A_{s_n} \sin\left(2\pi \frac{n}{T_F} t\right) \right\}. \end{aligned} \tag{2.3}$$

As shown in the above equation, the OFDM signal is composed of cosine and sine waveforms with different frequencies.

For simplicity, Figure 2.3 shows an example of OFDM time domain waveform, where the number of sub-carriers are assumed to be 128 (N = 128). As shown in Fig. 2.3, the OFDM signals cause the nonlinear distortion when passing through the high-power amplifier (HPA) because the peak-to-average power

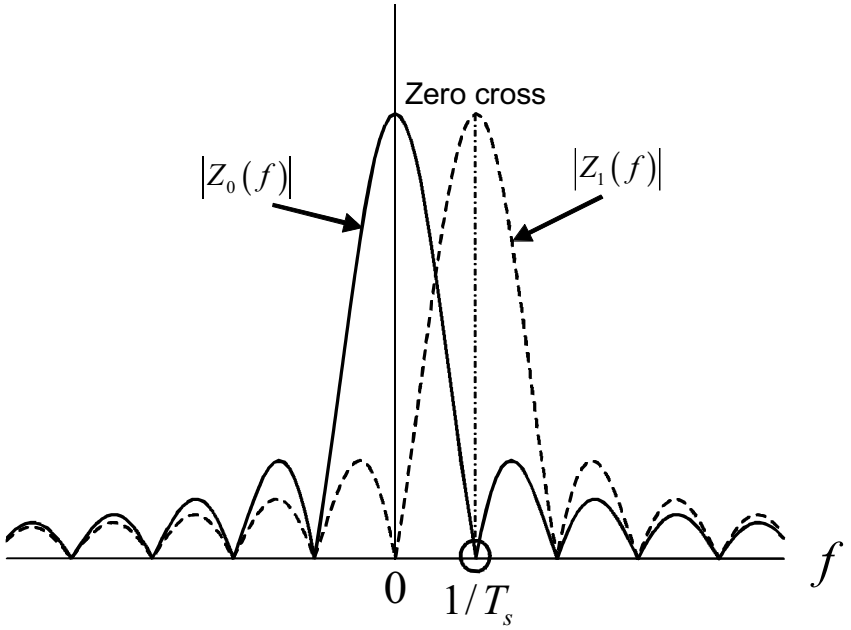

Figure 2.2: Frequency spectrum of adjacent sub-carriers in OFDM.

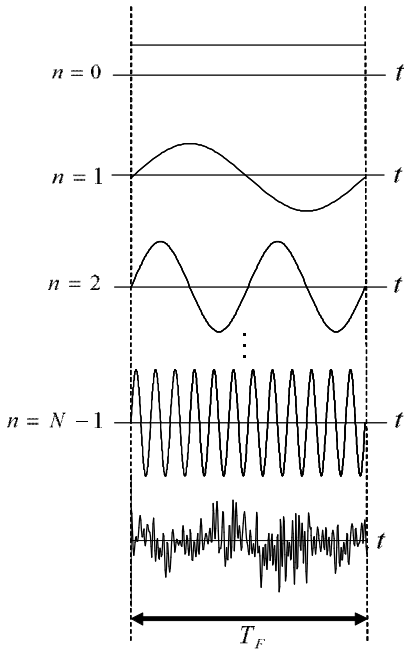

Figure 2.3: Combining of 128 sine waves.

ratio (PAPR) becomes extremely high.

The OFDM signal $z_F(t)$ in Eq. (2.3) can be rewritten as

$$\begin{aligned} z_F(t) &= \sum_{n=0}^{N-1}\left[\mathrm{Re}\left\{(A_{c_n} + jA_{s_n})e^{\left(j2\pi\frac{n}{T_F}t\right)}\right\}\right] \\ &= \mathrm{Re}\left[\sum_{n=0}^{N-1}\left\{(A_{c_n} + jA_{s_n})e^{\left(j2\pi\frac{n}{T_F}t\right)}\right\}\right]. \end{aligned} \tag{2.4}$$

If $z(t)$ is defined as

$$z(t) = \sum_{n=0}^{N-1}\left\{(A_{c_n} + jA_{s_n})e^{\left(j2\pi\frac{n}{T_F}t\right)}\right\}, \tag{2.5}$$

the OFDM signal which is upconverted to a carrier frequency f_c can be expressed by

$$\begin{aligned} s(t) &= \mathrm{Re}[z(t)e^{j2\pi f_c t}] \\ &= \mathrm{Re}[z(t)]\cos(2\pi f_c t) - \mathrm{Im}[z(t)]\sin(2\pi f_c t). \end{aligned} \tag{2.6}$$

By the way, it is convenient that discrete OFDM time domain waveform can be realized by just performing the IFFT processing. Suppose that N points are extracted from an OFDM symbol with the symbol period of T_F. The OFDM signal can be expressed as

$$z\left(\frac{k}{N}T_F\right) = \sum_{n=0}^{N-1}\left\{(A_{c_n} + jA_{s_n})\exp\left(j2\pi\frac{kn}{N}\right)\right\}. \tag{2.7}$$

From Eq. (2.7), it can be seen that the above formula is equivalent to the signal processing of IFFT. Therefore, OFDM signals are actually generated by the IFFT processing at the transmitter.

As described in the previous section, the OFDM signal with the symbol period of T_s can be realized by overlapping the square wave signals at frequency intervals of $1/T_s$. In this section, we show the frequency spectrum of OFDM signals after discussing the frequency spectrum of a sole rectangular signal with the symbol period of T_s.

If the amplitude of the square wave signal $x(t)$ is set to be 1, $x(t)$ can be expressed as

$$x(t) = \begin{cases} 1 & (0 \le t \le T_s) \\ 0 & (T_s \le t) \end{cases}. \tag{2.8}$$

Therefore, by using Fourier transform for the rectangular signal $x(t)$ in Eq. (2.8), the frequency spectrum $X(f)$ can be expressed as

$$X(f) = T_s\mathrm{sinc}\,(T_s\pi f). \tag{2.9}$$

Figure 2.4 shows the time domain waveform of the rectangular signal and its frequency spectrum. Now, the frequency spectrum of the rectangular signals which are overlapped at frequency intervals of $1/T_s$ is obtained by means of computer simulations, which corresponds to the basic principle of OFDM.

Figure 2.5 and Figure 2.6 show the frequency spectrums of OFDM signals

from different points of view. Comparing two figures, it can be said that the amplitude values at the carrier frequency of each sub-carrier in Fig. 2.5 is the same as these of each sub-carrier signal in Fig. 2.6, which indicates that the information data is not interfered by the neighboring sub-carriers even when the sub-carriers are placed at frequency intervals of $1/T_s$. In addition, thanks to overlapping the sub-carriers at frequency intervals of $1/T_s$, OFDM can provide higher frequency utilization efficiency than single carrier modulation or traditional multi-carrier modulation.

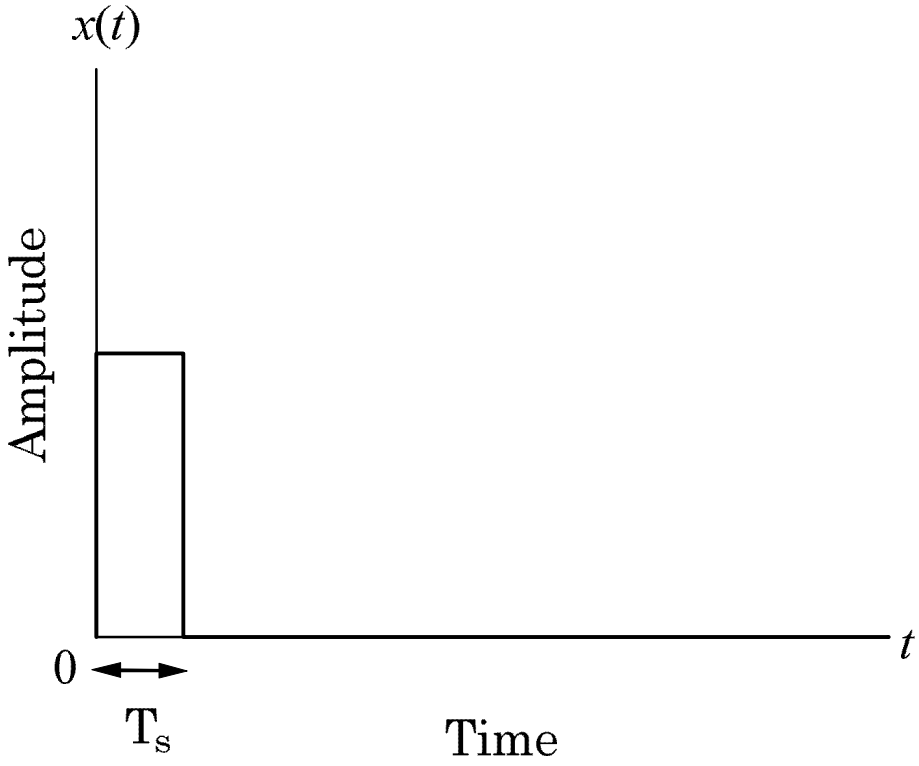

(a) Time waveform.

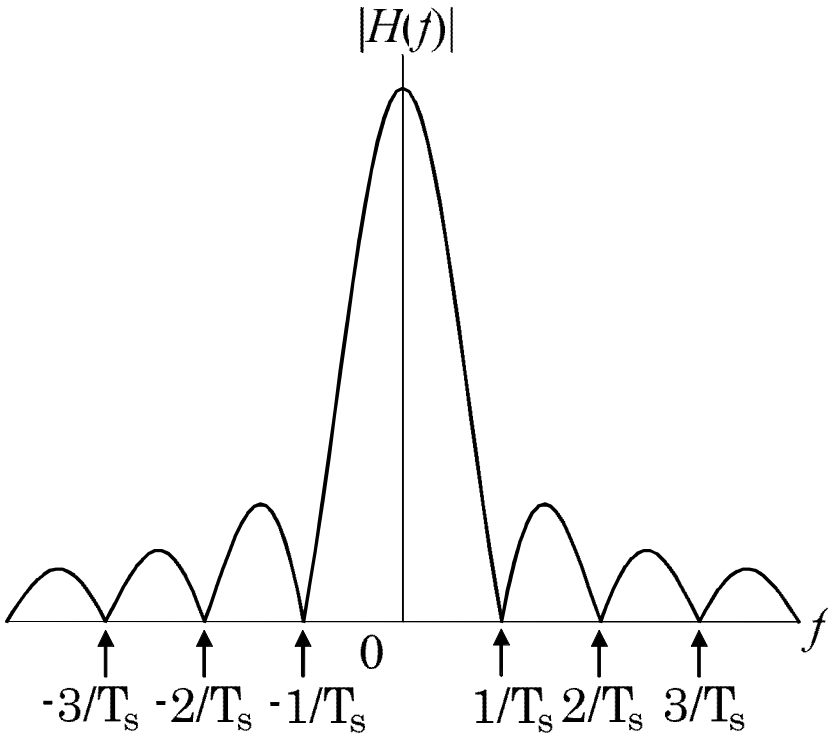

(b) Frequency spectrum.

Figure 2.4: Time waveform and frequency spectrum of rectangular signal.

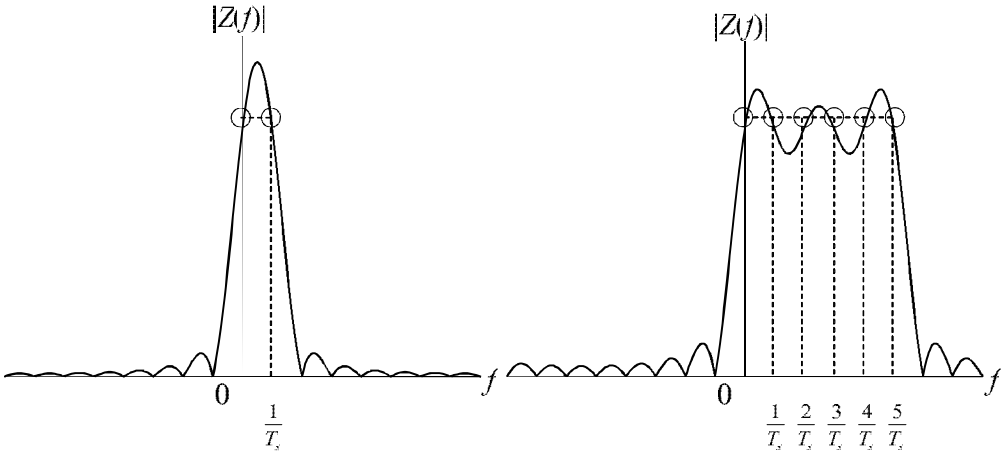

(a) Number of sub-carriers = 2 (b) Number of sub-carriers = 6

Figure 2.5: Frequency spectrum of an OFDM symbol.

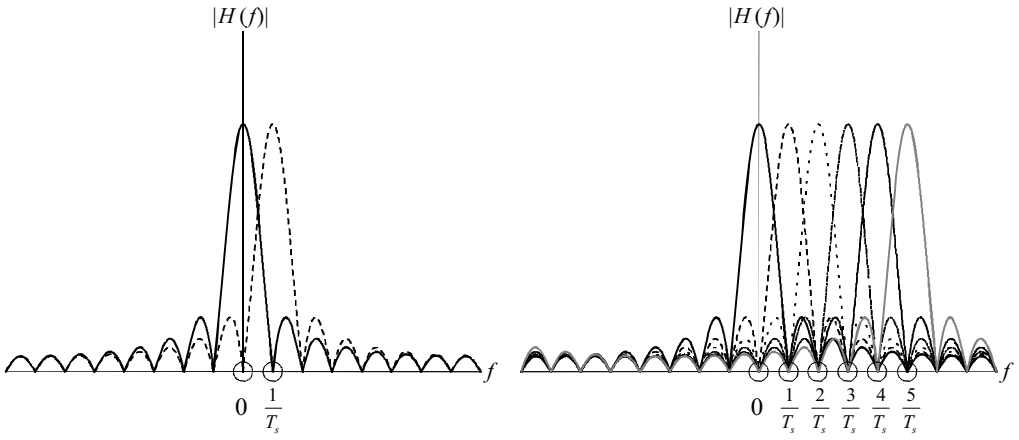

(a) Number of sub-carriers = 2 (b) Number of sub-carriers = 6

Figure 2.6: Sub-carrier spectrum included in an OFDM symbol.

In OFDM, the modulation process is performed in each sub-carrier and consequently, it is possible to transmit N modulated signals efficiently at the same time by means of the IDFT process. Thanks to this process, OFDM can realize high frequency utilization efficiency. Here, we introduce another property which is the strong robustness against frequency selective fading channels. Since frequency selective fading channels generate a number of delayed waves to the direct signal, the inter-symbol interference (ISI) is caused, which significantly degrades the transmission performance of OFDM. To overcome the ISI, OFDM makes use of the guard interval (GI) which is inserted between two successive OFDM symbols. Figure 2.7 shows the effect of the guard interval on OFDM, where the delayed wave is received with the multipath delay of τ. In Fig. 2.7, the effect of the ISI without the guard interval is also shown for reference. From Fig. 2.7 (a), it can be seen that the signal component of "Symbol 1"

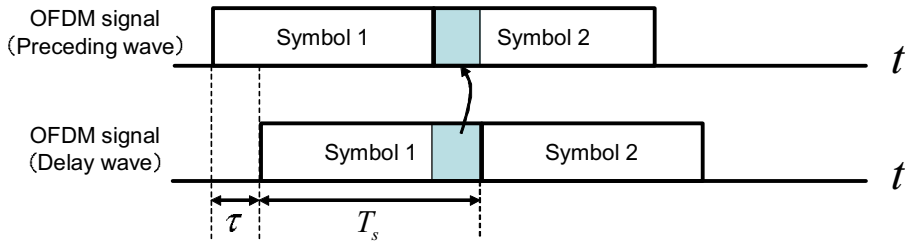

(a) w/o guard interval.

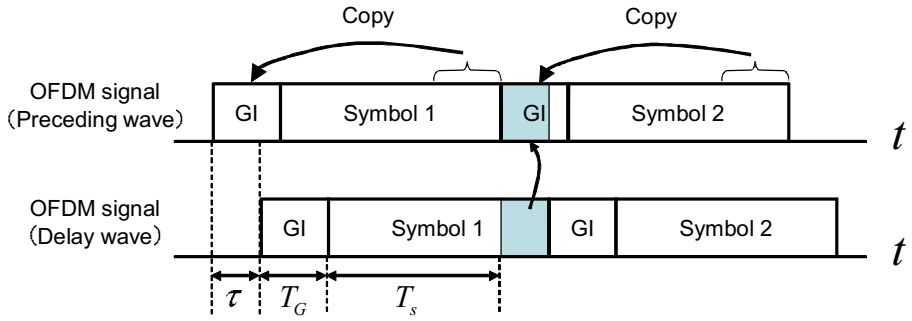

(b) w/ guard interval.

Figure 2.7: Effect of delay wave on an OFDM symbol with or without guard interval.

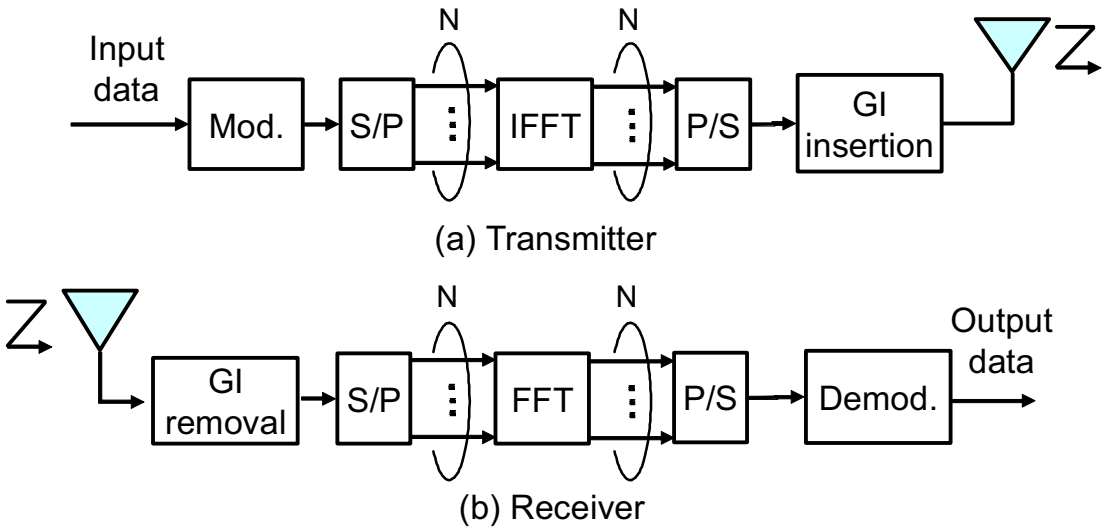

Figure 2.8: System configuration of OFDM scheme.

partially interferes "Symbol 2" in the observation period of "Symbol 2", which introduces the ISI. On the other hand, if the guard interval is given as the copy of the tail of the OFDM signal as shown in Fig. 2.7 (b), the guard interval can successively absorb the signal component of "Symbol 1", which implies that the signal component of "Symbol 1" does not interfere "Symbol 2" any more in the observation period of "Symbol 2". In this sense, the guard interval length T_G is generally set to be longer than the maximum delay.

In this section, we show the system configuration of the OFDM scheme and its transmission performance over AWGN channels, frequency non-selective fading channels, and frequency selective fading channels.

Figure 2.8 shows the system configuration of the OFDM transmission. Then, we evaluate the BER performance of OFDM transmission with a parameter of modulation scheme by means of computer simulations.

Figure 2.9 shows the BER performance of OFDM transmission over AWGN channels. Table 2.1 shows its simulation parameters. In Fig. 2.9, the solid line shows the theoretical performance of single carrier modulation for our comparison. Here, it should be noted that the theoretical formula for each modulation

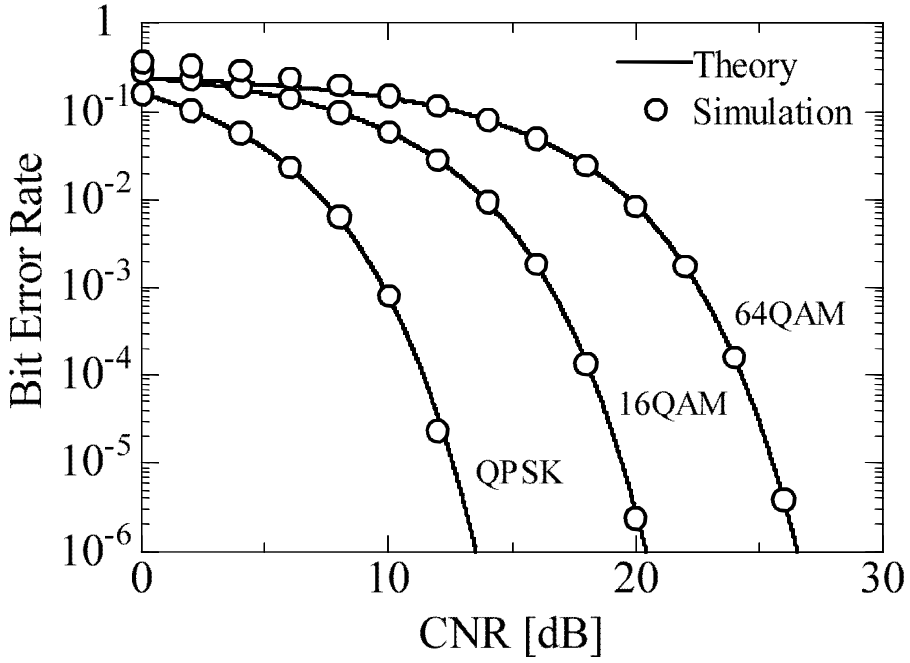

Figure 2.9: BER performance versus CNR of OFDM transmission over AWGN channels.

scheme is represented as [4]

$$P_b = \frac{1}{2}\mathrm{erfc}\sqrt{\frac{\gamma}{2}} \quad \text{(QPSK)}$$

$$P_b \simeq \begin{cases} \frac{3}{8}\mathrm{erfc}\sqrt{\frac{\gamma}{10}} & \text{(16QAM)} \\ \frac{7}{24}\mathrm{erfc}\sqrt{\frac{\gamma}{42}} & \text{(64QAM)} \end{cases}, \tag{2.10}$$

where γ denotes the CNR. From Fig. 2.9, it can be confirmed that the BER performance of OFDM over AWGN channels shows the same performance as that of single carrier modulation. This is because the sub-carrier orthogonality can be retained, which indicates that OFDM can be regarded as single carrier modulation in terms of the BER performance.

Figure 2.10 shows the BER performance of OFDM transmission over frequency non-selective fading channels. Table 2.2 shows its simulation param-

eters. In Fig. 2.10, the solid line shows the theoretical performance of single carrier modulation for our comparison. Here, it should be noted that the theoretical formula for each modulation scheme is represented as [7]

$$\begin{aligned} \bar{P}_b &= \frac{1}{2}\left(1 - \frac{1}{\sqrt{1+2/\Gamma}}\right) \quad \text{(QPSK)} \\ \bar{P}_b &\simeq \begin{cases} \frac{3}{8}\left(1 - \frac{1}{\sqrt{1+10/\Gamma}}\right) & \text{(16QAM)} \\ \frac{7}{24}\left(1 - \frac{1}{\sqrt{1+42/\Gamma}}\right) & \text{(64QAM)} \end{cases} \end{aligned}, \tag{2.11}$$

where Γ denotes the average CNR. From Fig. 2.10, as discussed above, it can be seen that the BER performance of OFDM transmission over frequency non-selective fading channels shows the same performance as that of single carrier transmission. This is because each sub-carrier is affected by flat attenuation, which implies that OFDM is influenced by the same impact as single carrier modulation.

From Figs. 2.9 and 2.10, OFDM can provide the same BER performance as the single carrier modulation while achieving high spectrum utilization efficiency. In this sense, OFDM can be seen as an attractive technique from a viewpoint of spectrum utilization.

Figure 2.11 shows the BER performance of OFDM with respect to the multipath delay, where double spike model is assumed as a radio propagation. Table 2.3 shows the simulation parameters, where T_{sam} denotes the sampling period of the OFDM signals. In Fig. 2.11, the solid line shows the theoretical performance in single carrier modulation over frequency non-selective fading chan-

Table 2.1: Simulation parameters.

Modulation	QPSK, 16QAM, 64QAM / OFDM
Number of subcarriers N	64
Channel model	AWGN

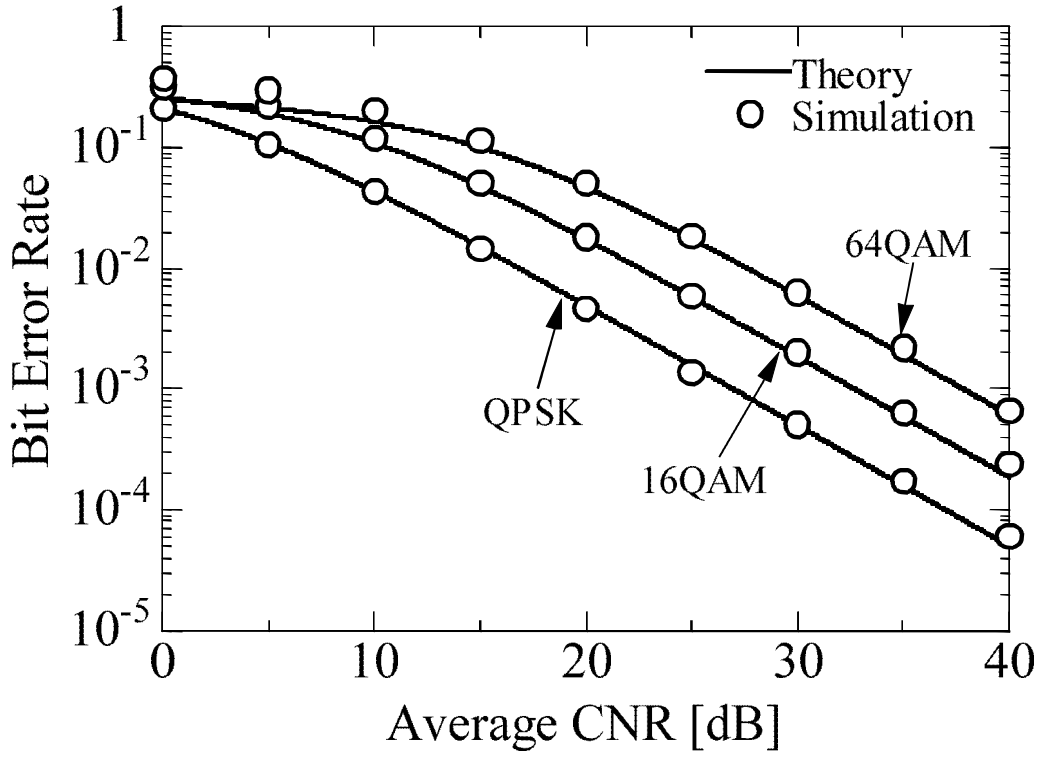

Figure 2.10: BER performance versus average CNR of OFDM transmission over frequency non-selective fading channels.

nels as shown in Eq. (2.11).

From Fig. 2.11, it can be seen that the BER degradation does not occur in the case that the delay time is within the length of the guard interval because OFDM scheme can absorb the influence of the delayed wave. However, the BER degradation is significantly introduced due to the ISI in the case that the

Table 2.2: Simulation parameters.

Modulation	QPSK, 16QAM, 64QAM / OFDM
Number of subcarriers N	64
Channel model	Flat Rayleigh fading
Channel estimation	Perfect

delay time exceeds the guard interval length.

In order to remove the ISI due to frequency selective fading channels, the guard interval length must be set to be longer than the maximum delay time. However, the guard interval length is expected to be as short as possible because the transmission efficiency is degraded with increase in the guard interval length.

Figure 2.12 and Figure 2.13 show the BER performance over frequency selective fading channels, where 16-ray exponentially decaying Rayleigh fading model is assumed as a radio propagation. Table 2.4 shows its simulation parameters. From Fig. 2.12, it can be seen that the BER performance of OFDM agrees with that of single carrier modulation regardless of the delay spread τ_{rms} and the modulation schemes. This is because the maximum multipath delay does not exceed the length of the guard interval length T_G. On the other hand, it can be seen from Fig. 2.13 that the BER performance of OFDM gets worse than that of single carrier modulation. This is because the multipath delay in excess of the guard interval length causes the ISI

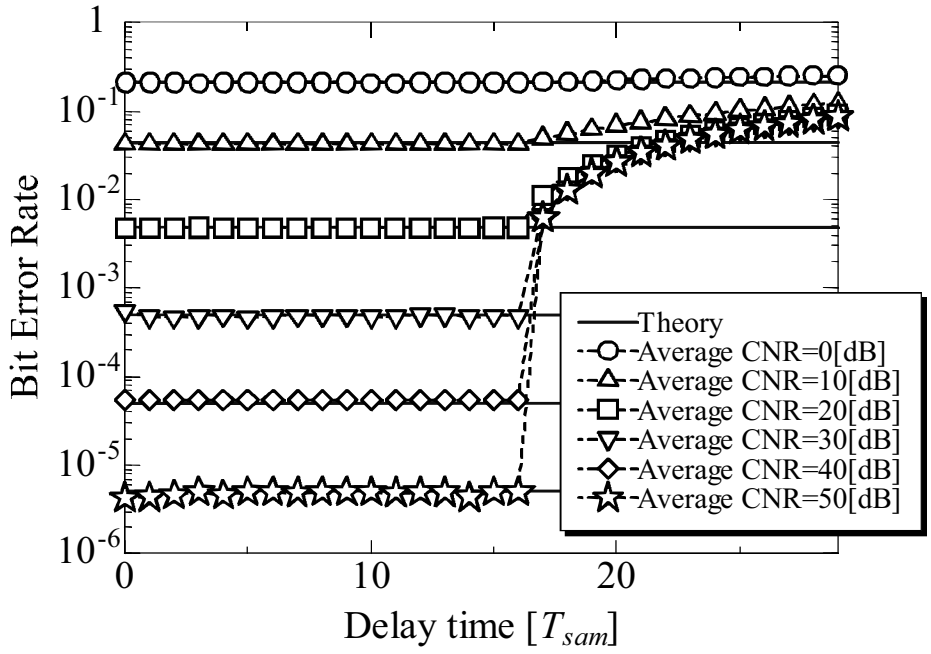

Figure 2.11: BER performance versus multipath delay in OFDM.

Table 2.3: Simulation parameters.

Modulation	QPSK / OFDM
Number of subcarriers N	64
Guard interval length T_G	$16T_{sam}$
Average CNR	0, 10, 20, 30, 40 [dB]
Channel model	Static equal gain 2-path

Table 2.4: Simulation parameters.

Modulation	QPSK, 16QAM, 64QAM / OFDM
Channel model	16-ray exponentially decaying Rayleigh fading channel
Channel estiomation	Perfect
$f_D T_{sam}$	0.0
Guard interval length T_G	$16T_{sam}$, $8T_{sam}$
Number of subcarriers N	64
FFT size	N

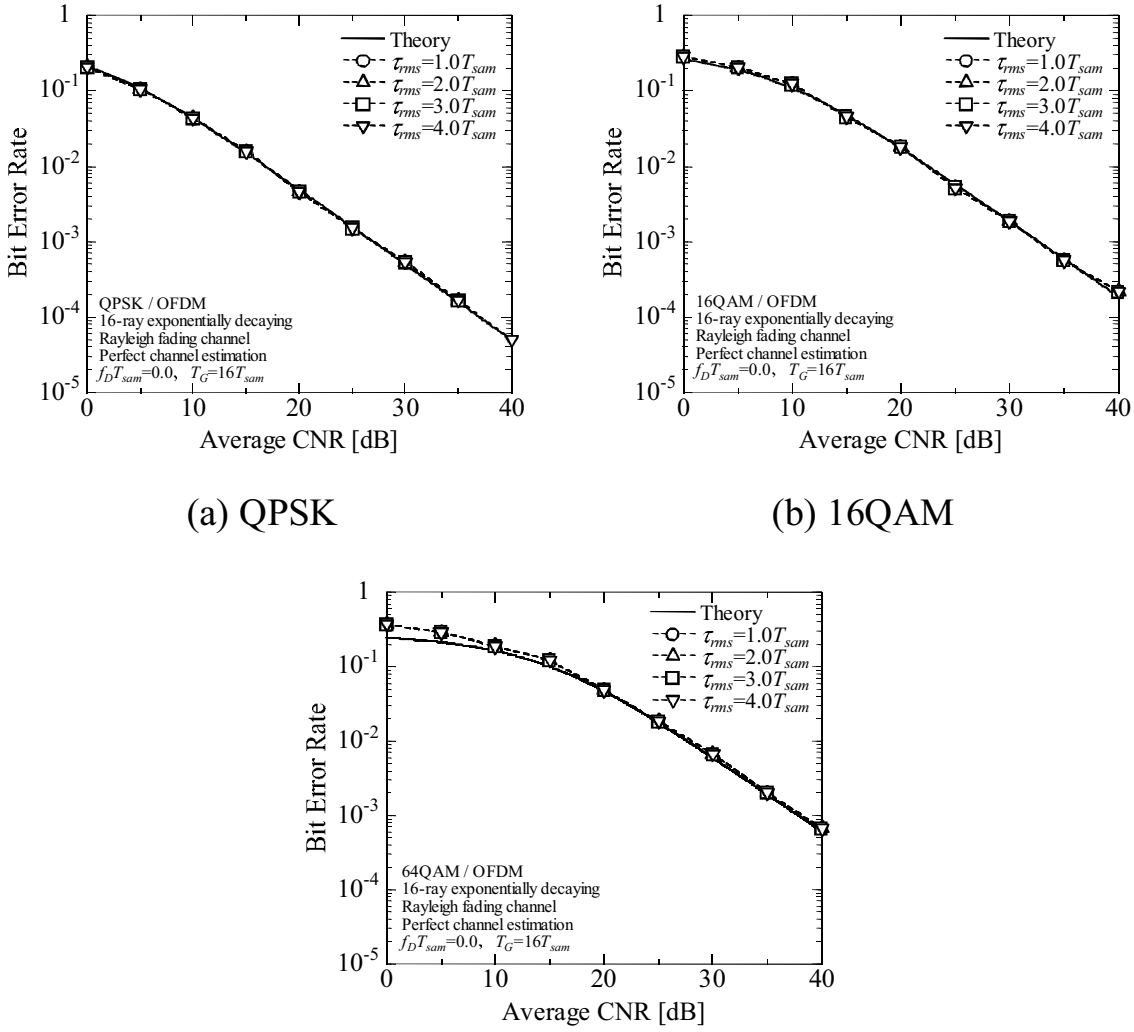

(a) QPSK (b) 16QAM

(c) 64QAM

Figure 2.12: BER performance versus average CNR of OFDM transmission over frequency selective fading channels. (T_G=16T_{sam})

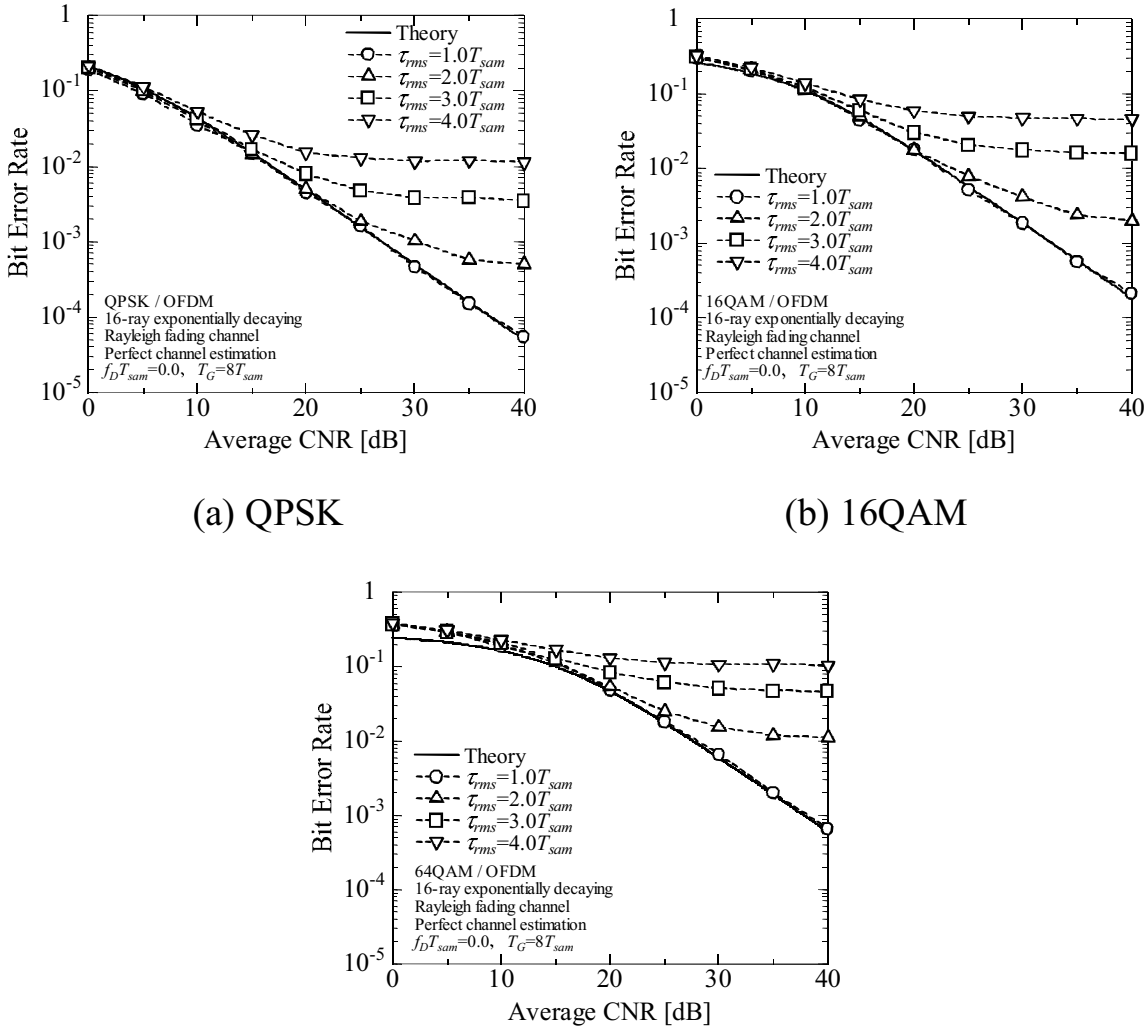

(a) QPSK (b) 16QAM

(c) 64QAM

Figure 2.13: BER performance versus average CNR of OFDM transmission over frequency selective fading channels. (T_G=8T_{sam})

2.2 Effect of Nonlinear Distortion on OFDM Signal

OFDM has a drawback of high peak power in the time domain waveform. This is because OFDM signals are inherently composed of a number of sinusoidal waves with different carrier frequencies. This peak power introduces the nonlinear distortion after passing through a high power amplifier (HPA) [10]-[12], [16], [17]. The influence of its nonlinearity on the OFDM signal is dependent on a HPA characteristic. In this chapter, we evaluate the influence of nonlinear distortion on OFDM signals in terms of the time waveform, the frequency spectrum, the signal constellation, the PAPR, and the BER performance.

Figure 2.14 shows an example of the input-output characteristics of HPA. As shown in Fig. 2.14, the HPA forces the output signal level to be a saturation level in a relatively high input signal level, while the output signal level is proportional to the input signal level in a relatively low input signal level. In this dissertation, we assume the soft envelope limiter model as a HPA characteristic

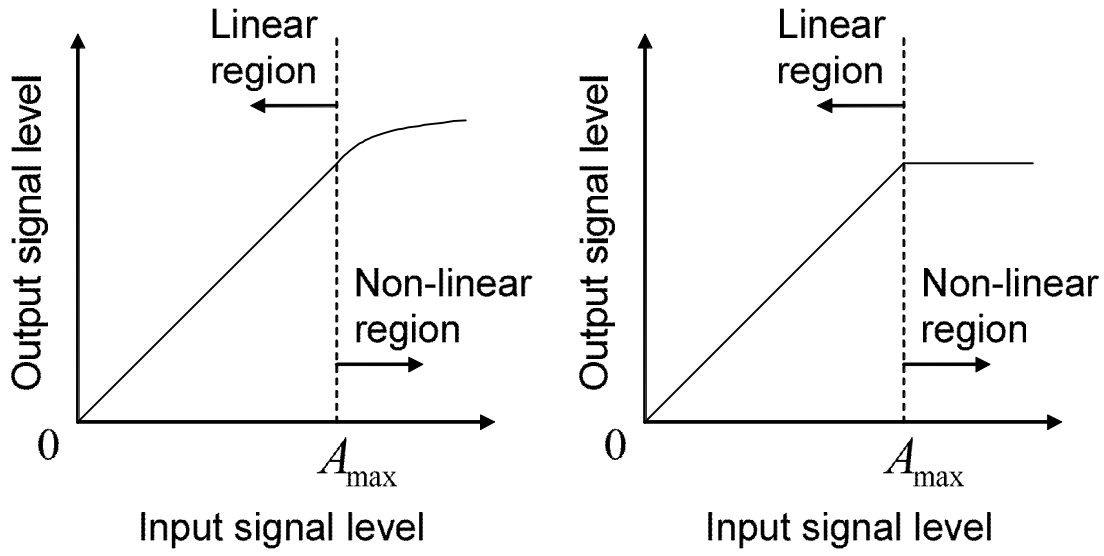

(a) General model (b) Soft limiter model

Figure 2.14: An example of input-output characteristics of HPA.

as shown in Fig. 2.14 (b) for our simplicity.

Input back off (IBO) is used as a criterion of the relationship between the input signal level and the nonlinearity in the HPA as shown in Fig. 2.14. Thus the IBO is defined as

$$\mathrm{IBO} = \frac{(A_{\max})^2}{P_{\mathrm{ave}}}, \tag{2.12}$$

where $A_{\max}$ is the maximum input amplitude to satisfy the linearity of the HPA and P_{ave} indicates the average input power, respectively. Therefore, the influence of nonlinear distortion becomes significant with decrease in the IBO.

Figure 2.15 shows the time domain waveform of the OFDM signal after passing through the HPA with a parameter of IBO. The OFDM signal input to the HPA is also shown for reference. Table 2.5 shows the simulation parameters. Here, it should be noted that oversampling is performed to take into account the effect of the out-of-band radiation. To suppress the aliasing effect due to the out-of-band radiation, the oversampling rate M is expected to be more than 4. From Fig. 2.15, it is found that the HPA clips the time domain waveform, which modifies the transmit OFDM signals and its change can be relaxed with increase in the IBO.

Figure 2.16 shows the frequency spectrum of the OFDM signal after passing through the HPA with a parameter of IBO. The OFDM signal input to the HPA is also shown for reference and the oversampling rate M is set to be 4 to prevent the aliasing effect. From Fig. 2.16, it can be confirmed that the out-of-band radiation becomes significant with decrease in the IBO. This is because the clipping effect becomes serious with the decrease in the IBO. Here, it should be noted that the out-of-band radiation lowers the spectrum utilization efficiency and hence the out-of-band radiation has to be suppressed as much as possible.

Figure 2.17 shows the signal constellation of the OFDM signal after passing through the HPA with a parameter of IBO. The OFDM signal input to the HPA is also shown for reference. From Fig. 2.17, it is confirmed that each signal point is distorted with decrease in the IBO. This is because the clipping effect

in the time domain gives a negative impact to each signal point which appears on the frequency domain.

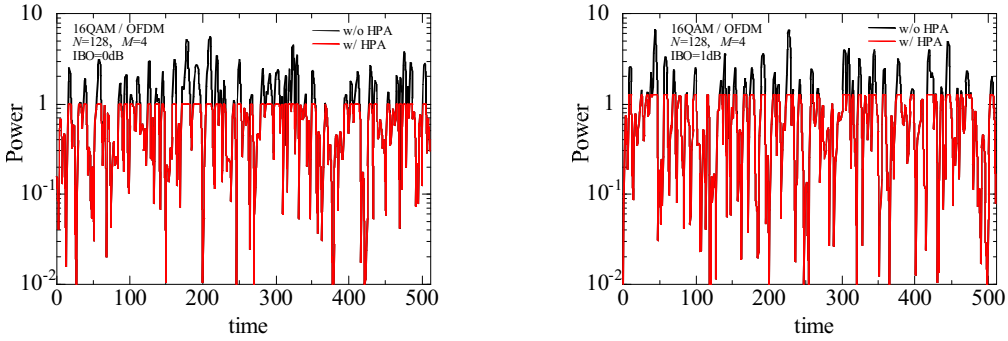

(a) IBO=0dB

(b) IBO=1dB

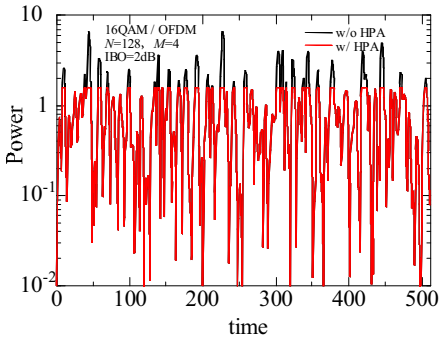

(c) IBO=2dB

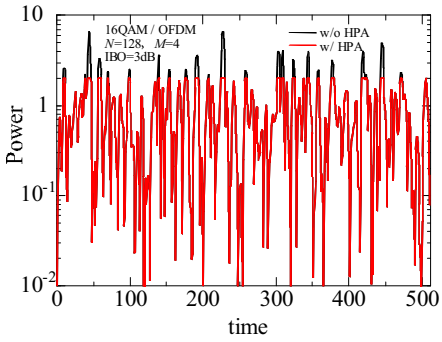

(d) IBO=3dB

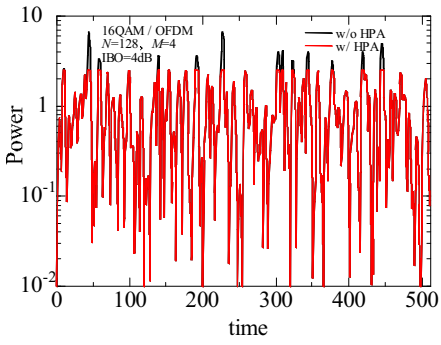

(e) IBO=4dB

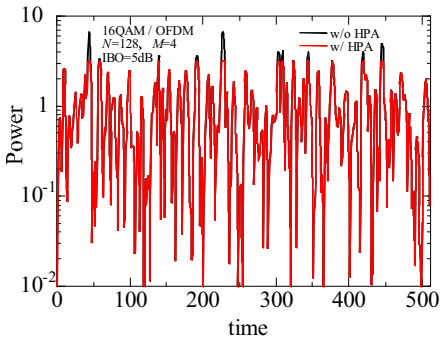

(f) IBO=5dB

Figure 2.15: Time domain waveform of OFDM signal after passing through HPA.

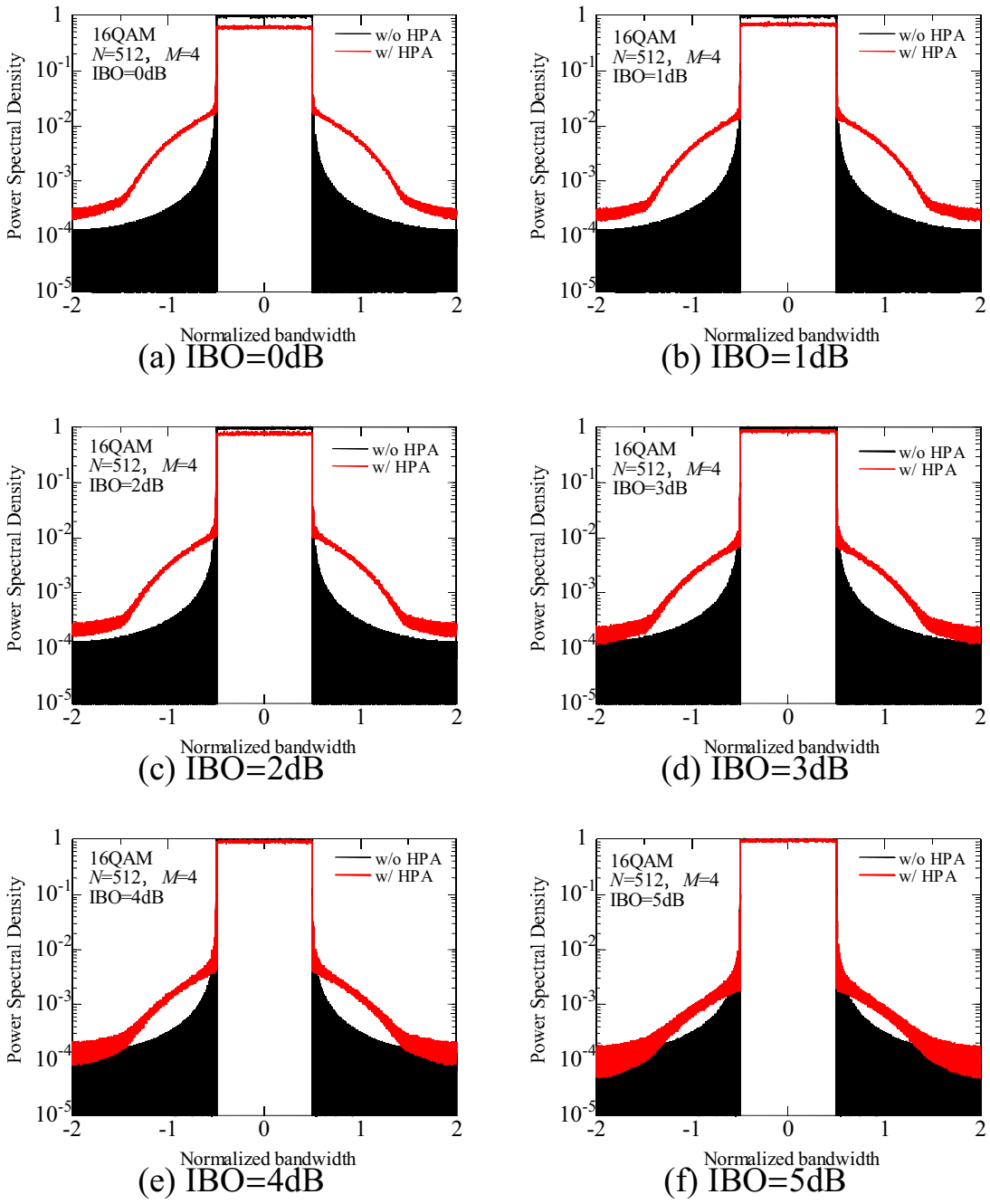

Figure 2.16: Frequency spectrum of OFDM signal after passing through HPA.

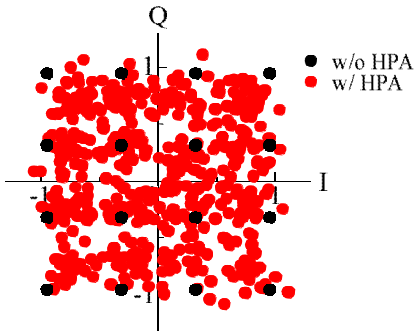

(a) IBO=0dB

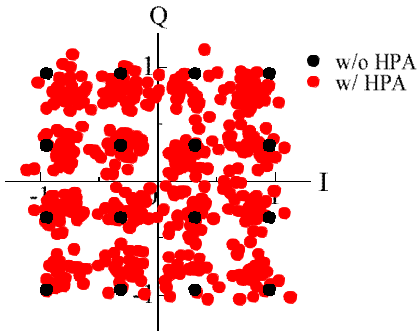

(b) IBO=1dB

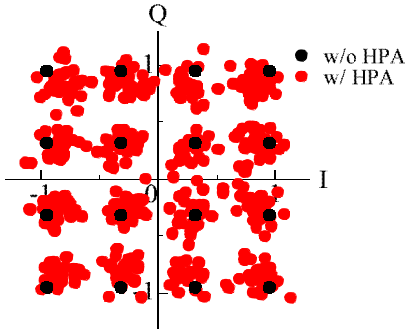

(c) IBO=2dB

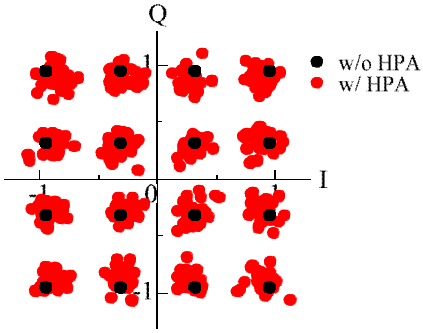

(d) IBO=3dB

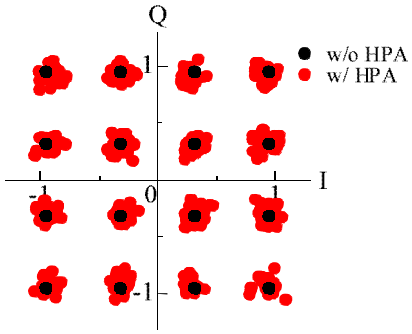

(e) IBO=4dB

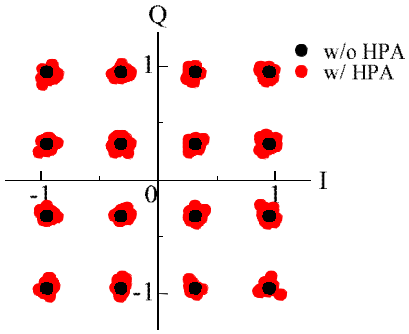

(f) IBO=5dB

Figure 2.17: Signal constellation of OFDM signal after passing through HPA.

Here, the influence of the number of sub-carriers on the peak-to-average power ratio (PAPR) is discussed and the definition of PAPR is defined as

$$\mathrm{PAPR} = \frac{P_{\max}}{P_{\mathrm{ave}}}, \tag{2.13}$$

where $P_{\max}$ is the maximum instantaneous power level in the time domain signals and P_{ave} denotes the average transmit power. From Eqs. (2.12) and (2.13), it can be said that, if PAPR $\leq$ IBO, the clipping effect does not occur and the OFDM signal is not distorted by the HPA. Thus the influence of the nonlinear distortion can be measured by comparing the PAPR with the IBO.

Figure 2.18 shows the PAPR performance of the OFDM signal with a parameter of the number of sub-carriers. Table 2.6 shows the simulation parameters. As shown in Fig. 2.18, it can be seen that the PAPR increases with increase in the number of sub-carriers. Moreover, the complementary cumulative distribution function (CCDF) of the PAPR is also shown to investigate the instantaneous peak power of the OFDM symbols. Figure 2.19 shows the CCDF performance of OFDM signal with a parameter of the number of sub-carriers. Table 2.7 shows the simulation parameters. As shown in Fig. 2.19, it can be seen that the PAPR increases with increase in the number of sub-carriers.

Here, the influence of the nonlinear distortion on the BER performance un-

Table 2.5: Simulation parameters.

Modulation	16QAM / OFDM
Number of subcarriers N	512
Oversampling rate M	4

Table 2.6: Simulation parameters.

Modulation	QPSK / OFDM
Number of subcarriers N	2〜1024

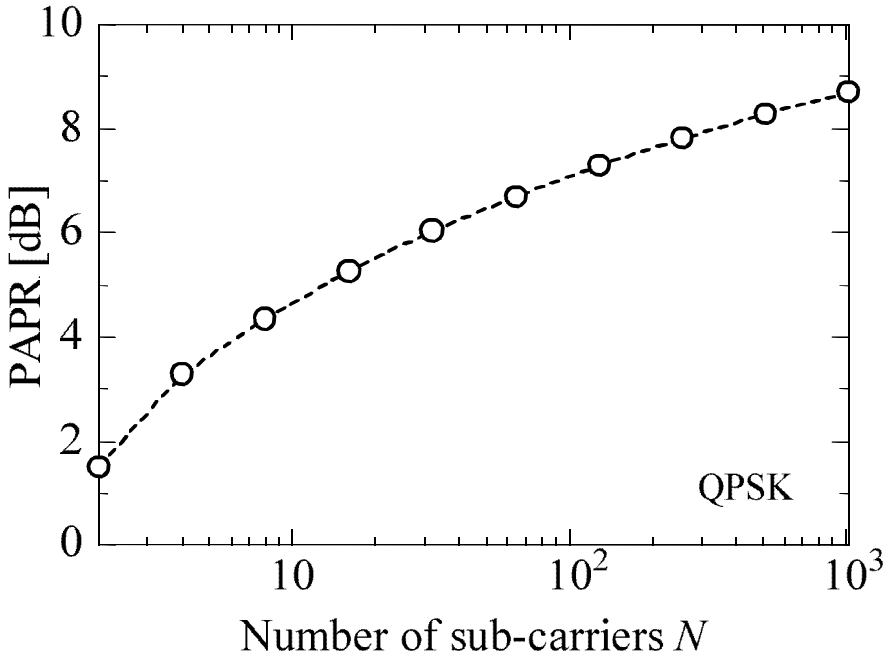

Figure 2.18: Number of sub-carriers versus PAPR performance of OFDM signal.

der AWGN and fading channels is investigated. Figure 2.20 shows the BER performance in the presence of the nonlinear distortion over AWGN channels and frequency selective fading channels. Table 2.8 shows the simulation parameters. From Fig. 2.20, it can be seen that the decrease in the IBO degrades the BER performance regardless of the channel model. Especially, this degradation becomes significant in use of a higher level modulation. This is because the higher level modulation uses the amplitude component which is significantly affected by the nonlinear distortion.

Table 2.7: Simulation parameters.

Modulation	QPSK / OFDM
Number of subcarriers N	64, 512

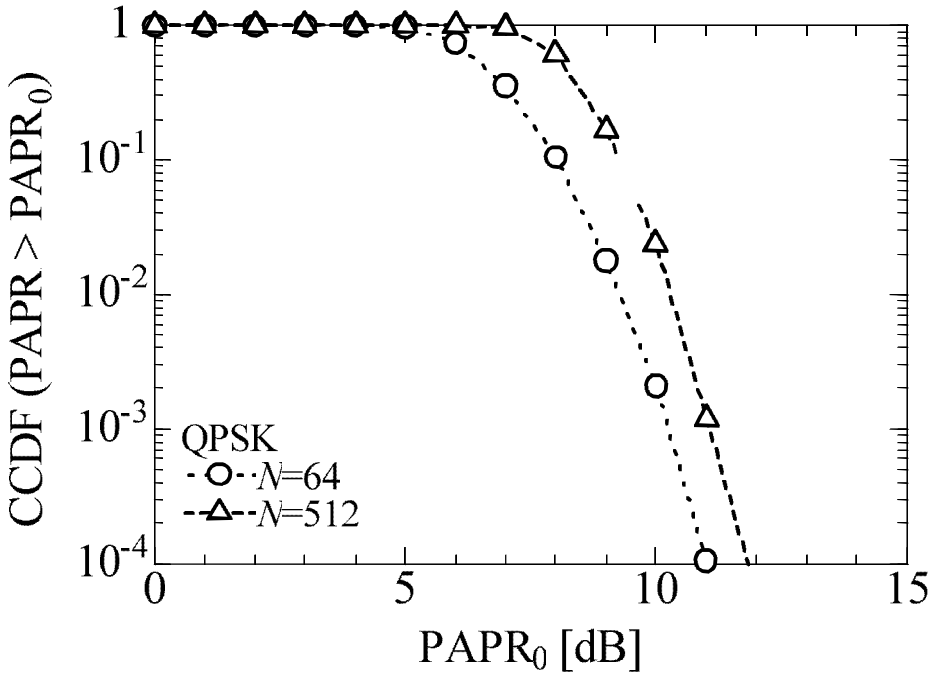

Figure 2.19: CCDF performance of OFDM signal with a parameter of the number of sub-carriers.

Table 2.8: Simulation parameters.

Modulation	QPSK, 16QAM, 64QAM / OFDM
Number of subcarriers N	512
Oversampling rate M	4
Guard interval length T_G	$128T_{sam}$
Channel model	AWGN, 128-ray exponentially decaying Rayleigh fading
Delay spread τ_{rms}	$36.0T_{sam}$
IBO	0, 1, 2, 3, 4, 5 [dB]

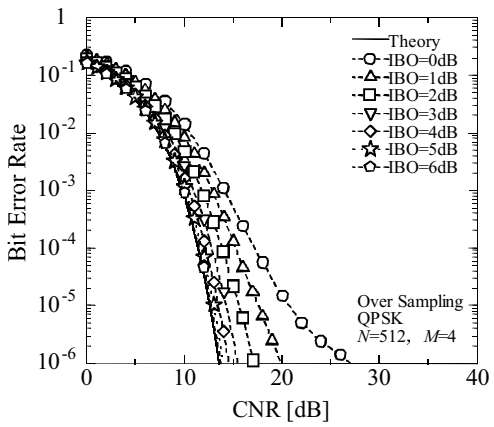

(a) QPSK (AWGN)

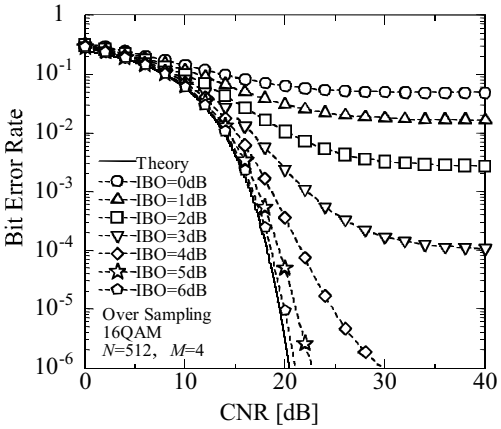

(b) 16QAM (AWGN)

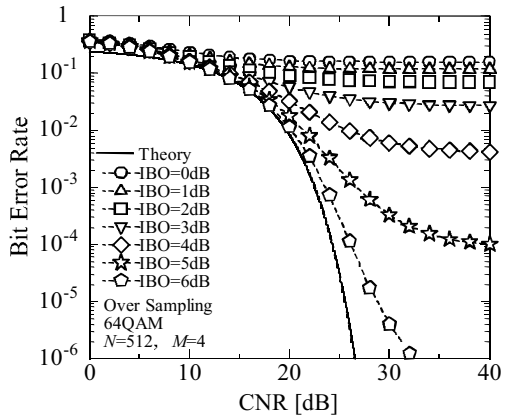

(c) 64QAM (AWGN)

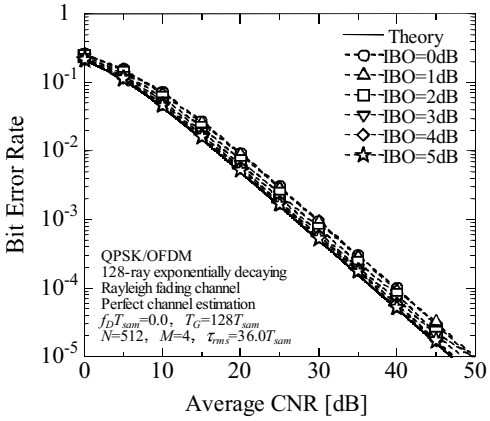

(d) QPSK (Fading)

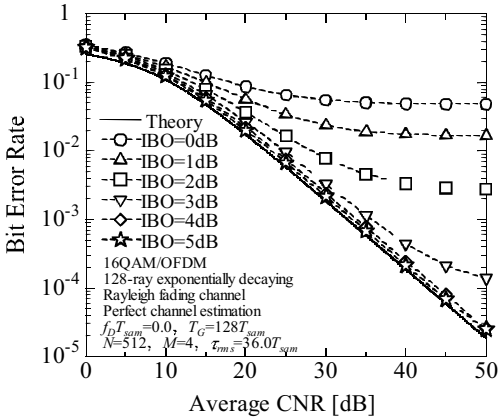

(e) 16QAM (Fading)

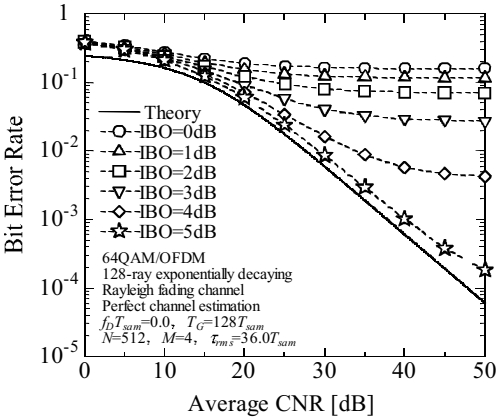

(f) 64QAM (Fading)

Figure 2.20: BER performance versus CNR in the presence of nonlinear distortion.

2.3 Summary

This chapter has described the principle and basic overview of OFDM systems and showed its transmission performance. In detail, the principle of frequency multiplexing, the signal generation, the frequency spectrum, and the guard interval which is essential to suppress the ISI due to multipath fading channels have been described. Next, the BER performance of OFDM systems over AWGN and multipath fading channels has been evaluated. Then the influence of the nonlinear distortion on OFDM signals has been described. In detail, the IBO and the PAPR have been described as the essential parameters in the analysis of the HPA and then the BER performance in the presence of the nonlinear distortion is evaluated under the AWGN and the multipath fading channels. From these results, the following things can be found.

- OFDM can realize the high spectrum utilization efficiency because of retaining orthogonality between sub-carriers.
- OFDM can perfectly suppress the ISI due to the multipath fading by inserting the guard interval.
- OFDM causes the significant degradation of the BER performance in the case that the maximum multipath delay exceeds the guard interval length.
- OFDM introduces the high PAPR, and its property causes the nonlinear distortion when passing through the HPA at the transmitter.
- The nonlinear distortion causes the out-of-band radiation as well as the BER degradation.

3 OFDM Clipping and Filtering Employing Transmit Power Control

OFDM has an inherent problem of the nonlinear distortion caused by the nonlinear characteristic of an HPA because OFDM time domain signals have high PAPR. In detail, the nonlinear distortion which is introduced after passing through the HPA causes the out-of-band radiation as well as the BER degradation.

In order to suppress the nonlinear distortion, a number of techniques have been proposed [18]. More specifically, clipping and filtering [19]-[22], partial transmit sequence [23], coding [26], [27], and predistortion [30] can be seen as well-known techniques. Among these techniques, partial transmit sequence and coding are effective to combat the nonlinear distortion, but both techniques require heavy transmission overhead and computational complexity. Predistorion is also an effective approach but the peak power level is not allowed to exceed the saturation level of the input-output characteristic of the HPA, which implies that the relatively high IBO is required in a realistic scenario.

From a practical point of view, clipping and filtering can be seen as an attractive technique because there are no constraints of the overhead, the computational complexity, and the IBO margin. However, clipping and filtering has a critical problem of the significant BER degradation because clipping significantly destroys the OFDM signals while suppressing the out-of-band radiation. Therefore, there are existing some effective approaches to overcome the BER degradation of clipping and filtering. For example, as for the transmitter side, the peak power reduction method employing peak reduction sub-carrier signals [31], [32] and the method to control the optimum clipping level considering the peak power regrowth after passing through a filter [33] have been proposed. On the other hand, as for the receiver side, the method to improve the BER by estimating and removing the nonlinear distortion component [34], [35] has been also proposed. Although these methods can effectively overcome the BER

degradation of clipping and filtering at the transmitter or the receiver side, these methods unfortunately require iterative processes, which consequently causes a considerable computational complexity.

So far, we have proposed the deterministic transmit power control scheme to enhance the SNDR in the presence of the nonlinear distortion [56]. In our proposed scheme, the discrete transmit power level is considered and the transmit power level is set to maximize the SNDR which is calculated by the theoretical formula. Therefore, this approach can determine the appropriate transmit power level without any heuristic calculation, which leads to a deterministic strategy for suppressing the nonlinear distortion while improving the BER performance. Considering that our transmit power control scheme can lower the transmit power level in a relatively high CNR, the application of our transmit power control scheme to clipping and filtering surely improve the BER performance while suppressing the out-of-band radiation. Moreover, considering that this proposed approach unfortunately restricts the range of the transmit power level and requires some cross correlation calculation at each transmit power level, we also propose the approach to derive the transmit power level with the maximum SNDR by using the closed form mathematical formula [36], which makes the dynamic range of the transmit power level limitless and enables us to automatically determine the best transmit power level satisfying the maximum SNDR just by a simple mathematical function. The effectiveness of the proposed method is demonstrated by means of computer simulations in comparison with the traditional clipping and filtering method [37]-[39].

The following section describes the operating principle of the OFDM clipping and filtering method. And next, Section 3.2 describes that of the proposed OFDM clipping and filtering method employing transmit power control based on SNDR.

3.1 OFDM Clipping and Filtering

3.1.1 System Concept

Clipping and filtering method has been well known as an effective technique to suppress the out-of-band radiation and therefore, its effectiveness has been extensively investigated [19]-[22]. Clipping and filtering method clips the time domain transmit OFDM signals by means of the clipping process and then eliminates the out-of-band radiation by means of the filtering process. In detail, the high peak power which is an inherent property of OFDM can be suppressed by clipping the time domain waveform and then the out-of-band radiation due to the clipping process is filtered out from the clipped OFDM signals. Therefore, clipping and filtering can be seen as a practical and effective technique to satisfy the spectral mask constraint. However, the clipping process causes the significant modification of the transmit OFDM signals and further modification is given by the specific frequency characteristic of the filtering process, which degrades the BER performance. In this context, although it can be said that clipping and filtering perfectly suppresses the out-of-band radiation, there is a critical problem of the significant BER degradation.

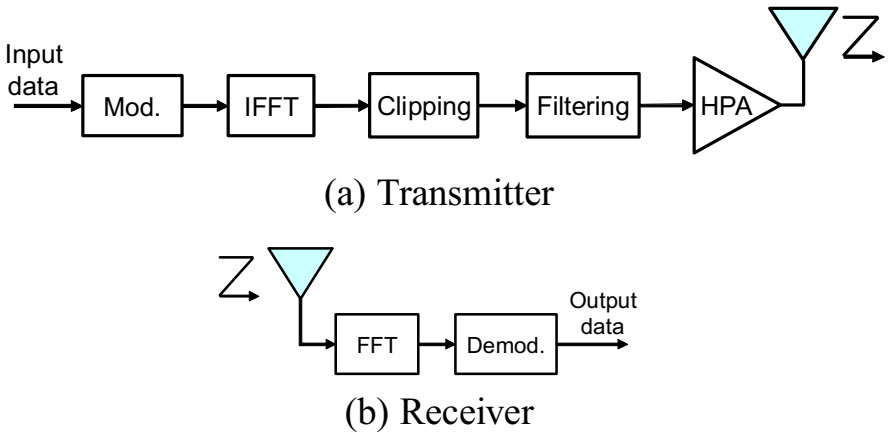

Figure 3.1: Overall configuration of traditional clipping and filtering method.

3.1.2 System Configuration

Figure 3.1 shows the overall configuration of the clipping and filtering method. As shown in Fig. 3.1, in order to reduce the peak power of the transmit signal, the OFDM signal is clipped by the clipping operation in the time domain. Here, clipping ratio (CR) is often used as a criterion of how much the time domain signal is clipped at the clipping process. Then the out-of-band radiation component caused by the clipping process is eliminated by the filtering operation in the frequency domain. In this dissertation, we assume the soft envelope limiter and the rectangular filter as the characteristics of clipping and filtering, respectively.

3.1.3 Numerical Results

In this section, we evaluate the performance of the clipping and filtering method in terms of the OFDM time domain waveform, the PAPR performance, the frequency spectrum, and the BER performance.

(a) OFDM time domain waveform

Figure 3.2 shows the OFDM time domain waveform of the clipping and filtering method with a parameter of a CR. Table 3.1 shows the simulation parameters. Here, the solid line in Fig. 3.2 indicates the clipping level (CL) in the clipping process for reference. From Fig. 3.2, we can confirm that the peak power of the OFDM time domain waveform after clipping and filtering can be suppressed in comparison with the case before clipping and filtering. Moreover, it can be observed that the peak power regrowth appears after performing the clipping and filtering method. This is because the filtering process additionally gives the modification of the clipped time domain waveform. Therefore, in general, the iterative signal processing is adopted for the clipping and filtering method in order to prevent this peak power regrowth problem.

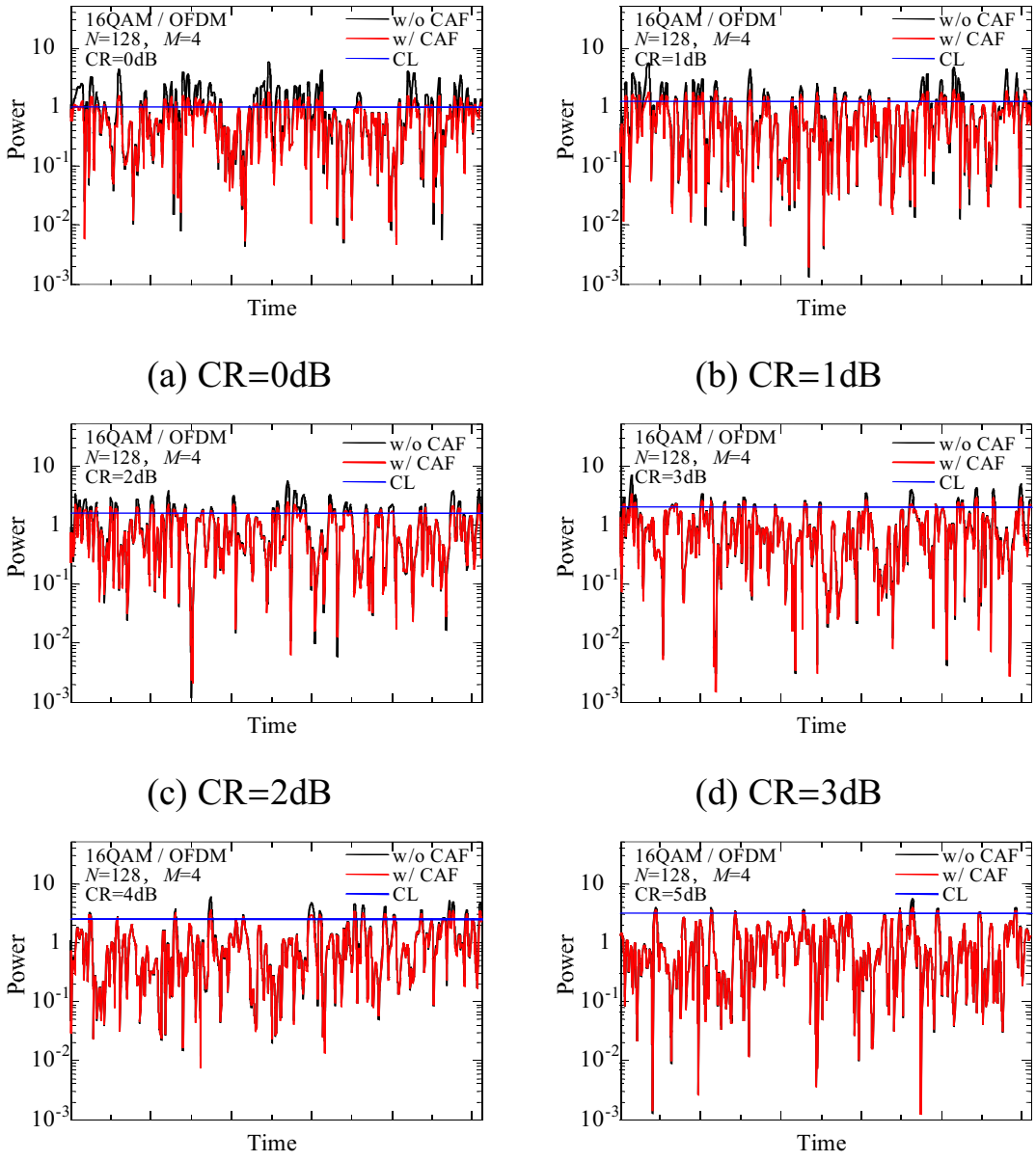

Figure 3.2: OFDM time domain waveform of clipping and filtering method with a parameter of clipping ratio.

Table 3.1: Simulation parameters.

Modulation	16QAM / OFDM
Number of subcarriers N	128
Oversampling rate M	4
CR	0, 1, 2, 3, 4, 5 [dB]

(b) PAPR performance

Figure 3.3 shows the PAPR performance with the clipping and filtering method. Table 3.2 shows the simulation parameters. Here, the performance with only the clipping process is also shown for reference. From this performance, we can see how much the effect of the peak power regrowth due to the filtering process. It is found from Fig. 3.3 that the peak power regrowth is caused by the filtering process regardless of the CR. Furthermore, it can be seen that the effect of the regrowth becomes more severe in the lower CR. This is because, the influence of the clipping process becomes significant in the lower CR and then, the more severe modification of the clipped signals is caused at the filtering process. This peak power regrowth gives the effect on the HPA and the appropriate value of the CR has to be determined considering the balance between the CR and the IBO. Therefore, in this performance evaluation, CR is set to be 2dB down from the IBO taking into account the effect of the peak power regrowth due to filtering.

Table 3.2: Simulation parameters.

Modulation	16QAM / OFDM
Number of subcarriers N	128
Oversampling rate M	4
CR	0, 3, 5 [dB]

Table 3.3: Simulation parameters.

Modulation	16QAM / OFDM
Number of subcarriers N	512
Oversampling rate M	4
CR	IBO-2 [dB]
IBO	0, 1, 2, 3, 4, 5 [dB]

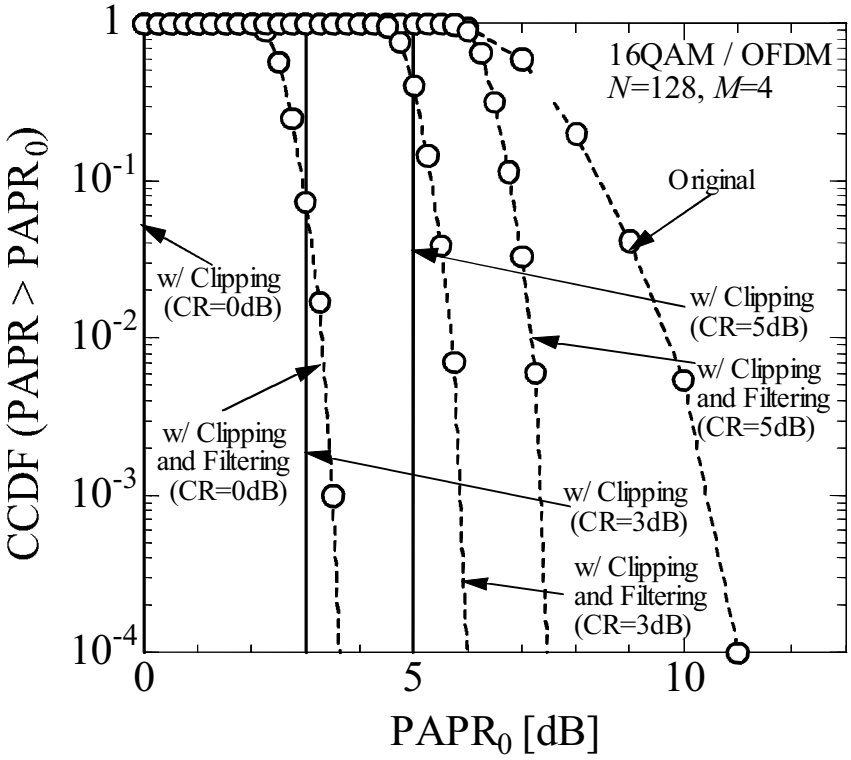

Figure 3.3: PAPR performance of clipping and filtering method.

(c) Frequency spectrum

Figure 3.4 shows the power spectral density performance of the clipping and filtering method with a parameter of the IBO. Table 3.3 shows the simulation parameters. Here, the performance without clipping and filtering is also shown for reference. It can be observed from Fig. 3.4 that the clipping and filtering method can significantly suppress the out-of-band radiation compared with the case without clipping and filtering. This is because the filtering process perfectly eliminates the out-of-band radiation due to the clipping process.

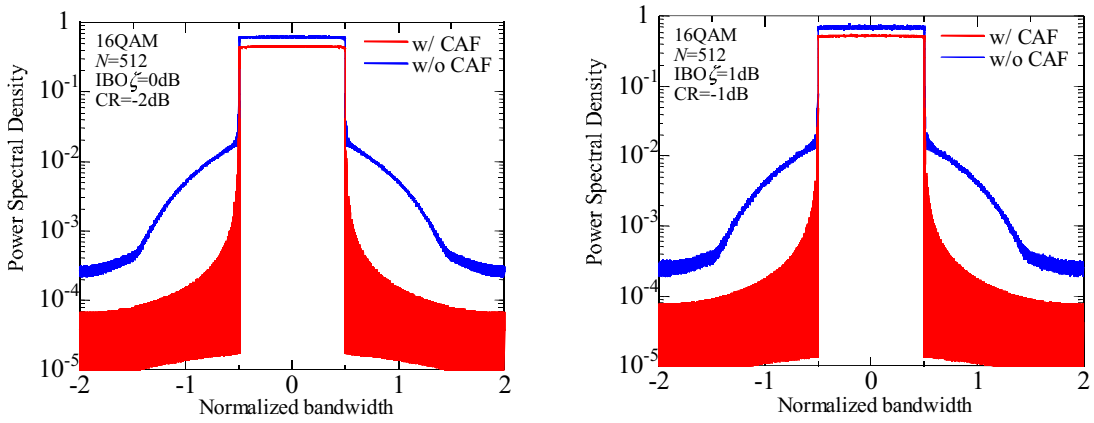

(a) IBO=0dB

(b) IBO=1dB

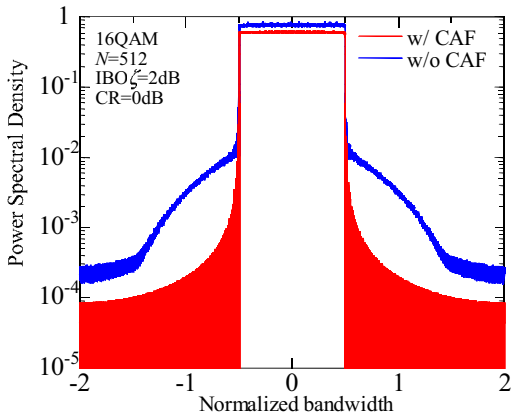

(c) IBO=2dB

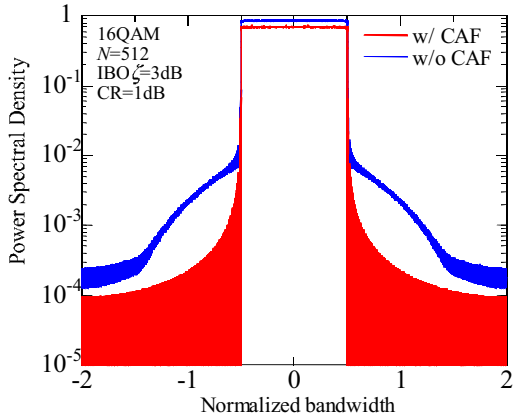

(d) IBO=3dB

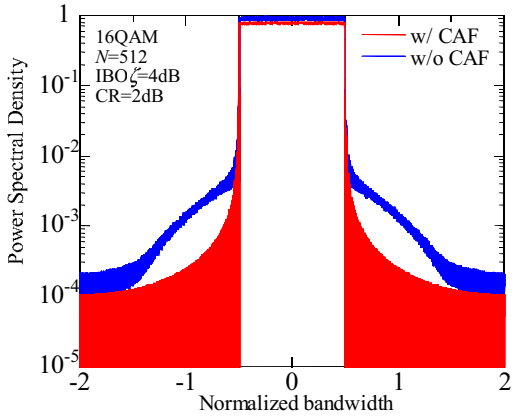

(e) IBO=4dB

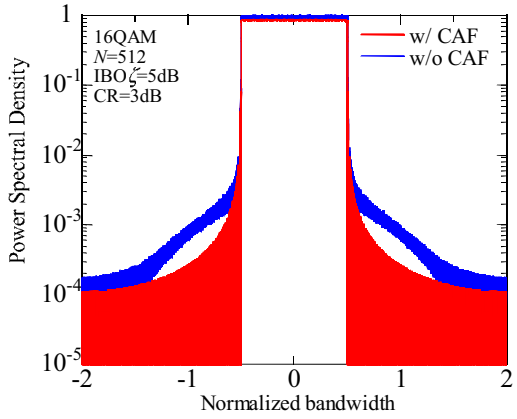

(f) IBO=5dB

Figure 3.4: Power spectral density performance of clipping and filtering method with a parameter of IBO.

(d) BER performance

Figure 3.5 and Figure 3.6 show the BER performance of the clipping and filtering method over AWGN and frequency selective fading channels. Table 3.3 shows the simulation parameters. It is found from Figs. 3.5 and 3.6 that the clipping and filtering method causes the BER degradation compared with the case without clipping and filtering regardless of the modulation scheme and the channel model. This is because clipping and filtering significantly modifies the transmit OFDM signals.

From the above simulation results, we can see that, although the clipping and filtering method is quite effective to suppress the out-of-band radiation, there is a critical problem of the clipping and the peak power regrowth, which leads to the BER degradation. Briefly speaking, clipping and filtering is an attractive method for complying with the bandwidth regulations, which contrarily sacrifices the BER performance.

Table 3.4: Simulation parameters.

Modulation	16QAM, 64QAM / OFDM
Number of subcarriers N	512
Oversampling rate M	4
Guard interval length T_G	$128T_{sam}$
Channel model	AWGN, 128-ray exponentially decaying Rayleigh fading
Delay spread τ_{rms}	$36.0T_{sam}$
CR	IBO-2 [dB]
IBO	0, 3, 5 [dB]

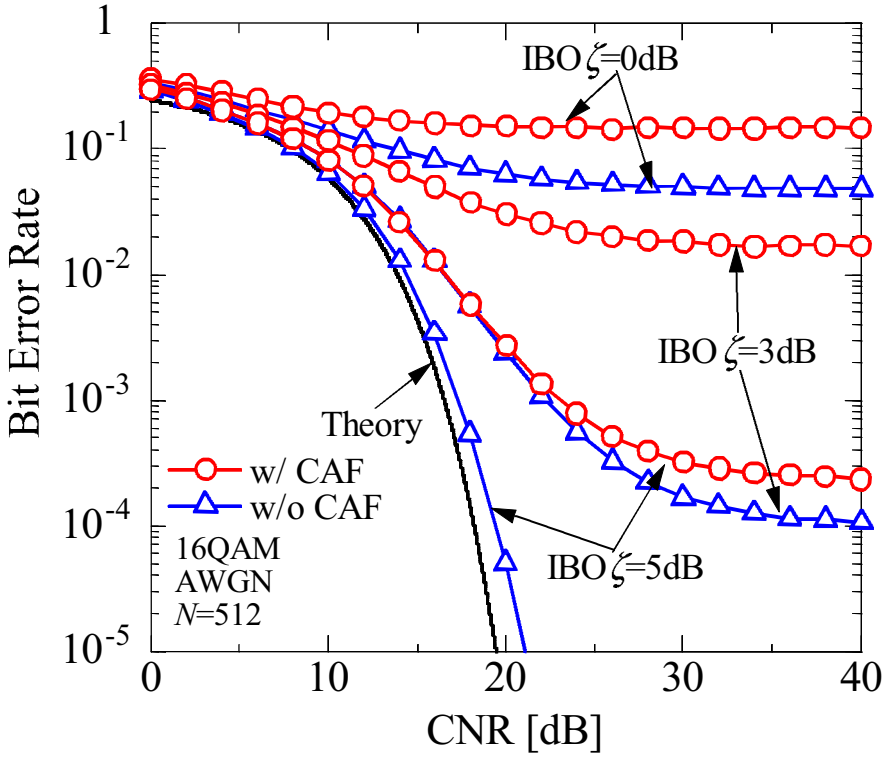

(a) 16QAM

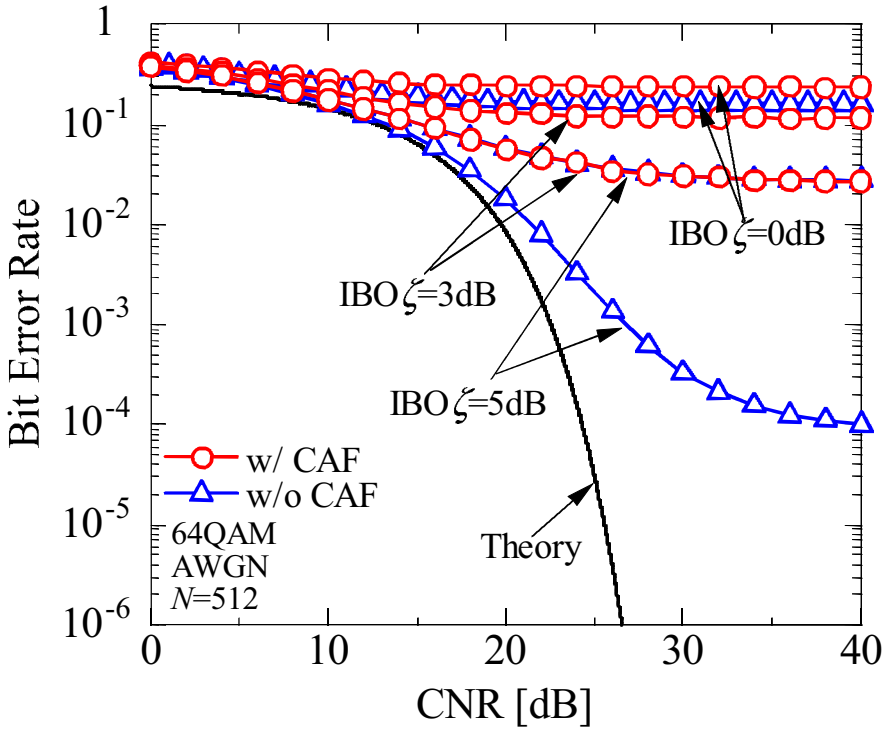

(b) 64QAM

Figure 3.5: BER performance of clipping and filtering method over AWGN channel.

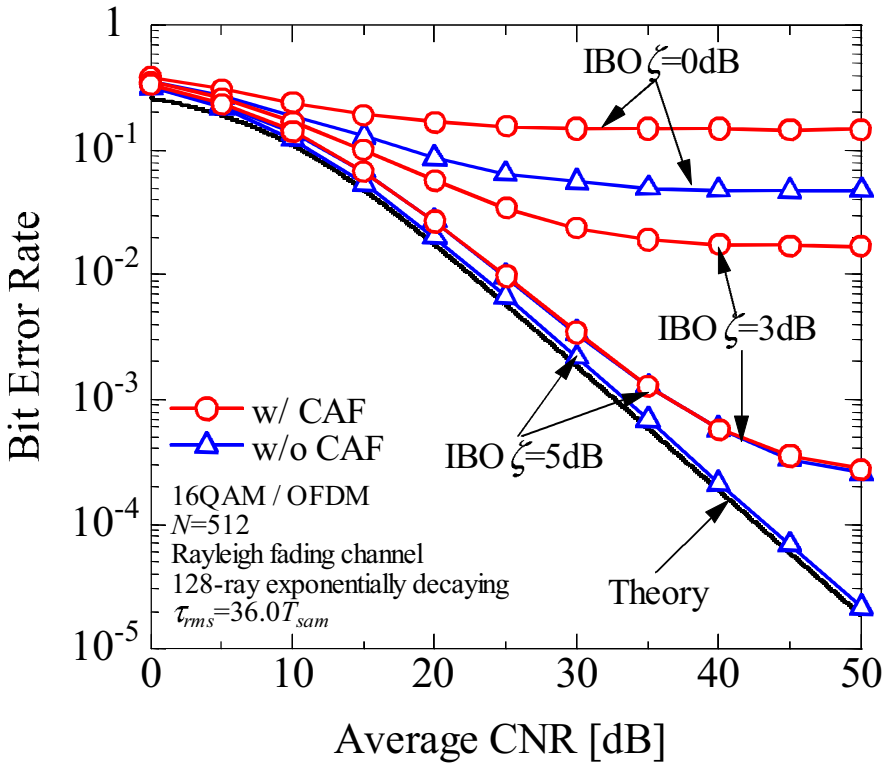

(a) 16QAM

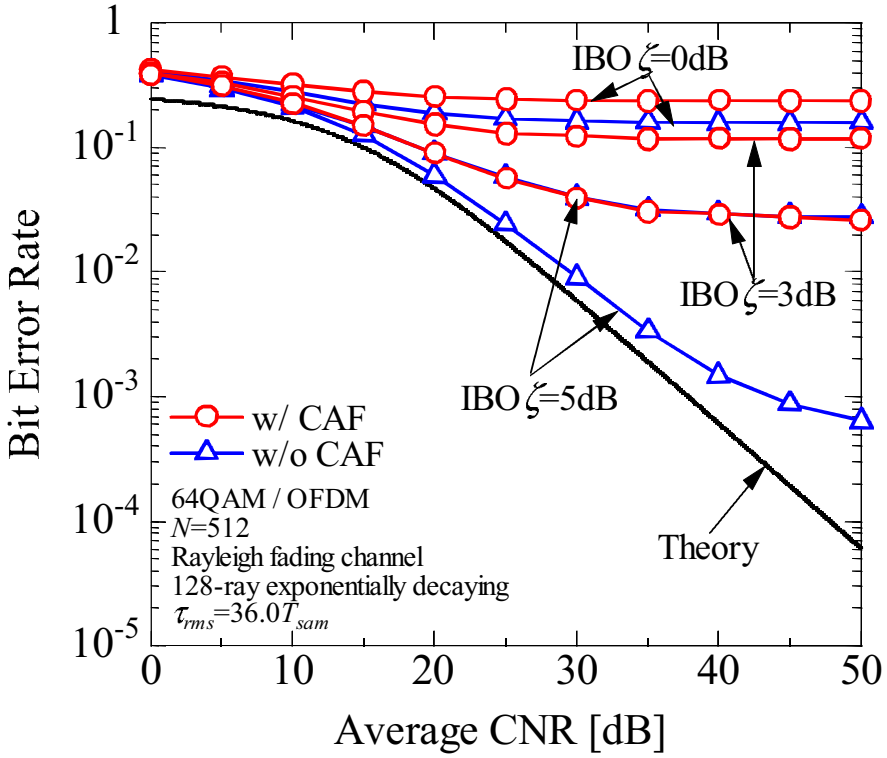

(b) 64QAM

Figure 3.6: BER performance of clipping and filtering method over frequency selective fading channel.

3.2 Application of Transmit Power Control to OFDM Clipping and Filtering

3.2.1 System Concept

In order to overcome the BER degradation of clipping and filtering, we propose the clipping and filtering employing the transmit power control based on SNDR [37]-[39]. Figure 3.7 shows the comparison in terms of the concept of clipping and filtering between the proposed method and the traditional method. As shown in Fig. 3.7, the proposed method deploys the transmit power control before the traditional clipping and filtering processes, which clearly shows the difference from the traditional method. Although clipping and filtering is quite effective to suppress the out-of-band radiation, there is still a critical problem of the BER degradation. This is because clipping and filtering significantly distorts the transmit OFDM time domain waveform. Simply speaking, clipping and filtering is attractive for complying with the bandwidth regulations, which contrarily sacrifices the BER performance. Therefore, the proposed method aims to improve the BER performance of clipping and filtering while suppressing the out-of-band radiation. The feature of the proposed method is to lower

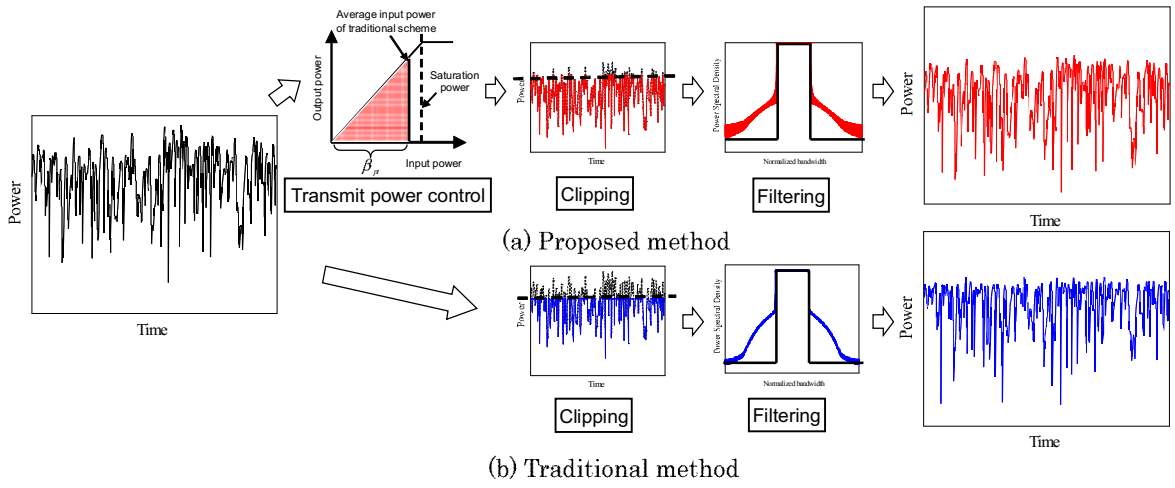

Figure 3.7: Relationship between proposed transmit power control and input-output characteristic of HPA.

the transmit power level input to the clipping process in order to alleviate the distortion appearing in clipping and filtering. This approach comes from the fact that the SNDR is increased by reducing the transmit power level in a relatively large CNR because the transmit power reduction essentially decreases the nonlinear distortion. It is observed from Fig. 3.7 that the proposed method employing transmit power control reduces the power level input to clipping and filtering in comparison with the traditional method and then consequently generates less distorted OFDM signals than the traditional method after clipping and filtering.

As discussed above, once the transmit power level input to the clipping process is properly determined based on the SNDR, it is expected that both improvement of the BER and suppression of the out-of-band radiation are successfully realized, which strongly motivates us to deploy the transmit power control before clipping and filtering.

Next, the basic mechanism of the SNDR-based transmit power control is described [56]. Figure 3.8 shows the relationship between transmit power control and input-output characteristic of HPA. As shown in Fig. 3.8, the increase in the transmit power level lowers the signal-to-distortion power ratio (SDR) while enhancing the signal-to-noise power ratio (SNR). On the other hand, the decrease in the transmit power level enhances the SDR while lowering the SNR. In this sense, there may have the optimal transmit power level to arbitrate between the SNR and the SDR. The main feature of the deterministic transmit power control is to determine the appropriate transmit power level satisfying the maximum SNDR by using the simple mathematical formula. In detail, we set the several transmit power levels and calculate the SNDR of each transmit power level. Then the transmit power level with the maximal SNDR is selected as the best transmit power level.

In this dissertation, we propose the different two approaches to realize the transmit power control : one is the discrete control approach and the other is the continuous control. Figure 3.9 shows the concept of proposed transmit power

control. As shown in Fig 3.9, the discrete control calculates the SNDR by using cross-correlation between the transmit signal and the clipped signal. In the discrete control, since the cross-correlation is obtained in a symbol-by-symbol manner, the symbol-wise transmit power control can be realized.

On the other hand, the continuous control performs the transmit power control by using the SNDR based on the statistical property, which enables to reduce the system complexity. Briefly speaking, the heavy calculation such as the symbol-wise calculation is not required in the continuous control. In the continuous control, the transmit power control is performed assuming that the effect of the nonlinear distortion on the OFDM signal is regarded as being constant. In this dissertation, the effectiveness of the proposed transmit power control method which can be realized by two approaches are investigated.

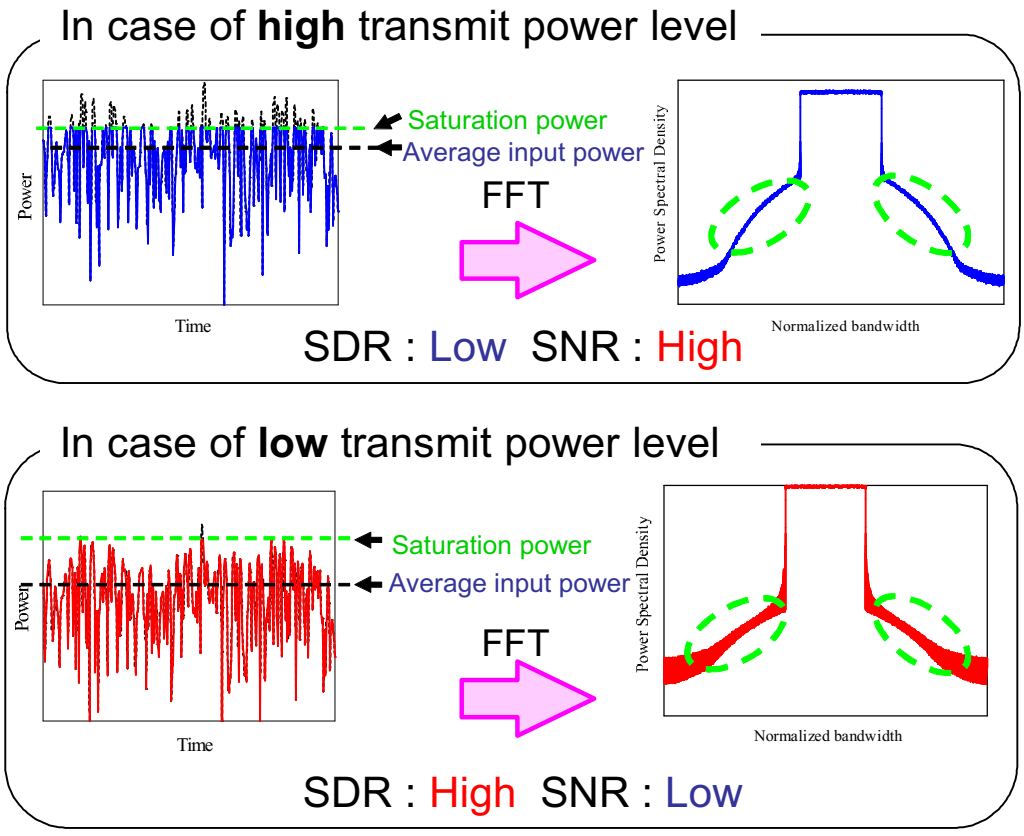

Figure 3.8: Relationship between transmit power control and input-output characteristic of HPA.

3.2.2 Theoretical Derivation of SNDR

In the case of a relatively large number of sub-carriers, the complex base-band OFDM signal can be modeled as a complex Gaussian process because the central limit theorem holds true [57]. Therefore, the analysis on the nonlinear distorted OFDM signals comes down to general results for nonlinear distorted Gaussian signals.

The SDR of the OFDM signals is derived by the use of Bussgang's theorem [58]-[61]. Since the extension of Bussgang's theorem to complex Gaussian inputs makes it possible to express the nonlinear distorted signal $s_d(t)$ as the sum of a desired component and an uncorrelated nonlinear distortion $n_d(t)$, the nonlinear distorted signal is expressed as

$$s_d(t) = \alpha s(t) + n_d(t), \tag{3.1}$$

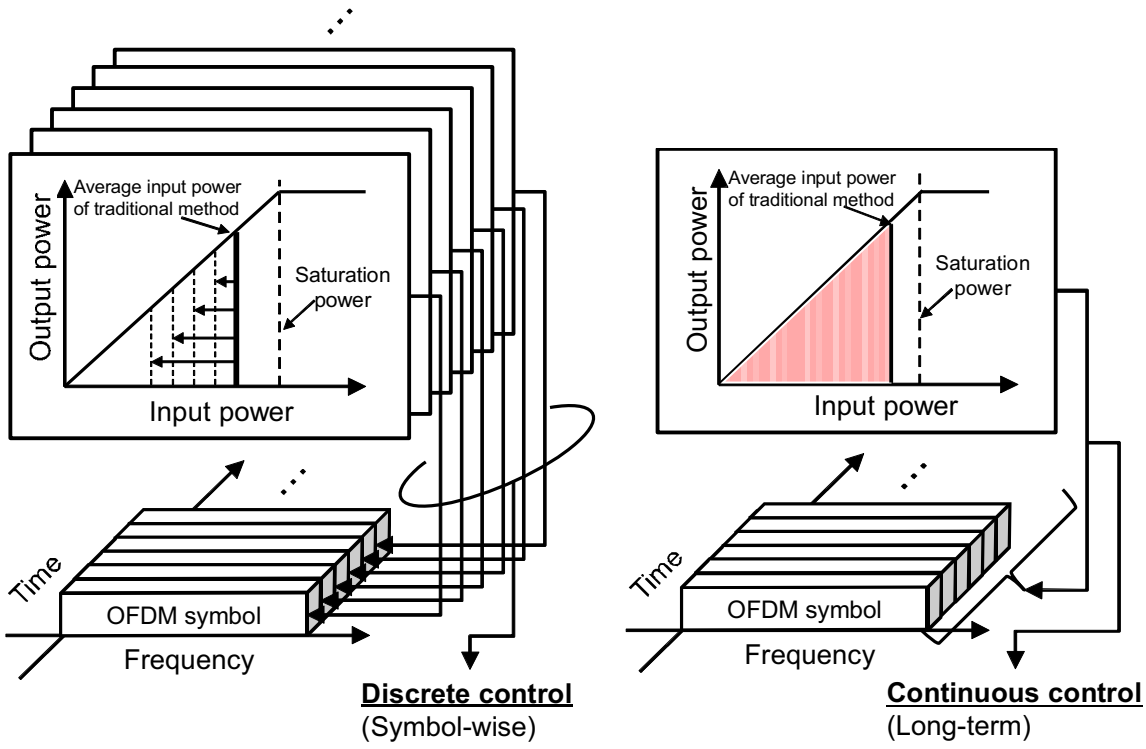

(a) Discrete control (b) Continuous control

Figure 3.9: Concept of proposed transmit power control.

where α is the attenuation coefficient due to the nonlinear distortion and $s(t)$ is the undistorted OFDM signal.

The complex version of the Bussgang's theorem introduces the expression of the autocorrelation of the nonlinear distorted signal $s_d(t)$ as given by

$$R_{s_d s_d}(\tau) = |\alpha|^2 \cdot R_{ss}(\tau) + R_{n_d n_d}(\tau), \tag{3.2}$$

where $R_{ss}(\tau) = \sigma_s^2$ and $R_{n_d n_d}(\tau)$ are the input autocorrelation function and the nonlinear distortion autocorrelation function, respectively.

The attenuation coefficient of the useful component is given by

$$\alpha = \frac{R_{s_d s}(0)}{R_{ss}(0)} = \frac{E[s_d^*(t)s(t)]}{\beta^2 {\sigma_s}^2}, \tag{3.3}$$

where $R_{s_d s}(\tau)$ denotes the input-output cross-correlation function, β is the coefficient of transmit power level, ${\sigma_s}^2$ is the average signal power without the transmit power control.

Hence, the SDR after transmit power control can be defined as the power ratio between the useful signal component and the nonlinear distortion component as given by

$$\begin{aligned} \Lambda &= \frac{|\alpha|^2 \cdot R_{ss}(0)}{R_{s_d s_d}(0) - |\alpha|^2 \cdot R_{ss}(0)} \\ &= \frac{|\alpha|^2 \beta^2 {\sigma_s}^2}{R_{s_d s_d}(0) - |\alpha|^2 \beta^2 {\sigma_s}^2}. \end{aligned} \tag{3.4}$$

Considering that the BER performance of the nonlinear distorted signal depends on the SNR as well as the SDR, the SNDR which takes these two factors into account needs to be derived. Let η and σ_n^2 denote the channel gain and the

noise variance, respectively, the SNDR γ_{nd} is defined as

$$\begin{aligned}\gamma_{nd} &= \frac{|\eta|^2 |\alpha|^2 \beta^2 {\sigma_s}^2}{\frac{|\eta|^2 |\alpha|^2 \beta^2 {\sigma_s}^2}{\Lambda} + \sigma_n^2} \\ &= \frac{|\alpha|^2 \beta^2}{\frac{|\alpha|^2 \beta^2}{\Lambda} + \frac{1}{\Gamma_0}},\end{aligned} \tag{3.5}$$

where $\Gamma_0 = |\eta|^2 {\sigma_s}^2 / \sigma_n^2$ is the average CNR at the receiver. Here, it should be noted that the average CNR Γ which requires less side information than the sub-carrier CNR is notified from the receiver.

In the discrete transmit power control, the transmit power level with the maximum SNDR calculated by using Eqs. (3.3)-(3.5) is selected from the discrete transmit power levels in a symbol-by-symbol manner. However, this approach requires the cross correlation calculation at each transmit power level and restricts the dynamic range of the transmit power level. On the other hand, the continuous transmit power control is just to derive the transmit power level to satisfy the maximum SNDR by using the simple closed form mathematical formula, which makes the dynamic range of the transmit power level limitless and enables us to easily determine the best transmit power level.

In the case of a relatively large number of sub-carriers, the amplitude distribution of the OFDM signals $p(r)$ is subject to Rayleigh distribution as given by

$$p(r) = \frac{2r}{\beta^2 \sigma_s^2} e^{-\frac{r^2}{\beta^2 \sigma_s^2}}. \tag{3.6}$$

Let $f(r) = g(r) \cdot e^{j\phi(r)}$ be a complex nonlinear distortion function, $s_d(t)$ is rewritten as

$$s_d(t) = f(r(t)) e^{j\theta(t)}, \tag{3.7}$$

where $r(t)$ and $\theta(t)$ are the amplitude and the phase of the undistorted signal $s(t)$,

respectively.

Using Eq. (3.6), the attenuation coefficient α and the autocorrelation of the nonlinear distorted signal $R_{s_d s_d}(\tau)$ are expressed as

$$\begin{aligned}\alpha &= \frac{R_{s_d s}(0)}{R_{ss}(0)} = \frac{E[s_d^*(t)s(t)]}{\beta^2 {\sigma_s}^2} \\ &= \frac{E[g(r)\cdot r]}{\beta^2\sigma_s^2} = \frac{1}{\beta^2\sigma_s^2}\int_0^\infty g(r)\cdot r\cdot p(r)dr \\ &= \frac{1}{\beta^2\sigma_s^2}\int_0^\infty g(r)\cdot r\cdot \frac{2r}{\beta^2\sigma_s^2} e^{-\frac{r^2}{\beta^2\sigma_s^2}} dr, \end{aligned} \tag{3.8}$$

$$\begin{aligned} R_{s_d s_d}(0) &= \int_0^\infty g^2(r)\cdot p(r)\, dr \\ &= \int_0^\infty g^2(r)\cdot \frac{2r}{\beta^2\sigma_s^2} e^{-\frac{r^2}{\beta^2\sigma_s^2}} dr. \end{aligned} \tag{3.9}$$

Assuming a soft envelope limiter, the nonlinear distortion function $f(r) = g(r)\dot{\phi}(r)$ is represented as

$$\begin{aligned} g(r) &= \begin{cases} r & r \le A \\ A & r > A \end{cases} \\ \phi(r) &= 0. \end{aligned} \tag{3.10}$$

Assuming a soft envelope limiter, the attenuation coefficient α and the autocorrelation of the nonlinear distorted signal $R_{s_d s_d}(\tau)$ are derived in a closed form formula and are expressed as

$$
\begin{aligned}
\alpha &= \frac{1}{\beta^2\sigma_s^2}\int_0^\infty g(r)\cdot r\cdot p(r)\,dr \\
&= \frac{1}{\beta^2\sigma_s^2}\left\{\int_0^A r^2\cdot p(r)\,dr+\int_A^\infty A\cdot r\cdot p(r)\,dr\right\} \\
&= -\frac{1}{\beta^2\sigma_s^2}\left\{\int_0^A r^2\cdot q'(r)\,dr+\int_A^\infty A\cdot r\cdot q'(r)\,dr\right\} \\
&= -\frac{1}{\beta^2\sigma_s^2}\left\{\left[r^2q(r)\right]_0^A-\int_0^A 2r\cdot q(r)\,dr+\left[A\cdot r\cdot q(r)\right]_A^\infty-A\int_A^\infty q(r)\,dr\right\} \\
&= -\frac{1}{\beta^2\sigma_s^2}\left\{A^2\cdot q(A)+\sigma_s^2\int_0^A q'(r)\,dr-A^2\cdot q(A)-A\int_A^\infty q(r)\,dr\right\} \\
&= -\frac{1}{\beta^2\sigma_s^2}\left\{\beta^2\sigma_s^2\left[q(r)\right]_0^A-A\int_A^\infty e^{-\frac{r^2}{\beta^2\sigma_s^2}}dr\right\} \\
&= -\frac{1}{\beta^2\sigma_s^2}\left\{\beta^2\sigma_s^2\left(q(A)-1\right)-A\int_{\frac{A}{\beta\sigma_s}}^\infty e^{-t^2}\cdot\beta\sigma_s dt\right\} \\
&= \frac{1}{\beta^2\sigma_s^2}\left[\beta^2\sigma_s^2\left(1-e^{-\frac{A^2}{\beta^2\sigma_s^2}}\right)+\frac{A\beta\sigma_s\sqrt{\pi}}{2}\mathrm{erfc}\left(\frac{A}{\beta\sigma_s}\right)\right] \\
&= 1-e^{-\frac{A^2}{\beta^2\sigma_s^2}}+\frac{A\sqrt{\pi}}{2\beta\sigma_s}\mathrm{erfc}\left(\frac{A}{\beta\sigma_s}\right) \\
&= 1-e^{-\frac{\zeta}{\beta^2}}+\frac{\sqrt{\pi\zeta}}{2\beta}\mathrm{erfc}\left(\frac{\sqrt{\zeta}}{\beta}\right), \qquad (3.11)
\end{aligned}
$$

$$
\begin{aligned}
R_{s_ds_d}(0) &= \int_0^A r^2\cdot p(r)\,dr+\int_A^\infty A^2\cdot p(r)\,dr \\
&= -\left\{\int_0^A r^2\cdot q'(r)\,dr+\int_A^\infty A^2\cdot q'(r)\,dr\right\} \\
&= -\left\{\left[r^2\cdot q(r)\right]_0^A-\int_0^A 2r\cdot q(r)\,dr+A^2\left[q(r)\right]_A^\infty\right\} \\
&= -\left\{A^2\cdot q(A)+\beta^2\sigma_s^2\int_0^A q'(r)\,dr+A^2\left(-q(A)\right)\right\} \\
&= -\beta^2\sigma_s^2\left\{q(A)-1\right\} \\
&= \beta^2\sigma_s^2\left(1-e^{-\frac{\zeta}{\beta^2}}\right), \qquad (3.12)
\end{aligned}
$$

where $\zeta = A^2/\sigma_s^2$ is the input-backoff (IBO) and $q(r) = \exp\left(-r^2/\sigma_s^2\right)$.

Substituting Eqs. (3.11) and (3.12) into Eq. (3.4), the SDR Λ is successfully represented in closed form as given by

$$\begin{aligned}\Lambda &= \frac{|\alpha|^2\beta^2{\sigma_s}^2}{R_{s_d s_d}(0) - |\alpha|^2\beta^2{\sigma_s}^2} \\ &= \frac{\left\{1 - e^{-\frac{\zeta}{\beta^2}} + \frac{\sqrt{\pi\zeta}}{2\beta}\mathrm{erfc}\left(\frac{\sqrt{\zeta}}{\beta}\right)\right\}^2}{\left(1 - e^{-\frac{\zeta}{\beta^2}}\right) - \left\{1 - e^{-\frac{\zeta}{\beta^2}} + \frac{\sqrt{\pi\zeta}}{2\beta}\mathrm{erfc}\left(\frac{\sqrt{\zeta}}{\beta}\right)\right\}^2}.\end{aligned} \tag{3.13}$$

Since the transmission performance of the nonlinearly distorted signal depends on not only the SDR but also the SNR, we have to derive the SNDR including the effect of these two factors. The SNDR γ_{nd} is represented again as

$$\begin{aligned}\gamma_{nd} &= \frac{|\eta|^2\,|\alpha|^2\,\beta^2{\sigma_s}^2}{\frac{|\eta|^2\,|\alpha|^2\,\beta^2{\sigma_s}^2}{\Lambda} + \sigma_n^2} \\ &= \frac{|\alpha|^2\beta^2}{\frac{|\alpha|^2\beta^2}{\Lambda} + \frac{1}{\Gamma_0}}.\end{aligned} \tag{3.14}$$

By substituting Eqs. (3.11) and (3.13) into Eq. (3.14), it is observed that the SNDR γ_{nd} results in the closed form solutions, which implies that the continuous transmit power control approach can easily find the optimal transmit power level β satisfying the maximum SNDR. Figure 3.10 shows the SNDR with respect to the transmit power level β, where the IBO $\zeta = 0, 3, 5$ dB and the average CNR $\Gamma_0 = 30$ dB. Here, it should be noted that the SNDR γ_{nd} is obtained in intervals of $\beta = 0.01$. From Fig. 3.10, the optimal value of β satisfying the maximum SNDR γ_{nd} can be found regardless of the IBO.

3.2.3 System Configuration

Figure 3.11 shows the overall system configuration of the proposed method employing the discrete control and continuous control. At the transmitter, in-

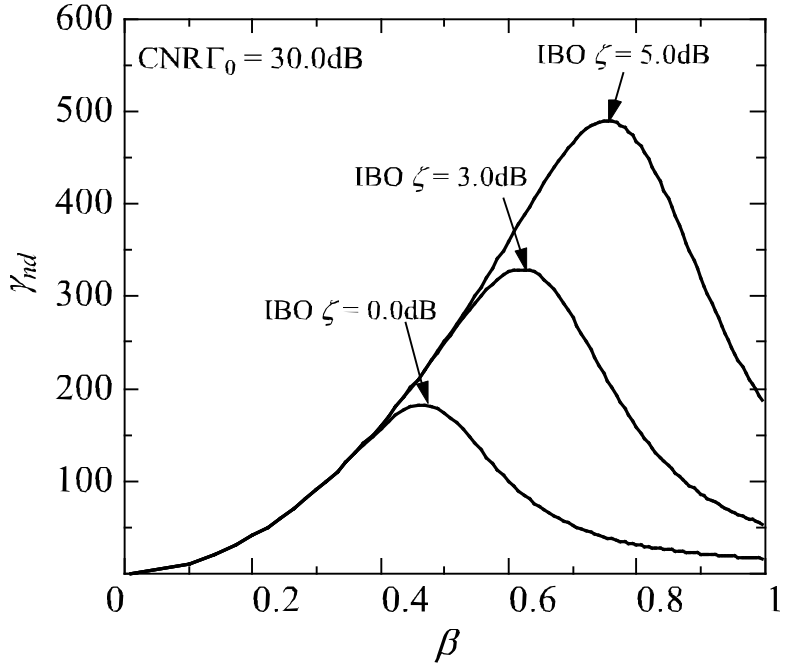

Figure 3.10: Relationship between SNDR γ_{nd} and normalized transmit power level β.

coming information bits are encoded and then are mapped into the sub-carrier signals with an arbitrary modulation level. Then the N-parallel modulated signals are fed into the N-point IFFT circuit so as to be converted into the time domain OFDM signals with the sampling period of T_{sam}. Here, in the discrete control, there are several input power levels to be predetermined, the SNDR of each input power level β_i is theoretically calculated by using Eqs. (3.3)-(3.5) in a symbol-by-symbol manner. On the other hand, in the continuous control, the optimal transmit power level β_{opt} is determined by using Eqs. (3.11), (3.13), and (3.14) as a closed form solution. Then, the optimal input power level β_{opt} is determined by selecting the input power level satisfying the maximum SNDR. Especially in the continuous control, the SNDR characteristic as a function of the transmit power level β can be easily investigated, which enables us to find the optimal transmit power level. Here, it is assumed that the average CNR Γ_0 is perfectly sent from the receiver. After the time domain signals are scaled to the optimal transmit power level, the time domain OFDM signals are input to clipping and filtering and then are amplified by the HPA. In clipping and filter-

ing, the maximum input signal level to clipping is set to be 2 dB down from the target saturation level of the nonlinear amplifier to prevent the effect of the peak power regrowth after filtering.

At the receiver, the OFDM signals which are distorted by both nonlinear amplification and multipath fading are received and then amplified according to the transmit power level β_{opt}. Next, the received OFDM signals are fed into the N-point FFT circuit and are converted into the N-channel signals. Finally, transmit data are recovered by means of channel decoder. Here, it should be noted that, although β has to be notified from the transmitter to the receiver, the degradation in the transmission efficiency becomes negligible. This is because the notification period can be set to be much longer than an OFDM symbol period.

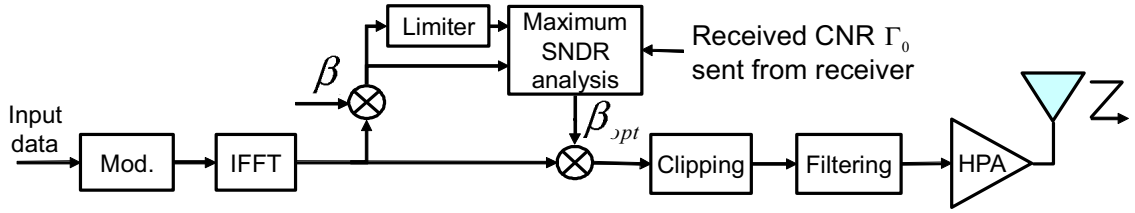

(a) Transmitter (Discrete control)

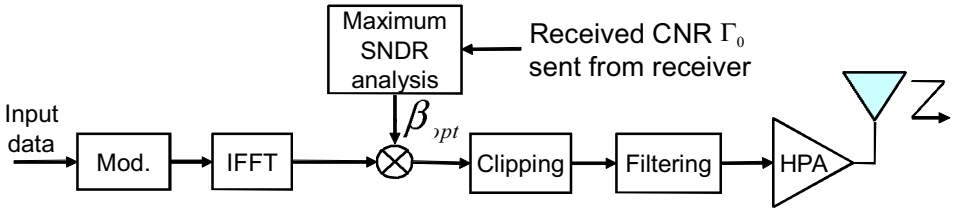

(b) Transmitter (Continuous control)

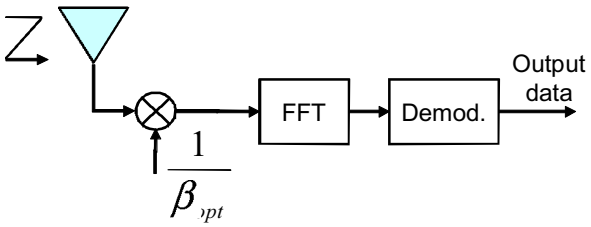

(c) Receiver

Figure 3.11: Overall configuration of proposed method.

3.2.4 Numerical Results

In this section, we evaluate the performance of the proposed method in terms of the output power reduction ratio of HPA, the OFDM time domain waveform, the PAPR performance, the frequency spectrum, and the BER performance.

(a) Output power reduction ratio of HPA

Figure 3.12 and Figure 3.13 show the output power reduction ratio of the HPA with the proposed method employing the discrete control and continuous control. Table 3.5 shows the simulation parameters. The output power reduction ratio is defined as the ratio of the average output power of the proposed method after passing through the HPA. Since this power reduction ratio is normalized by the traditional method without transmit power control, we can see that the effect of transmit power reduction by means of the proposed method. It is found from Figs. 3.12 and 3.13 that the output power of the HPA with the proposed method is reduced compared with the traditional method and moreover, its effect is remarkable in the higher CNR. This is because the transmit power reduction is performed in the nonlinear distortion dominant condition which corresponds to the high CNR. In the low CNR region, the output power ratio does not change so much, which implies that the SNR takes the priority over the SDR. Moreover, it can be seen from Fig. 3.12 that the output reduction ratio performance is dependent on the number of sub-carriers because of its different PAPR characteristic. From Fig. 3.13, it is observed that the output reduction ratio is lowered with decrease in the IBO. This is because the continuous control does not have the dynamic range of the transmit power level which is required by the discrete control.

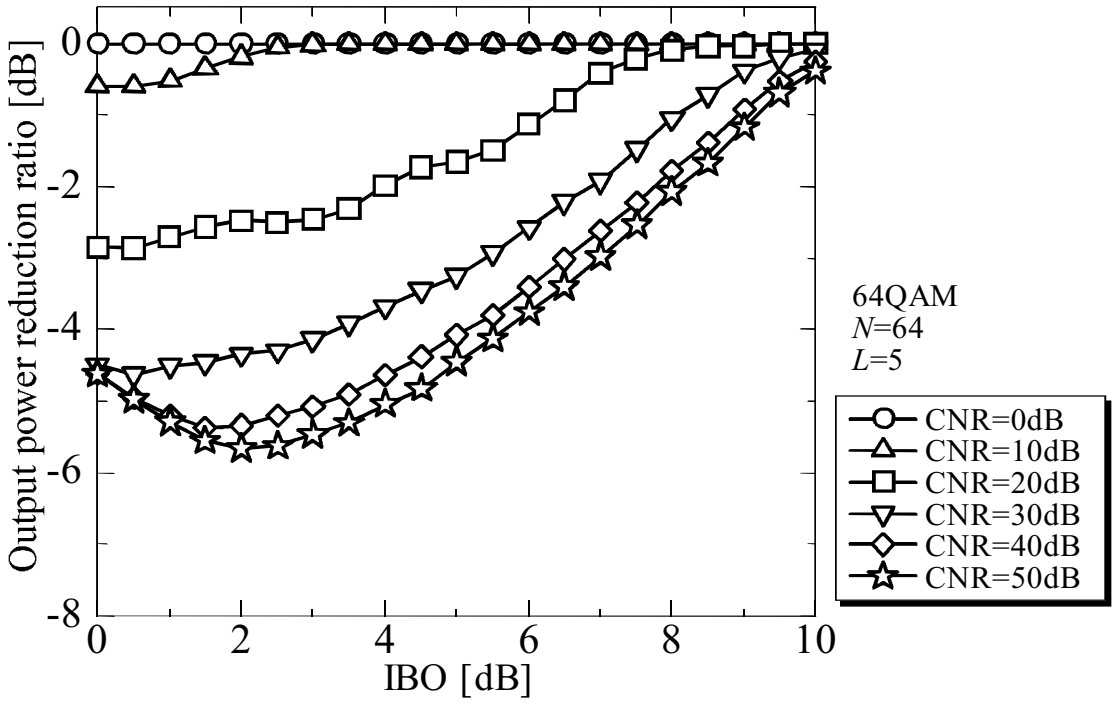

(a) N=64

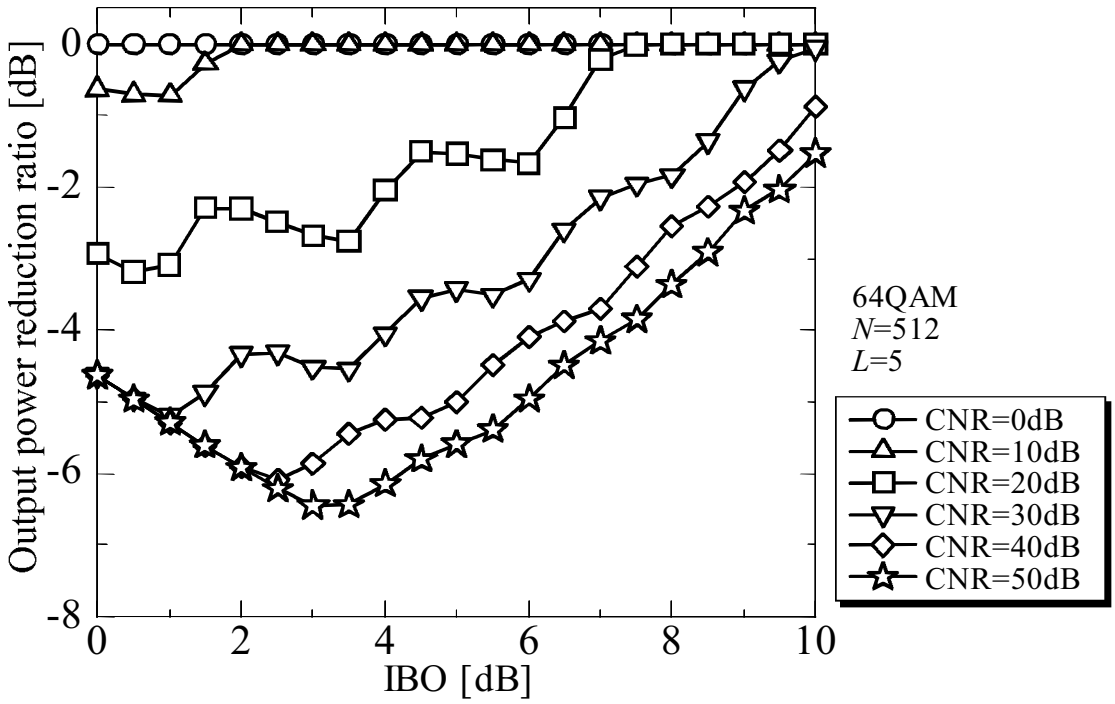

(b) N=512

Figure 3.12: Output power reduction ratio of proposed method employing discrete control.

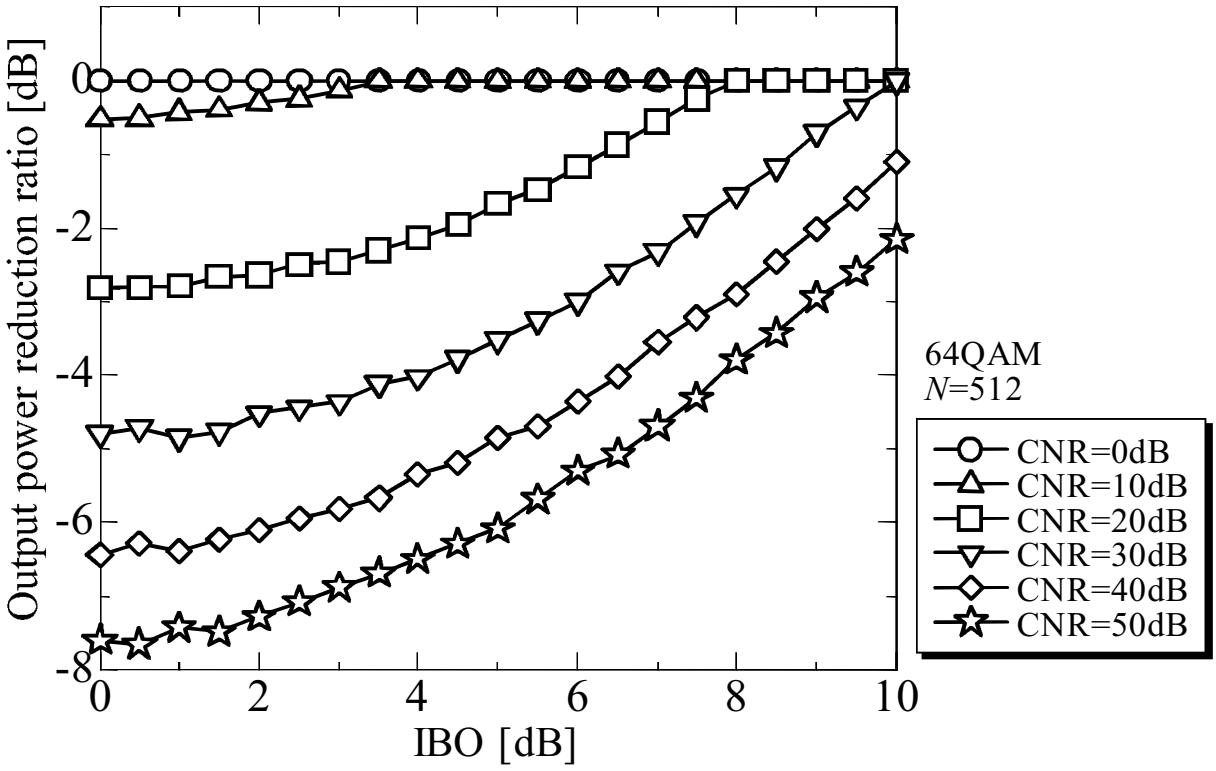

Figure 3.13: Output power reduction ratio of proposed method employing continuous control.

Table 3.5: Simulation parameters.

Modulation	64QAM / OFDM
Number of subcarriers N	512
Oversampling rate M	4
CNR γ	0, 10, 20, 30, 40, 50 [dB]
Number of transmit power levels L	5
Input power ratio between switches ΔP_i	2.0 [dB]

(b) PAPR performance

Figure 3.14 shows the PAPR performance with the proposed method employing the discrete control and continuous control. Table 3.6 shows the simulation parameters and the average power used for measuring the PAPR is defined as the average transmit power without the effect of transmit power control. It can be seen from Fig. 3.14 that the proposed and traditional methods significantly reduce the PAPR compared with the case without clipping and filtering. This is because the peak power reduction effect can be also obtained by clipping and filtering in the proposed and traditional methods. In addition, it is also confirmed that the proposed method can decrease the PAPR with increase in the CNR because the transmit power level is reduced by the proposed transmit power control.

Table 3.6: Simulation parameters.

Modulation	64QAM / OFDM
Number of subcarriers N	512
Oversampling rate M	4
CR	3 [dB]
CNR γ	10, 20, 30, 40, 50 [dB]
Number of transmit power levels L	5
Input power ratio between switches ΔP_i	2.0 [dB]

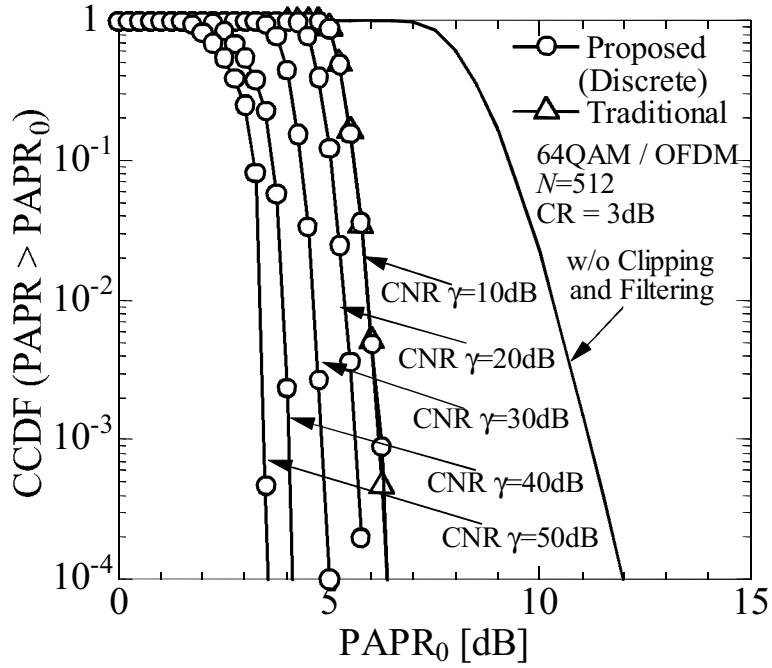

(a) Discrete control

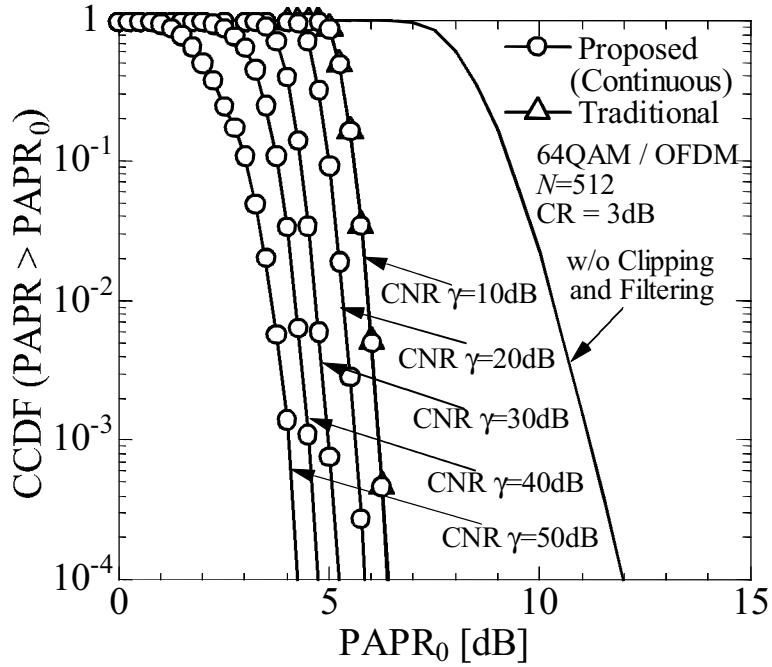

(b) Continuous control

Figure 3.14: Performance comparison, in terms of PAPR, between proposed and traditional methods.

(c) Frequency spectrum

Figure 3.15 and Figure 3.16 show the frequency spectrum of the proposed methods employing the discrete and continuous controls. Table 3.7 shows the simulation parameters. It can be seen from Figs. 3.15 and 3.16 that the proposed and traditional methods significantly reduce the out-of-band radiation compared with the case without clipping and filtering. This is because the filtering process perfectly eliminates the out-of-band radiation. Moreover, it is also confirmed that the proposed method can reduce the out-of-band radiation with increase in the CNR. This is because the proposed method makes the transmit power level reduce with increase in the CNR.

Table 3.7: Simulation parameters.

Modulation	16QAM
Number of subcarriers N	512
Oversampling rate M	4
CR	IBO-2 [dB]
IBO	0, 1, 2, 3, 4, 5 [dB]
CNR γ	0 [dB]
Number of transmit power levels L	5
Input power ratio between switches ΔP_i	2.0 [dB]

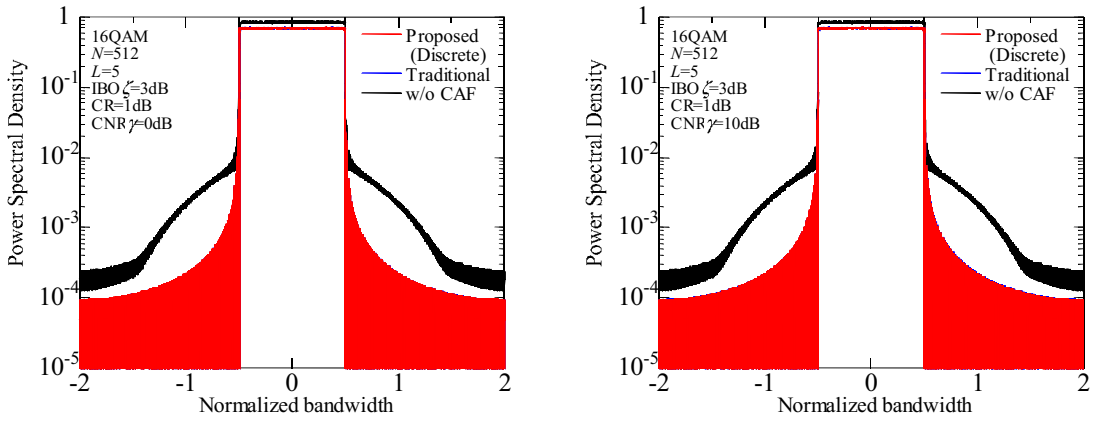

(a) CNR=0dB

(b) CNR=10dB

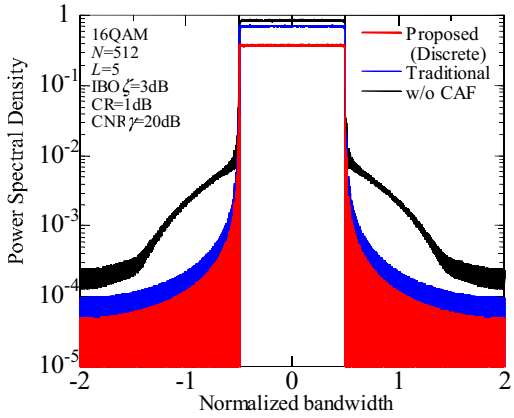

(c) CNR=20dB

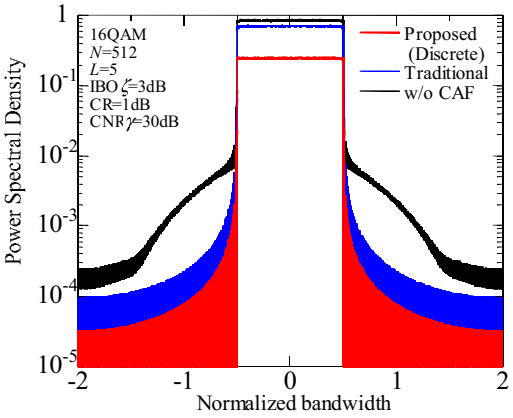

(d) CNR=30dB

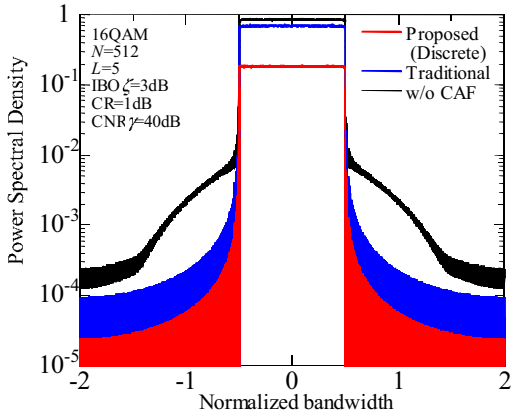

(e) CNR=40dB

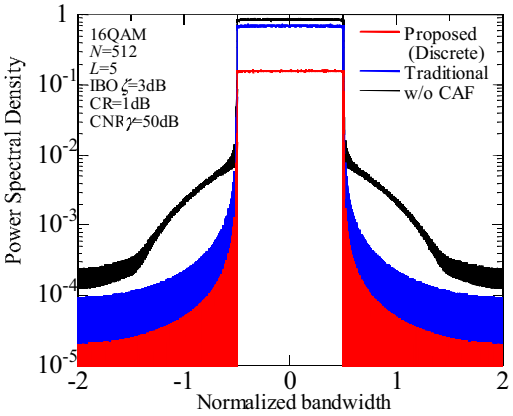

(f) CNR=50dB

Figure 3.15: Performance comparison, in terms of power spectral density, between proposed method employing discrete control and traditional method.

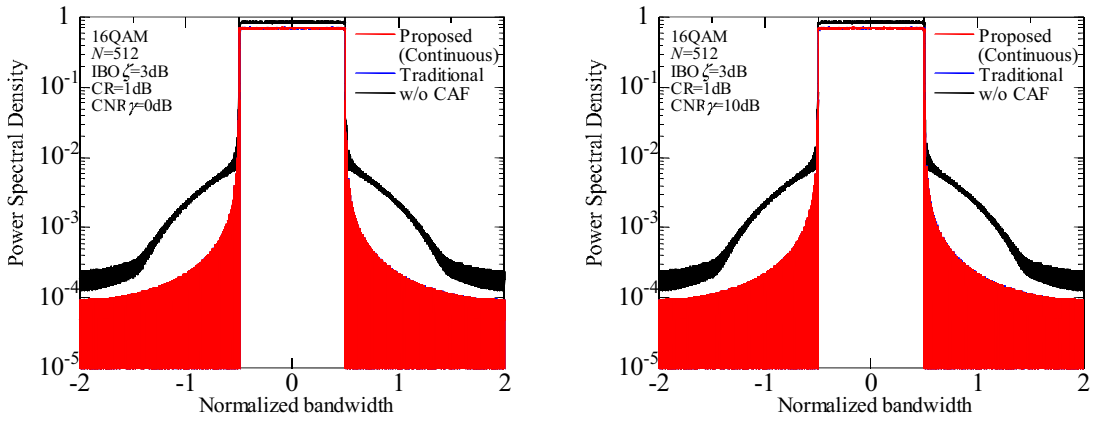

(a) CNR=0dB

(b) CNR=10dB

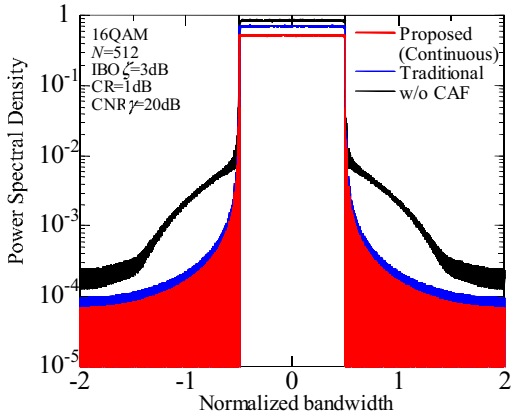

(c) CNR=20dB

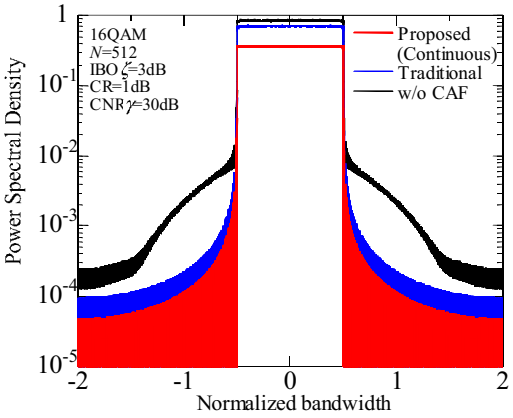

(d) CNR=30dB

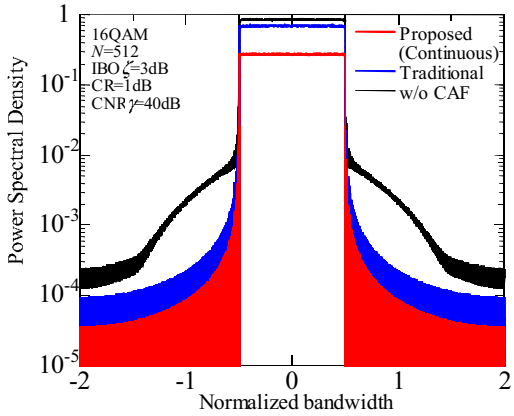

(e) CNR=40dB

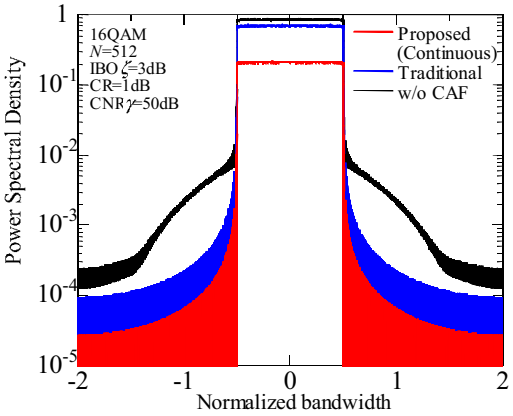

(f) CNR=50dB

Figure 3.16: Performance comparison, in terms of power spectral density, between proposed method employing continuous control and traditional method.

(d) BER performance

Figure 3.17 and Figure 3.18 show the BER performances of the proposed method employing different transmit power control over AWGN channel. Table 3.8 shows the simulation parameters. It is found from Figs. 3.17 and 3.18 that the proposed method provides better BER than the traditional method regardless of the form of the transmit power control. In addition, its effectiveness can be found irrespective of the modulation scheme and the IBO. This is because the proposed method effectively alleviates the effect of the nonlinear distortion by reducing the transmit power level while the traditional method distorts the transmit OFDM signals in the clipping process. Moreover, the discrete control provides better BER than the continuous control especially in the low IBO. This is because the discrete control can realize the symbol-by-symbol transmit power control while the continuous control based on the statistical property is obliged to be performed in a relatively long term.

Figure 3.19 and Figure 3.20 show the BER performances of the proposed method employing different transmit power control over frequency selective fading channel. It is also found from Figs. 3.19 and 3.20 that the proposed method provides better BER than the traditional method regardless of the modulation scheme and the IBO. Furthermore, it can be also confirmed that the discrete control provides better BER than the continuous control especially in the low IBO as discussed in the case of AWGN channel.

To further confirm the effectiveness of the proposed method, the BER performance in adoption of channel coding is evaluated. Figure 3.21 and Figure 3.22 show the BER performance of the proposed method. It can be seen from Figs. 3.21 and 3.22 that the proposed methods provide much better BER performance than the traditional method regardless of the IBO.

Figure 3.23 and Figure 3.24 show the performance comparison, in terms of the BER versus the IBO, between the proposed method and traditional method over frequency selective fading channel in the case of the average CNR = 20 dB. It is observed from Figs. 3.23 and 3.24 that the proposed methods exhibit

better BER performance than the traditional method especially in a relatively low IBO. This is because the proposed transmit power control can effectively prevent the nonlinear distortion especially in severe nonlinear channels such as the IBO = 0 dB.

Table 3.8: Simulation parameters.

Modulation	16QAM, 64QAM / OFDM
FEC	None, Convolutional coding/ Viterbi decoding $R = 1/2,\ K = 7$
Number of subcarriers N	512
Oversampling rate M	4
Guard interval length T_G	$128T_{sam}$
Channel model	AWGN, 128-ray exponentially decaying Rayleigh fading
Delay spread τ_{rms}	$36.0T_{sam}$
CR	IBO-2 [dB]
Number of transmit power levels L	5
Input power ratio between switches ΔP_i	2.0 [dB]

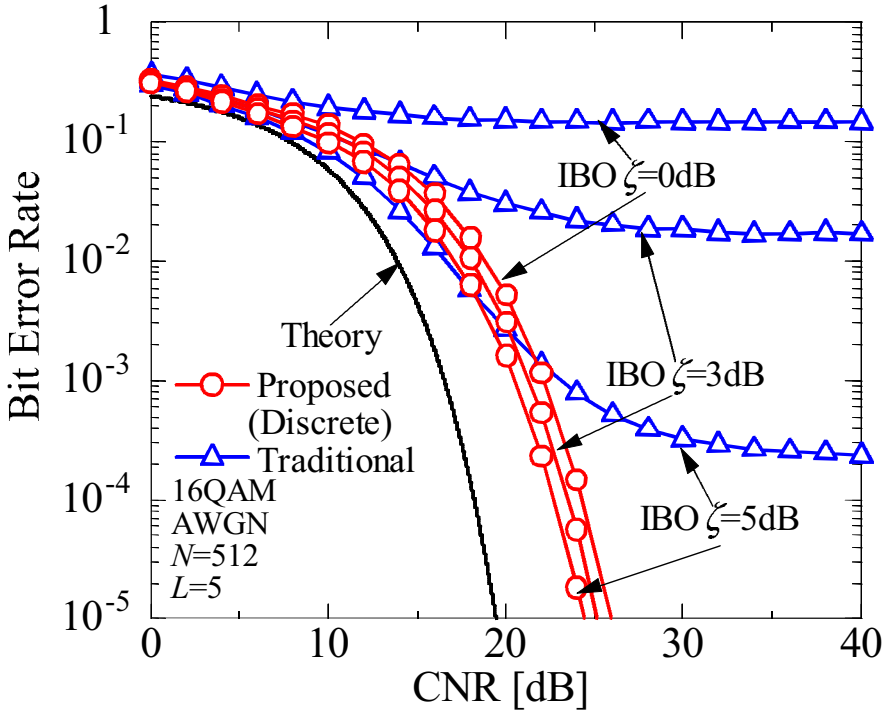

(a) 16QAM

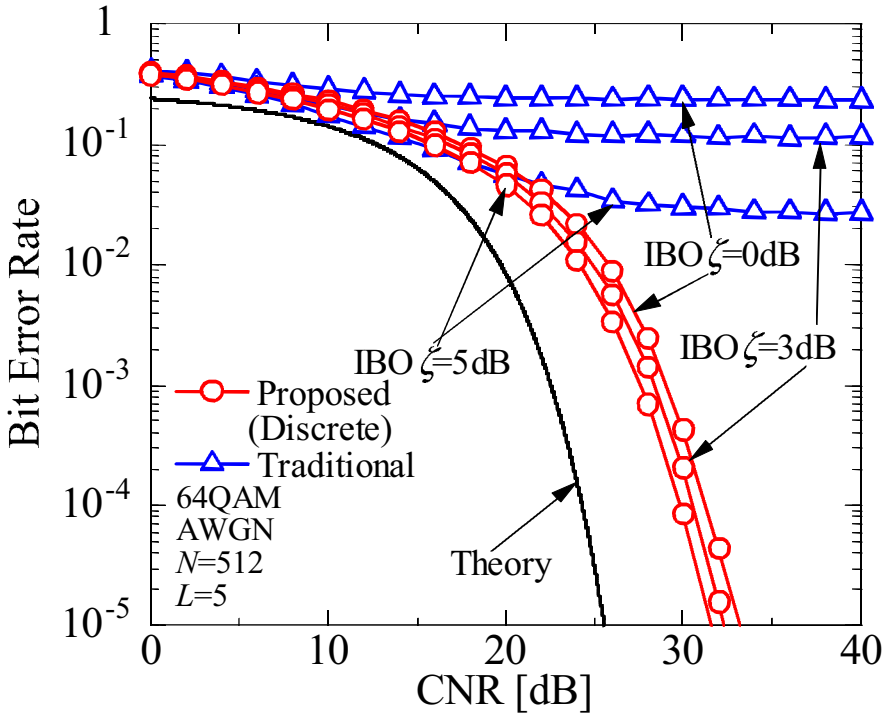

(b) 64QAM

Figure 3.17: Performance comparison, in terms of BER performance versus CNR, between proposed method employing discrete control and traditional method over AWGN channels, where channel coding is not adopted.

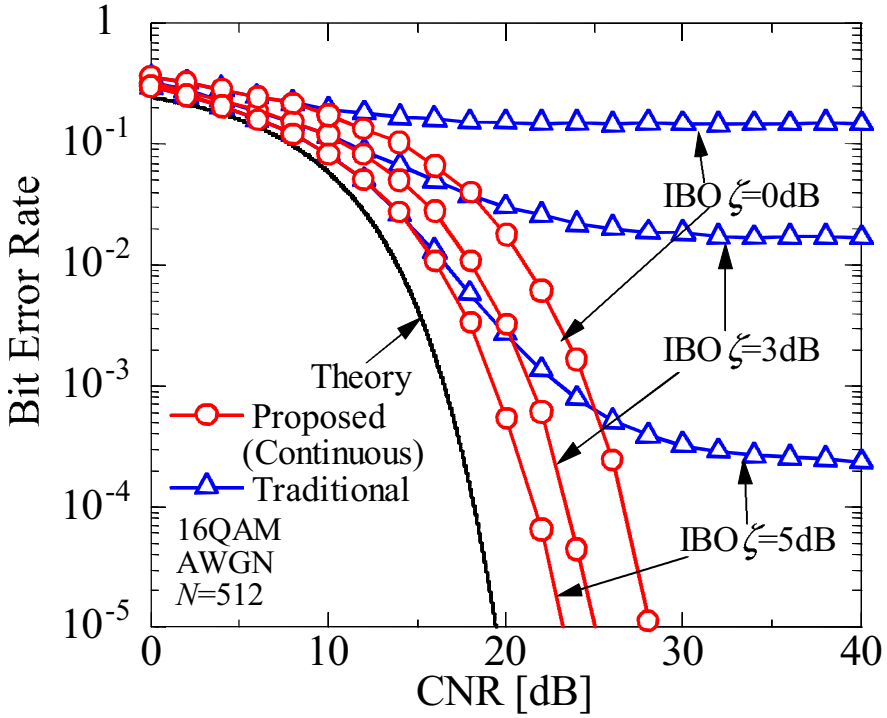

(a) 16QAM

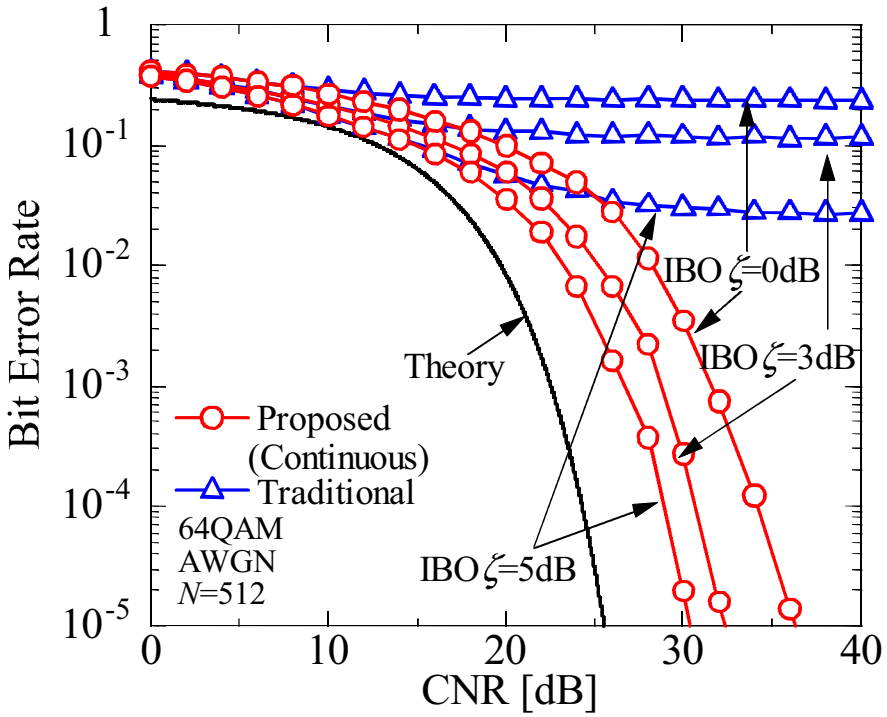

(b) 64QAM

Figure 3.18: Performance comparison, in terms of BER performance versus CNR, between proposed method employing continuous control and traditional method over AWGN channels, where channel coding is not adopted.

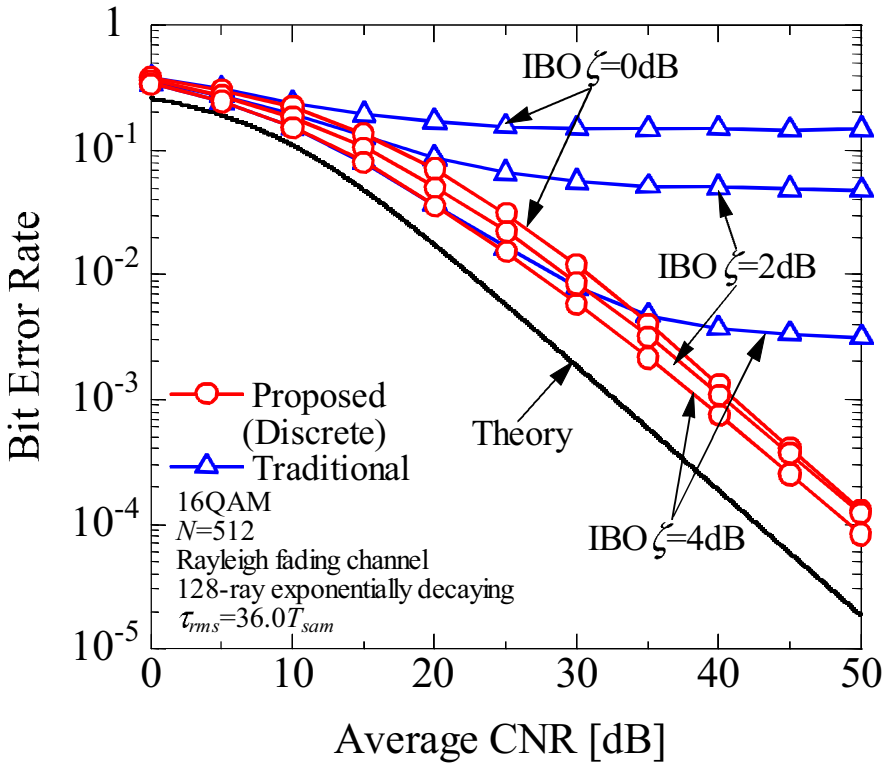

(a) 16QAM

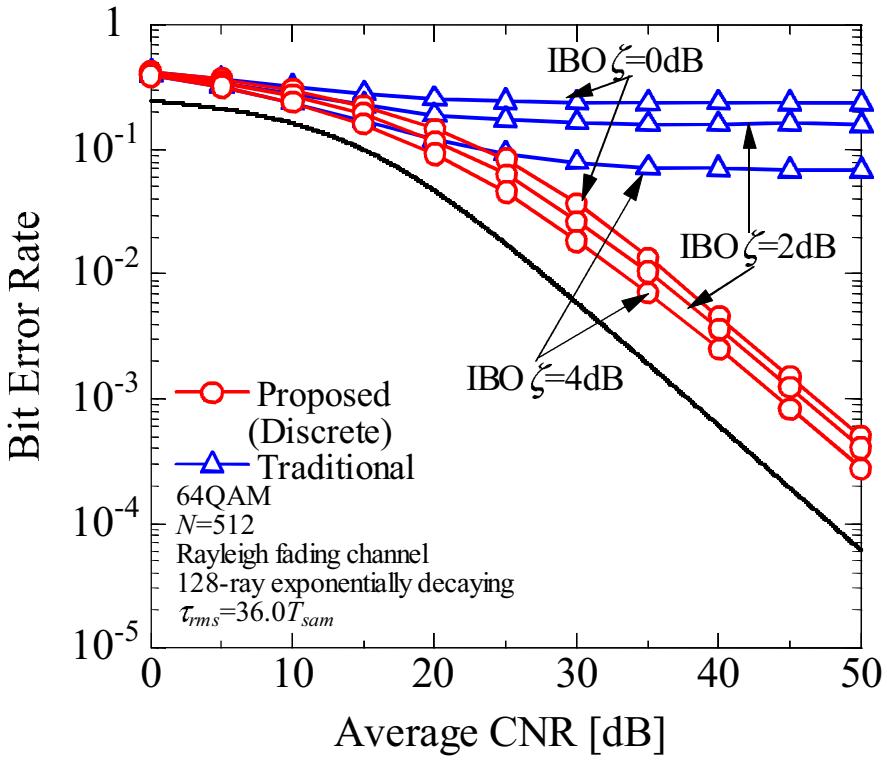

(b) 64QAM

Figure 3.19: Performance comparison, in terms of BER performance versus average CNR, between proposed method employing discrete control and traditional method over frequency selective fading channel, where channel coding is not adopted.

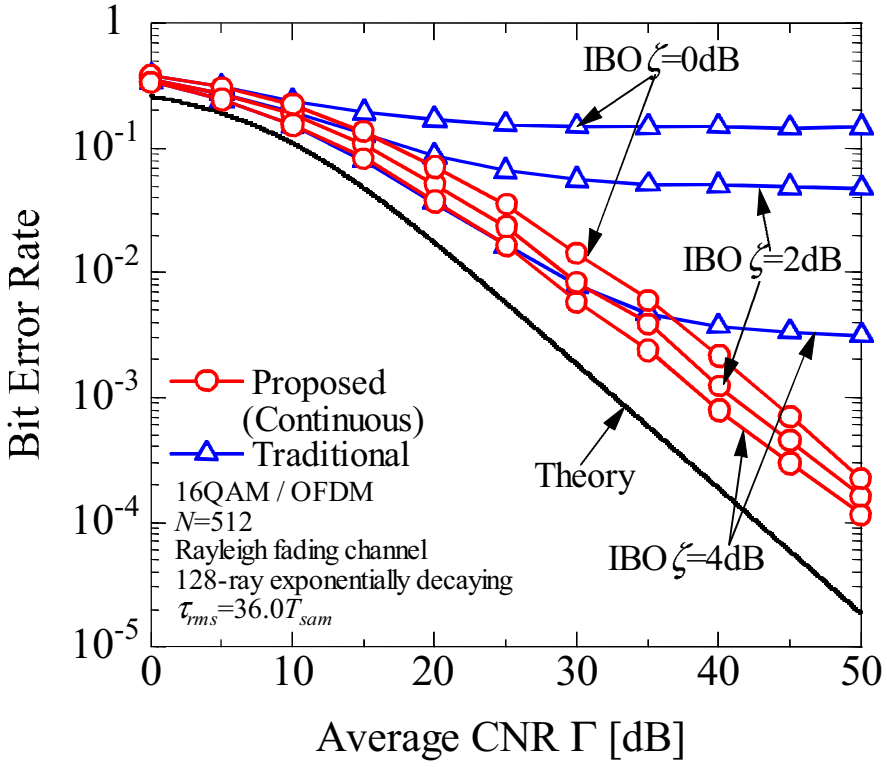

(a) 16QAM

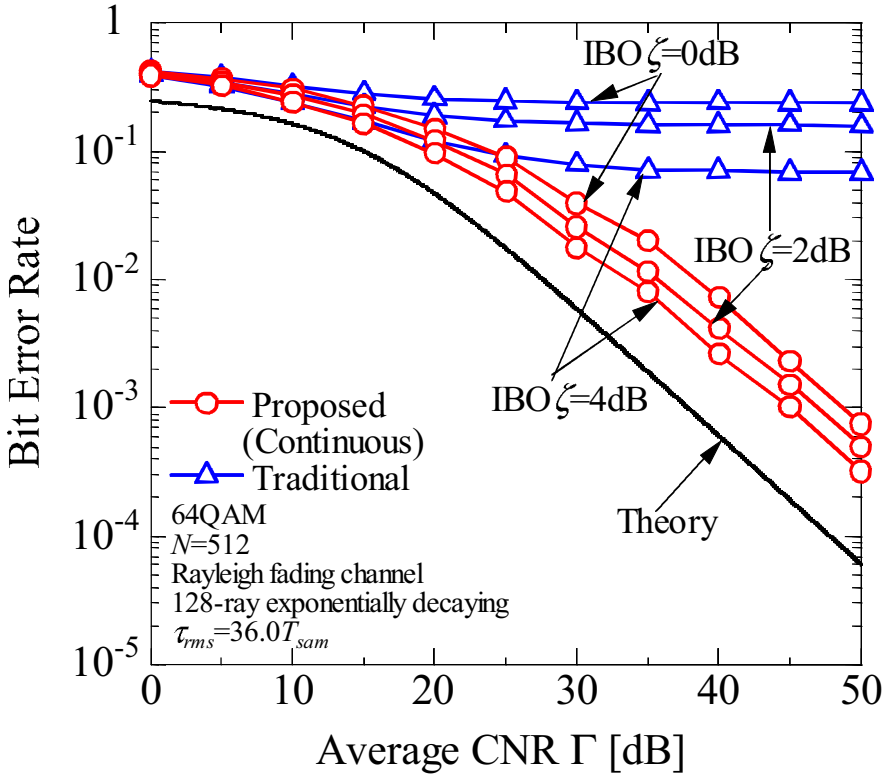

(b) 64QAM

Figure 3.20: Performance comparison, in terms of BER performance versus average CNR, between proposed method employing continuous control and traditional method over frequency selective fading channel, where channel coding is not adopted.

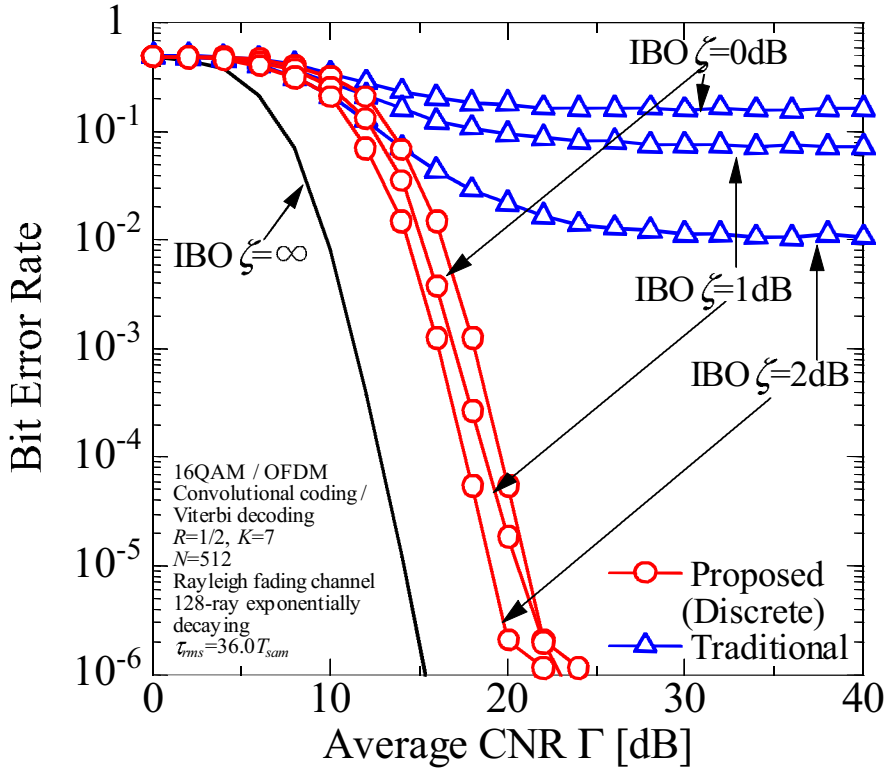

(a) 16QAM

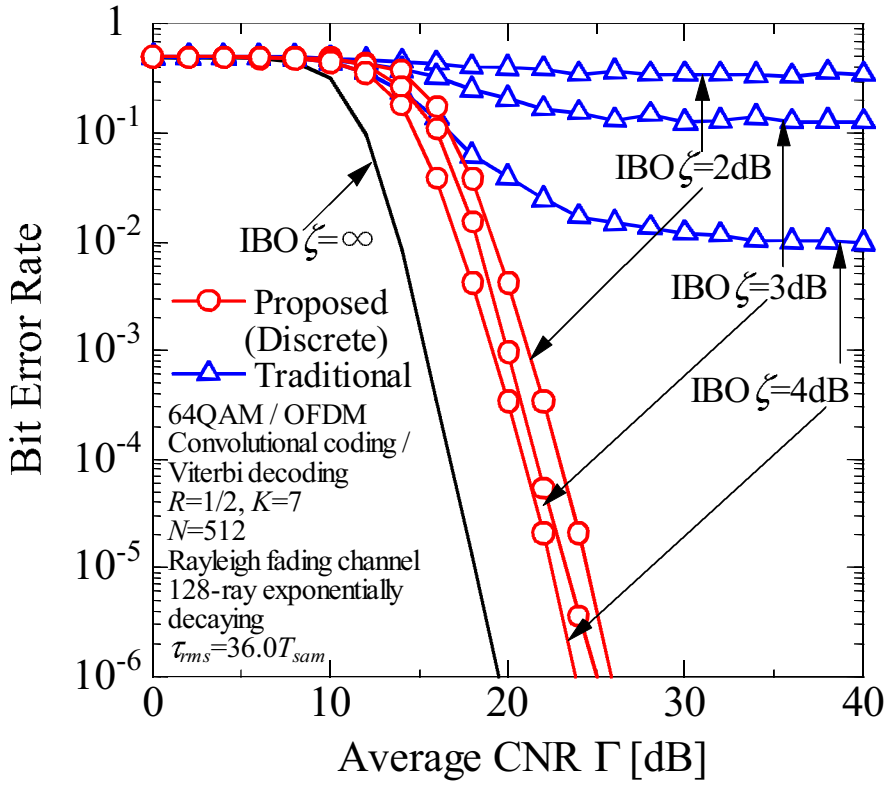

(b) 64QAM

Figure 3.21: Performance comparison, in terms of BER performance versus average CNR, between proposed method employing discrete control and traditional method over frequency selective fading channel, where channel coding is adopted.

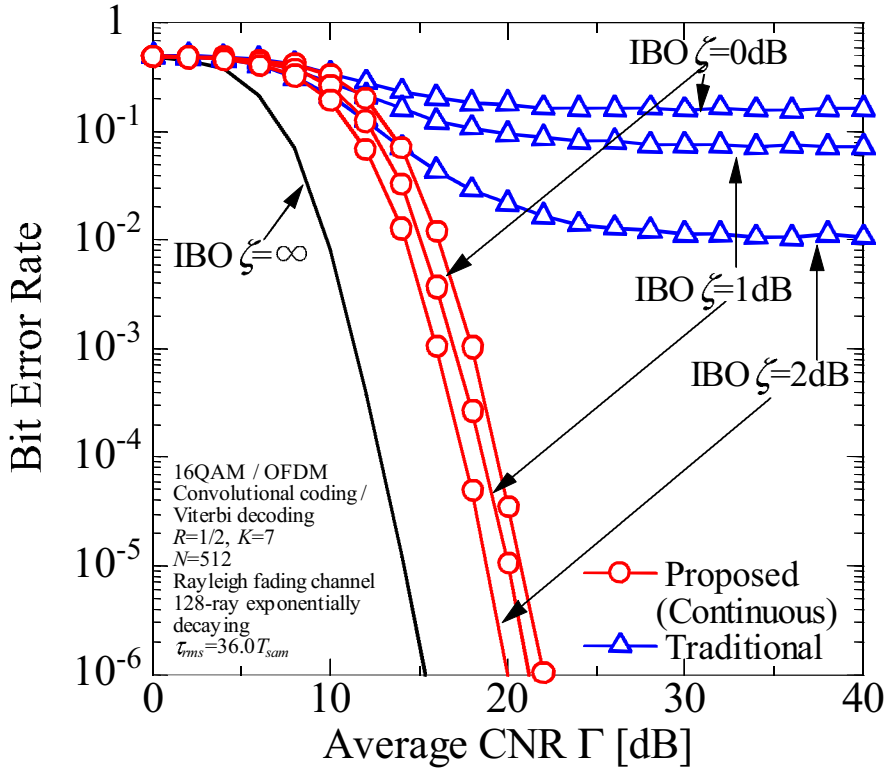

(a) 16QAM

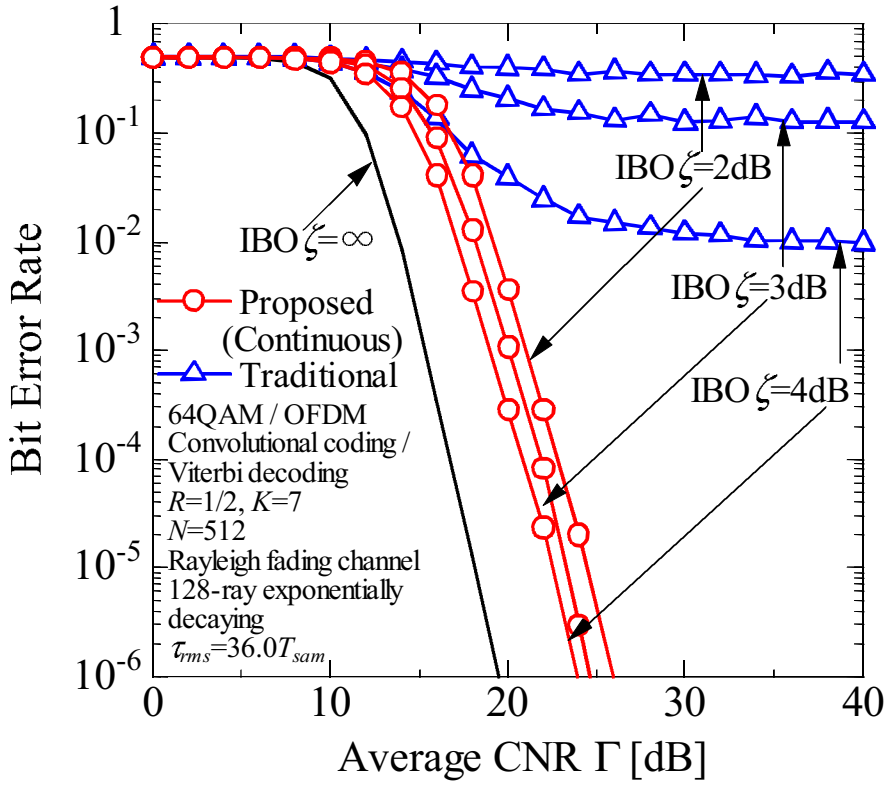

(b) 64QAM

Figure 3.22: Performance comparison, in terms of BER performance versus average CNR, between proposed method employing continuous control and traditional method over frequency selective fading channel, where channel coding is adopted.

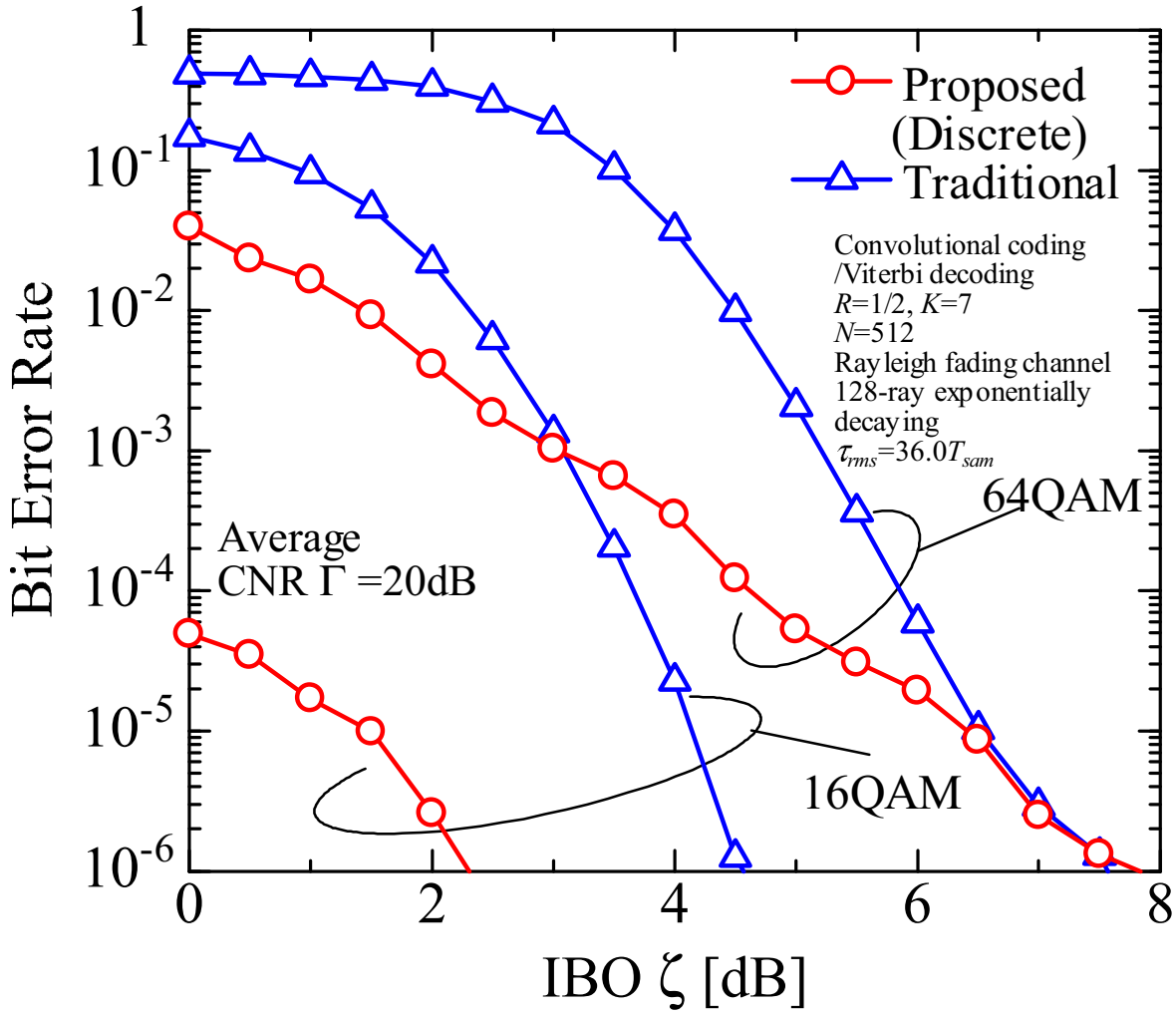

Figure 3.23: Performance comparison, in terms of BER performance versus IBO, between proposed method employing discrete control and traditional method over frequency selective fading channel, where channel coding is adopted.

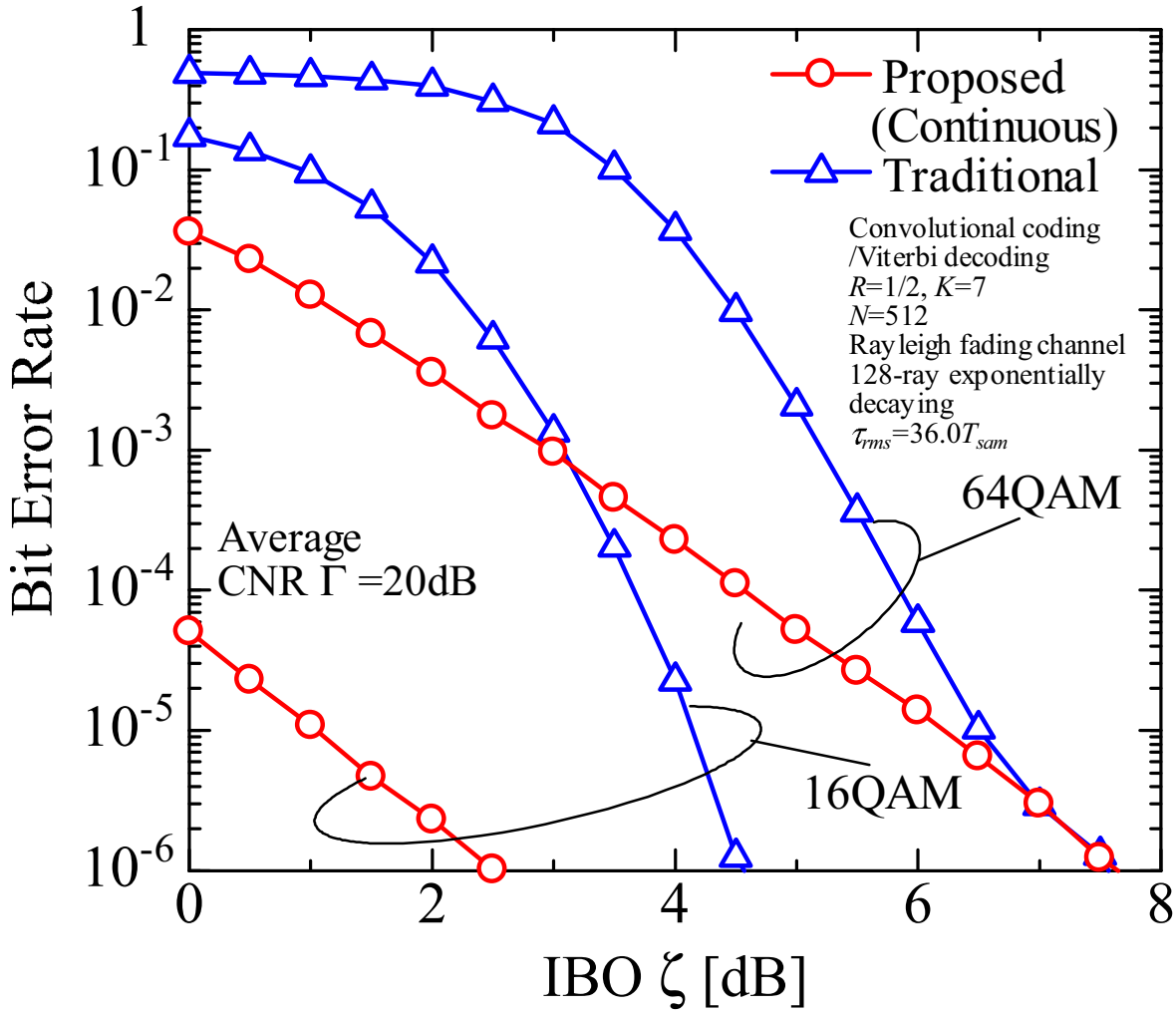

Figure 3.24: Performance comparison, in terms of BER performance versus IBO, between proposed method employing continuous control and traditional method over frequency selective fading channel, where channel coding is adopted.

3.3 Summary

In this chapter, the proposed clipping and filtering employing transmit power control based on the SNDR has been described and its effectiveness is demonstrated by means of computer simulations. Firstly, the traditional clipping and filtering method has been described. In detail, the concept and the system configuration of the traditional method have been described and its performance in terms of the OFDM time domain waveform, the PAPR performance, the frequency spectrum, the BER performance has been clarified. Next, the concept and the configuration of the proposed method have been described and its effectiveness in terms of the frequency spectrum and the BER has been demonstrated in comparison with the traditional clipping and filtering method with the constant transmit power level. From these results, the following things can be found.

- Although the traditional clipping and filtering can effectively suppress the out-of-band radiation, the BER degradation is caused by clipping and the peak power regrowth.
- Considering that the filtering process causes the peak power regrowth, the clipping ratio in the clipping process should be smaller than the IBO of the HPA.
- The proposed clipping and filtering method provides far better BER performance than the traditional method regardless of the IBO and the channel model while perfectly suppressing the out-of-band radiation.
- The continuous transmit power control can be realized thanks to the simple mathematical formula which represents the relationship between the transmit power level and the SNDR.

4 OFDM Clipping and Filtering Employing Transmit Power Control for SU-MIMO Systems

Single user multiple input multiple output (SU-MIMO) has become a promising technique for achieving high-speed transmission of the single user by using multiple input antennas and multiple output antennas [40], [41]. Furthermore, the combination of SU-MIMO with OFDM (SU-MIMO-OFDM) has much attracted as the further improvement of transmission quality, and it has already been adopted in wireless LAN, broadcasting, and so on [46]-[50]. In this chapter, the proposed clipping and filtering method is adopted for SU-MIMO and its effectiveness is investigated by means of computer simulations [45].

4.1 Problems in SU-MIMO-OFDM Systems

As described above, SU-MIMO has become a promising technique for achieving high-speed transmission in single user systems and the combination of SU-MIMO with OFDM is quite effective to meet the requirement to simultaneously realize high-speed transmission and inter-symbol interference suppression due to multipath fading channels.

However, SU-MIMO-OFDM has an inherent problem of the BER degradation in the presence of the nonlinear distortion, which significantly loses the channel capacity. Figure 4.1 shows the concept of SU-MIMO-OFDM systems in the presence of nonlinear distortion. As shown in Fig. 4.1, the effect of the nonlinear distortion at each transmit antenna causes the BER degradation at the receiver side, which leads to the fact that the BER performance of SU-MIMO-OFDM is worse than that of single user single input single output OFDM (SU-SISO-OFDM) [45].

Considering the background described above, we adopt the proposed clipping and filtering method for SU-MIMO-OFDM and clarify the effectiveness of the proposed approach in comparison with the traditional clipping and filtering method [45].

4.2 System Configuration

In this section, we explain the overall configuration of the proposed clipping and filtering method deployed on SU-MIMO-OFDM systems. Figure 4.2 shows the overall configuration of proposed method deployed on SU-MIMO-OFDM systems. Here, both the discrete control and the continuous control are considered as the form of the transmit power control. At the transmitter, multiple data streams are generated and each data stream is mapped into the sub-carrier signals with an arbitrary modulation level. The N-parallel modulated signal are fed into the N-point IFFT circuit so as to be converted into the time domain OFDM signals with the sampling period of T_{sam}. At each transmit antenna, the SNDR of each input power level is theoretically calculated and the input power level to satisfy the maximum SNDR is determined. Then the transmit time domain signals scaled to the appropriate power level is power level is input to the clipping and filtering process. It should be noted that the optimal power level β_{opt} has to be determined at each transmit antenna because the effect of the nonlinear

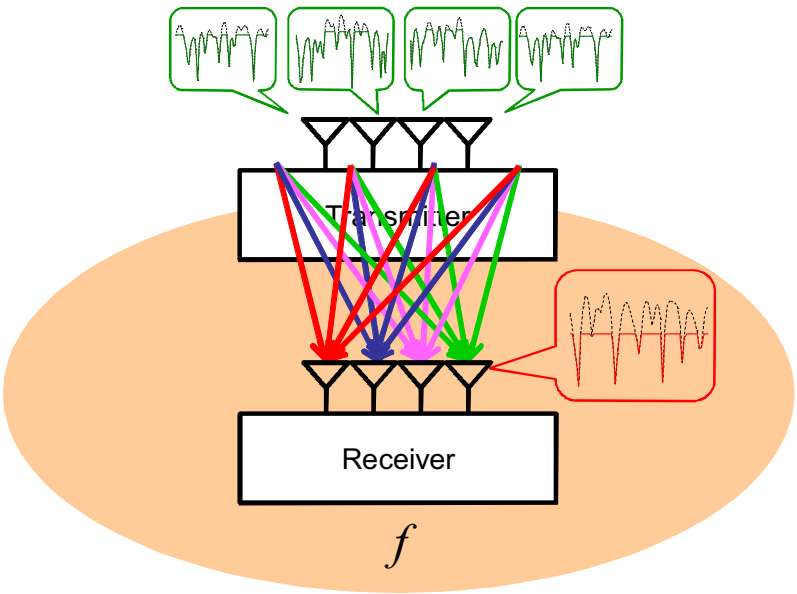

Figure 4.1: Concept of SU-MIMO-OFDM Systems in the Presence of Nonlinear Distortion.

distortion and average CNR is not always the same among different transmit antennas. After passing through the clipping and filtering process, the transmit OFDM signals are amplified by the HPA and are transmitted at each transmit antenna.

At the receiver, the overlapped OFDM signals are received at each received antenna. At each antenna, the received OFDM signals are converted into frequency domain signals and are input to MIMO signal detection, where overlapped OFDM signals are decomposed into single transmit data streams by a signal detection scheme. In MIMO signal detection, the channel estimates including the effect of the transmit power level of the j-th transmit antenna β_{optj} is essential to eliminate the effect of the transmit power control. Therefore, the modified channel estimates from the j-th transmit antenna to the i-th received antenna are given by

$$h'_{ij} = \beta_{optj} h_{ij}. \tag{4.1}$$

Here, it should be noted that the transmit power levels of all antennas have to be notified to the receiver and then are used for MIMO signal separation. Although this notification of the transmit power level causes some degradation in the transmission efficiency, its degradation is negligible considering the number of sub-carriers. After FFT processing at each antenna, MIMO signal detection recovers the single transmit data streams from the overlapped OFDM signals.

4.3 Numerical Results

In this section, the BER performance of the proposed method is evaluated and then its performance is compared with the traditional clipping and filtering with the constant transmit power level in order to clarify the effectiveness of the proposed approach.

Figure 4.3 and Figure 4.4 show the BER performance of the proposed method, where 2×2 SU-MIMO-OFDM is assumed. Table 4.1 shows the simulation parameters. It is found from Figs.4.3 and 4.4 that the proposed method provides

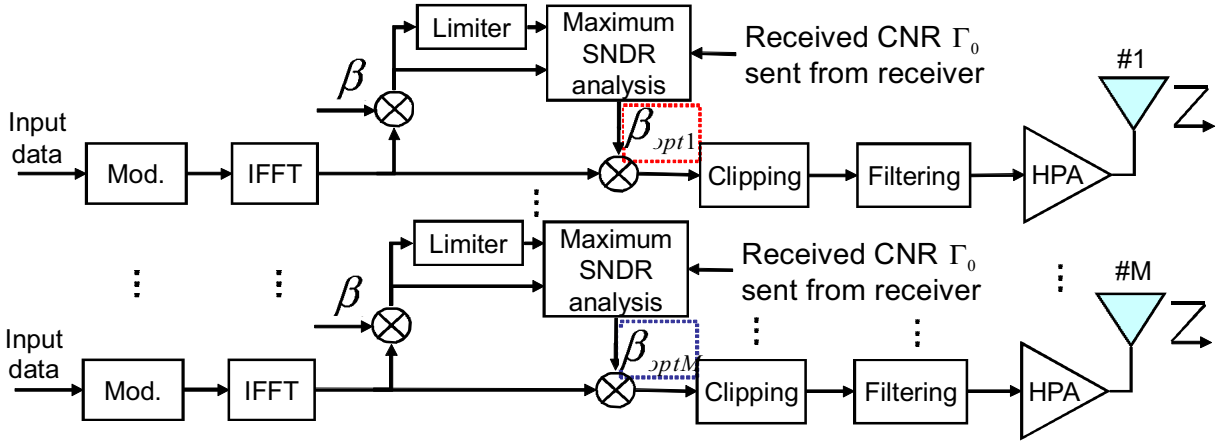

(a) Transmitter (Discrete control)

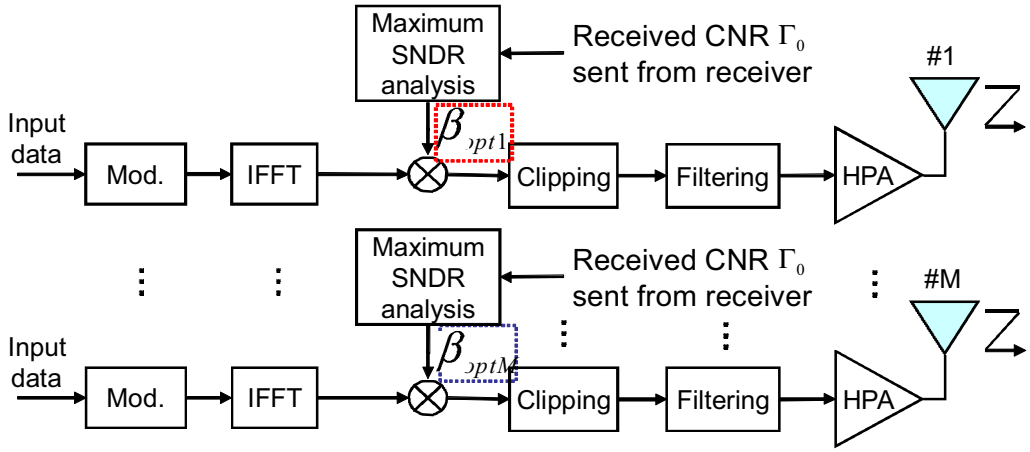

(b) Transmitter (Continuous control)

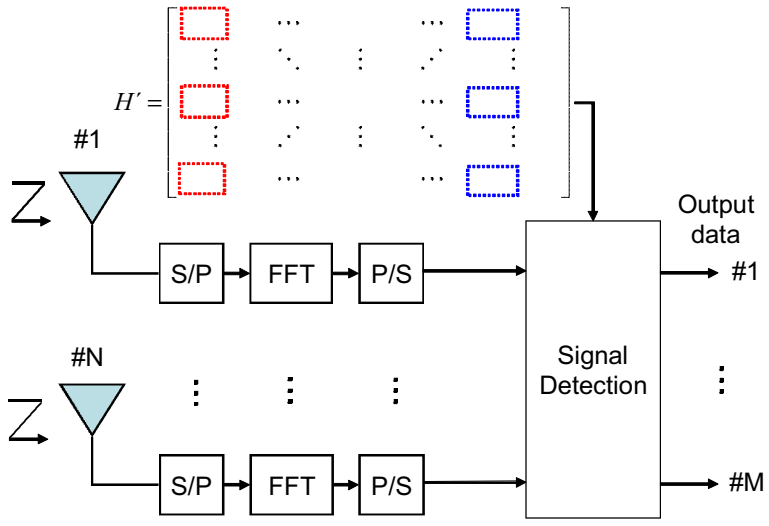

(c) Receiver

Figure 4.2: Overall configuration of proposed method deployed on SU-MIMO-OFDM systems.

better BER than the traditional method regardless of the form of the transmit power control. In addition, its effectiveness can be found irrespective of the modulation scheme and the IBO. This is because the proposed method effectively alleviates the effect of the nonlinear distortion by reducing the transmit power level while the traditional method distorts the transmit OFDM signals in the clipping process.

Moreover, in the case of ZF, MMSE, and V-BLAST, the discrete control provides slightly better BER than the continuous control especially in the low IBO. This is because the discrete control can realize the symbol-by-symbol transmit power control while the continuous control based on the statistical property is obliged to be performed in a relatively long term.

On the other hand, in the case of MLD, the continuous control eliminates the error floor while there is the error floor in the discrete method. This is because MLD is much sensitive to the nonlinear distortion than ZF and MMSE and the continuous control can find out more appropriate transmit power level thanks to being no dynamic range of the transmit power control.

Next, Figure 4.5 and Figure 4.6 show the BER performance of the proposed method, where 4×4 SU-MIMO-OFDM is assumed. It can be also confirmed from Figs.4.5 and 4.6 that the proposed method provides better BER than the traditional method regardless of the form of the transmit power control. In addition, its effectiveness can be found irrespective of the modulation scheme and the IBO. In the case of V-BLAST and MLD, it is observed that the proposed method exploits much more diversity benefit than 2×2 MIMO case shown in Figs. 4.3 and 4.4, while the BER of the traditional method is slightly worse than that of 2×2 MIMO case. Thus it can be said that the proposed method using transmit power control contributes to retaining the reasonable space diversity benefit originally coming from MIMO.

Figures 4.7-4.10 show the BER performance of the proposed method in adoption of channel coding. From these results, it can be seen that the effectiveness of the proposed methods is still retained in adoption of channel coding.

Finally, Figure 4.11 and Figure 4.12 show the BER performance of the proposed method as a function of the IBO, where the average CNR Γ = 15dB. It is observed from Figs. 4.11 and 4.12 that the proposed method provides better BER performance than the traditional method regardless of the number of transmit and receive antennas. Especially in a relatively low IBO, the effectiveness of the proposed method becomes remarkable because the proposed method employing transmit power control alleviates the nonlinear distortion caused by clipping and filtering and effectively retains the reasonable space diversity benefit.

From these results, it is concluded that the proposed clipping and filtering method dramatically improves the BER performance compared with the traditional clipping and filtering method thanks to performing the transmit power control before clipping and filtering at each transmit antenna. Moreover, since the proposed method can sufficiently retain the reasonable space diversity benefit, it can be said that the proposed method contributes to enhancing the channel capacity of SU-MIMO-OFDM.

Table 4.1: Simulation parameters.

Modulation	16QAM, 64QAM / OFDM
FEC	None, Convolutional coding/ Viterbi decoding $R = 1/2, K = 7$
Number of subcarriers N	64
Oversampling rate M	4
Guard interval length T_G	$16T_{sam}$
Channel model	16-ray exponentially decaying Rayleigh fading
Delay spread τ_{rms}	$4.0T_{sam}$
CR	IBO-2 [dB]
Number of transmit power levels L	5
Input power ratio between switches ΔP_i	2.0 [dB]
Signal decision	ZF, MMSE, V-BLAST, MLD

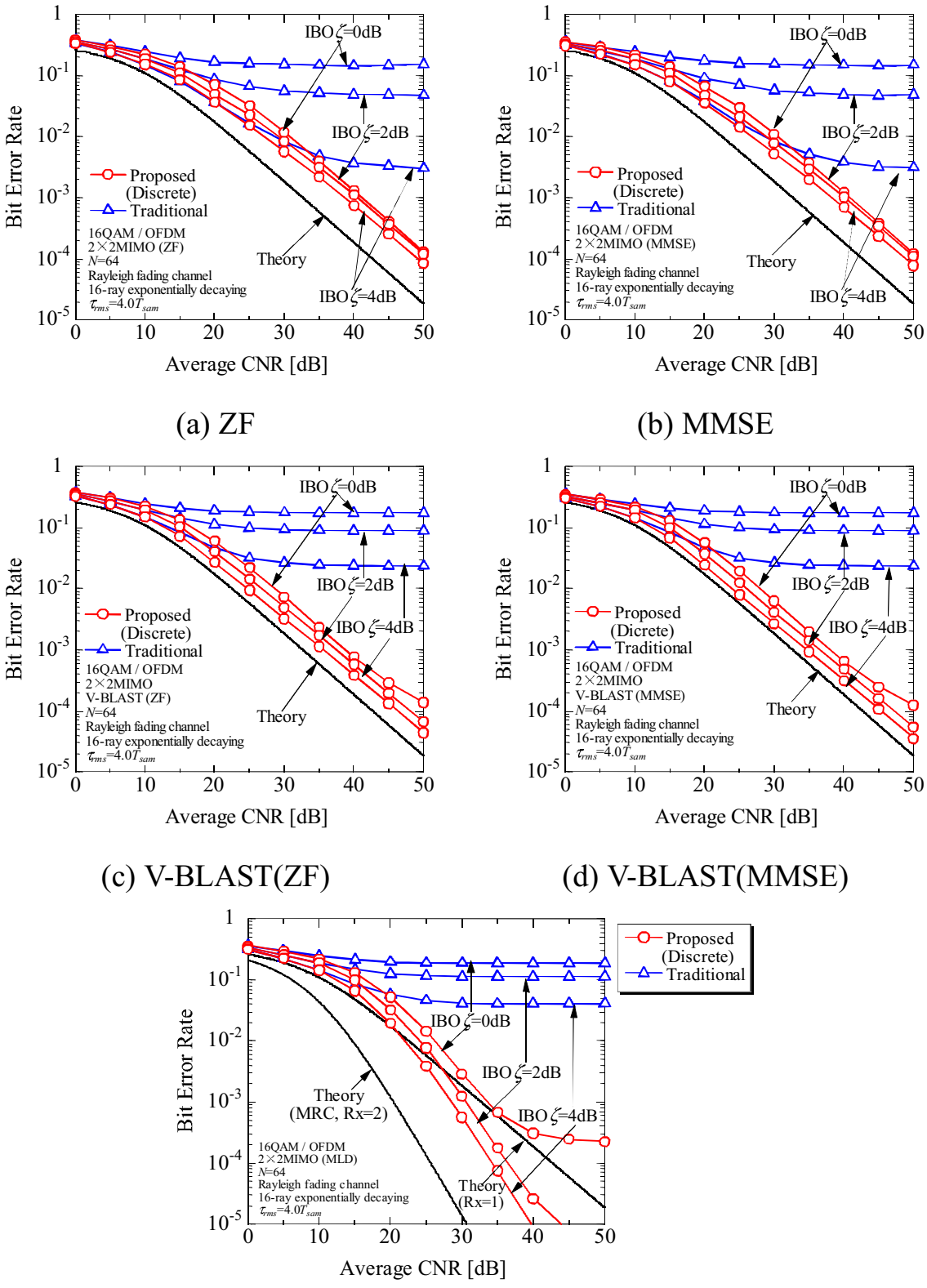

Figure 4.3: Performance comparison, in terms of BER performance versus average CNR, between proposed method and traditional method, where 2×2 SU-MIMO-OFDM is assumed.

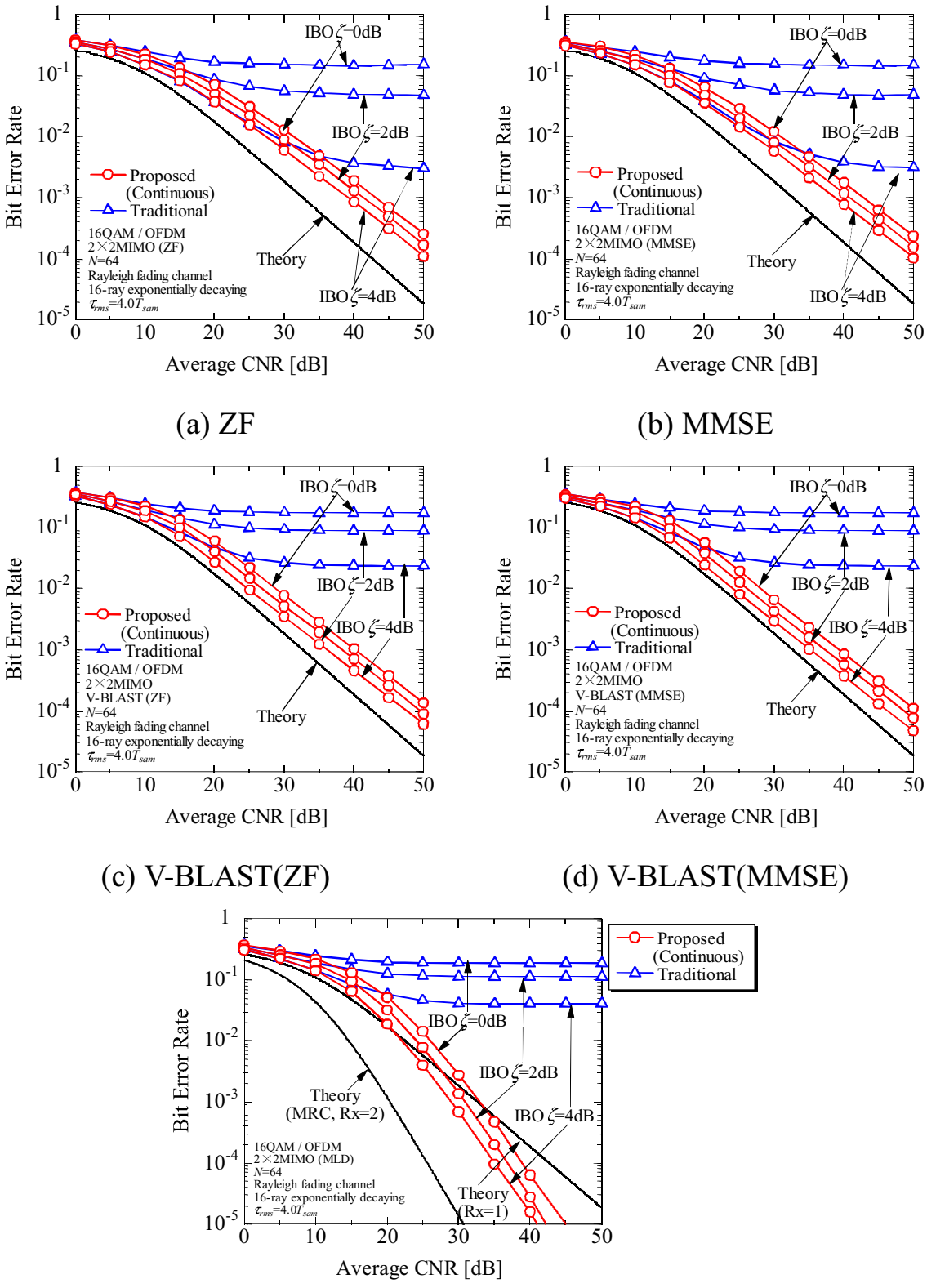

Figure 4.4: Performance comparison, in terms of BER performance versus average CNR, between proposed method and traditional method, where 2×2 SU-MIMO-OFDM is assumed.

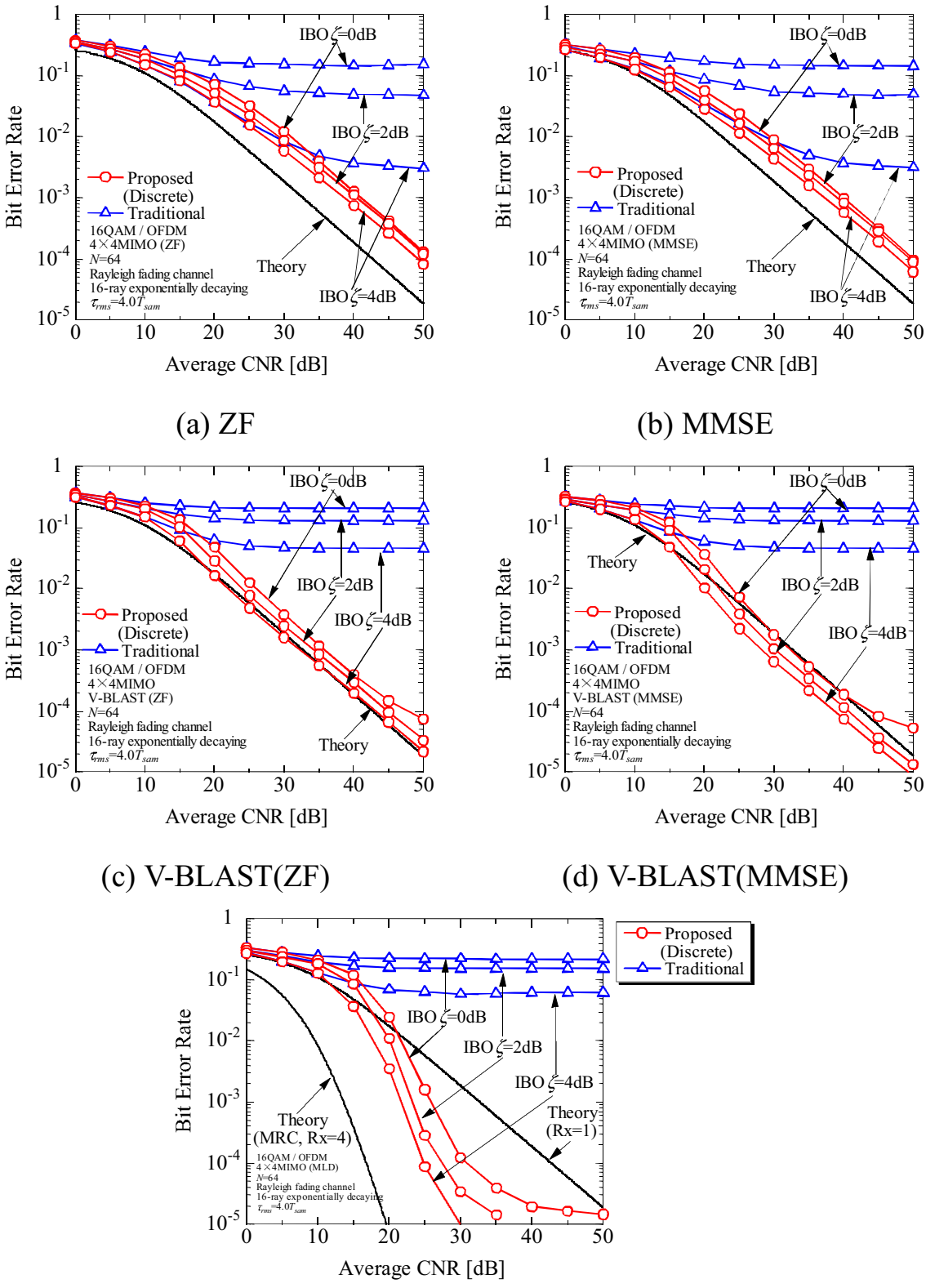

Figure 4.5: Performance comparison, in terms of BER performance versus average CNR, between proposed method and traditional method, where 4×4 SU-MIMO-OFDM is assumed.

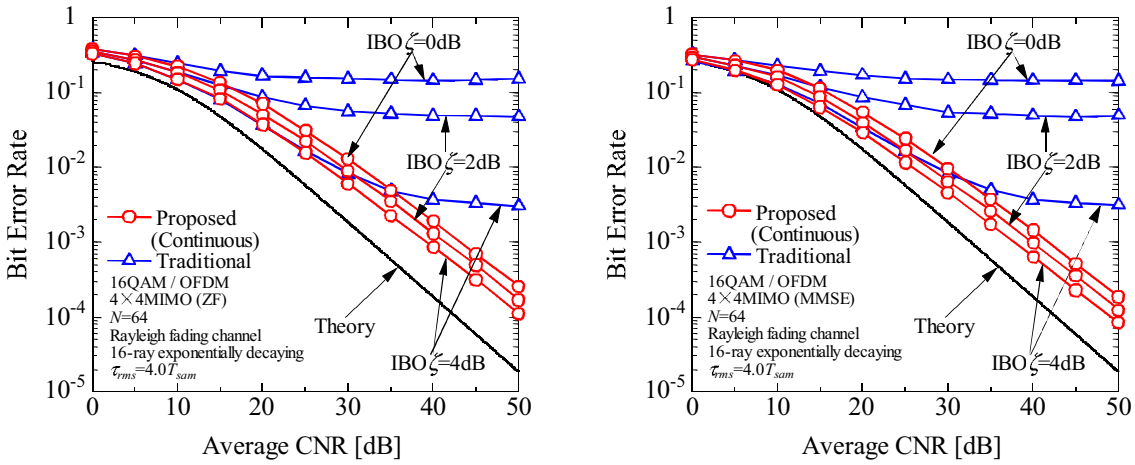

(a) ZF

(b) MMSE

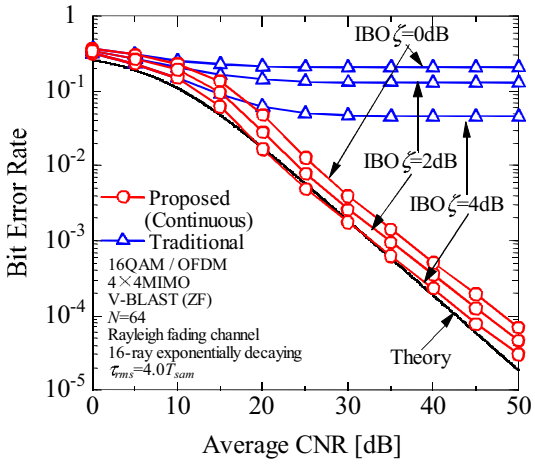

(c) V-BLAST(ZF)

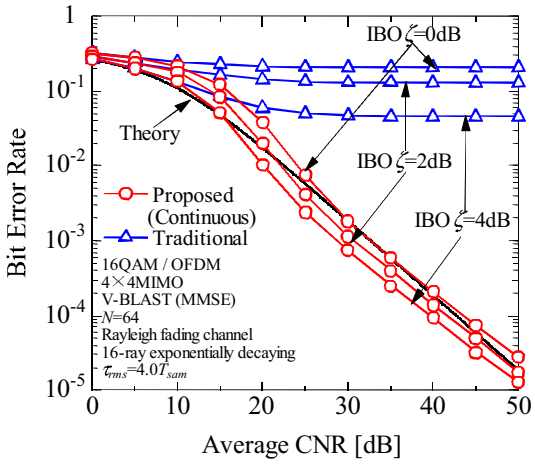

(d) V-BLAST(MMSE)

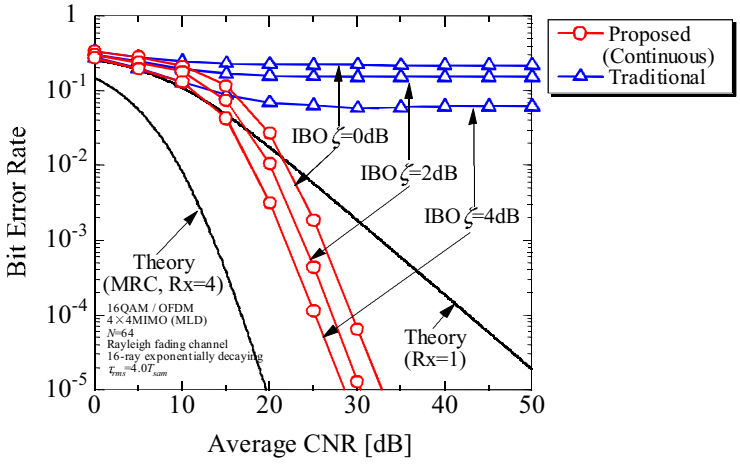

(e) MLD

Figure 4.6: Performance comparison, in terms of BER performance versus average CNR, between proposed method and traditional method, where 4×4 SU-MIMO-OFDM is assumed.

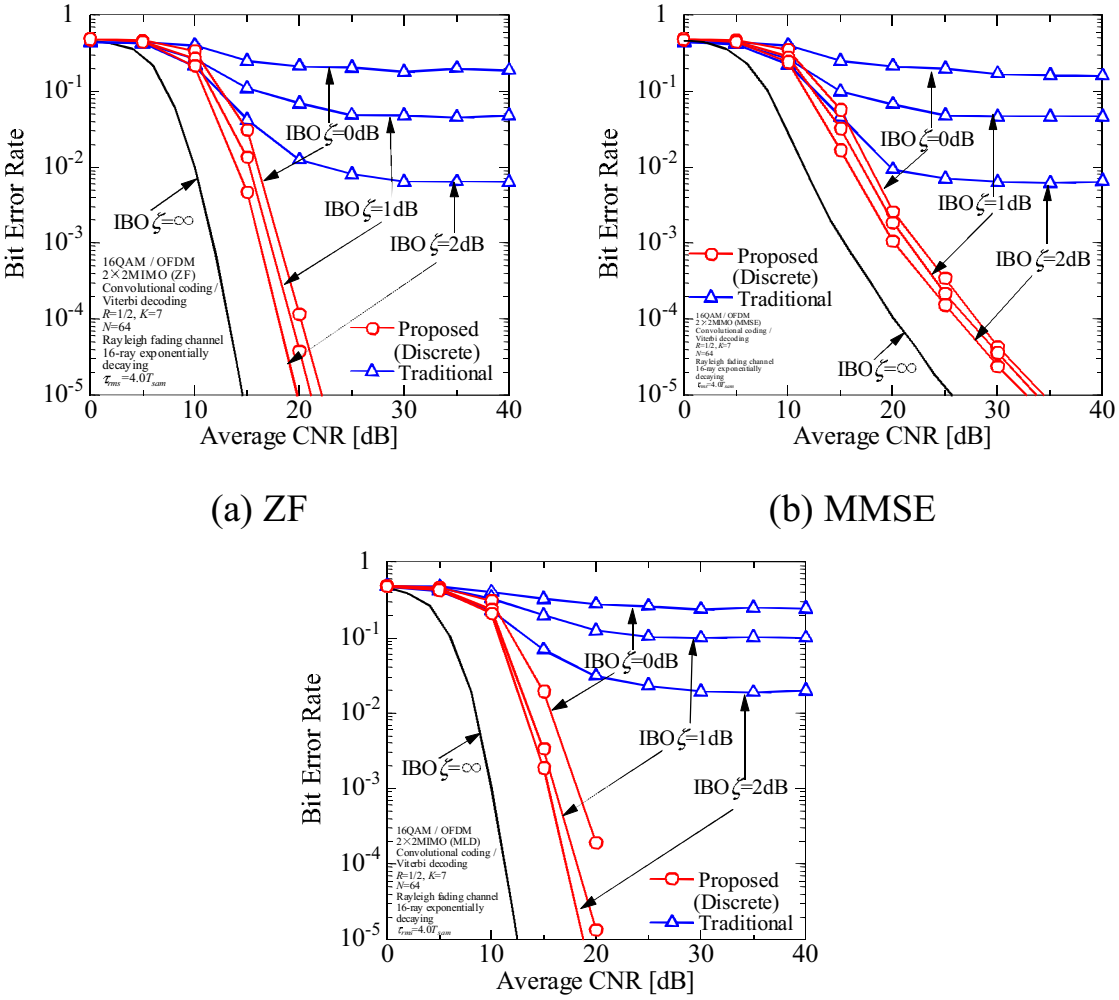

Figure 4.7: Performance comparison, in terms of BER performance versus average CNR, between proposed method and traditional method, where 2×2 SU-MIMO-OFDM is assumed and channel coding is adopted.

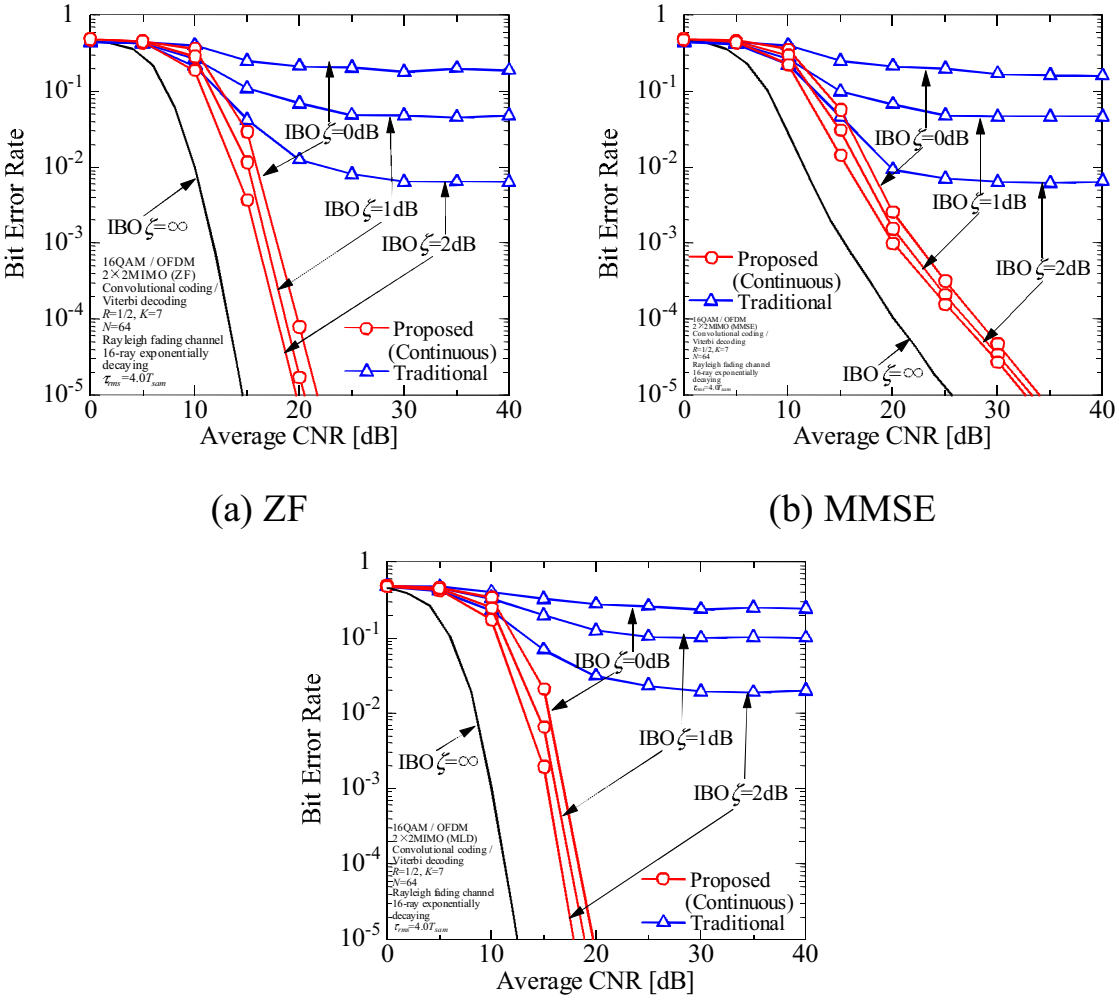

(a) ZF (b) MMSE

(c) MLD

Figure 4.8: Performance comparison, in terms of BER performance versus average CNR, between proposed method and traditional method, where 2×2 SU-MIMO-OFDM is assumed and channel coding is adopted.

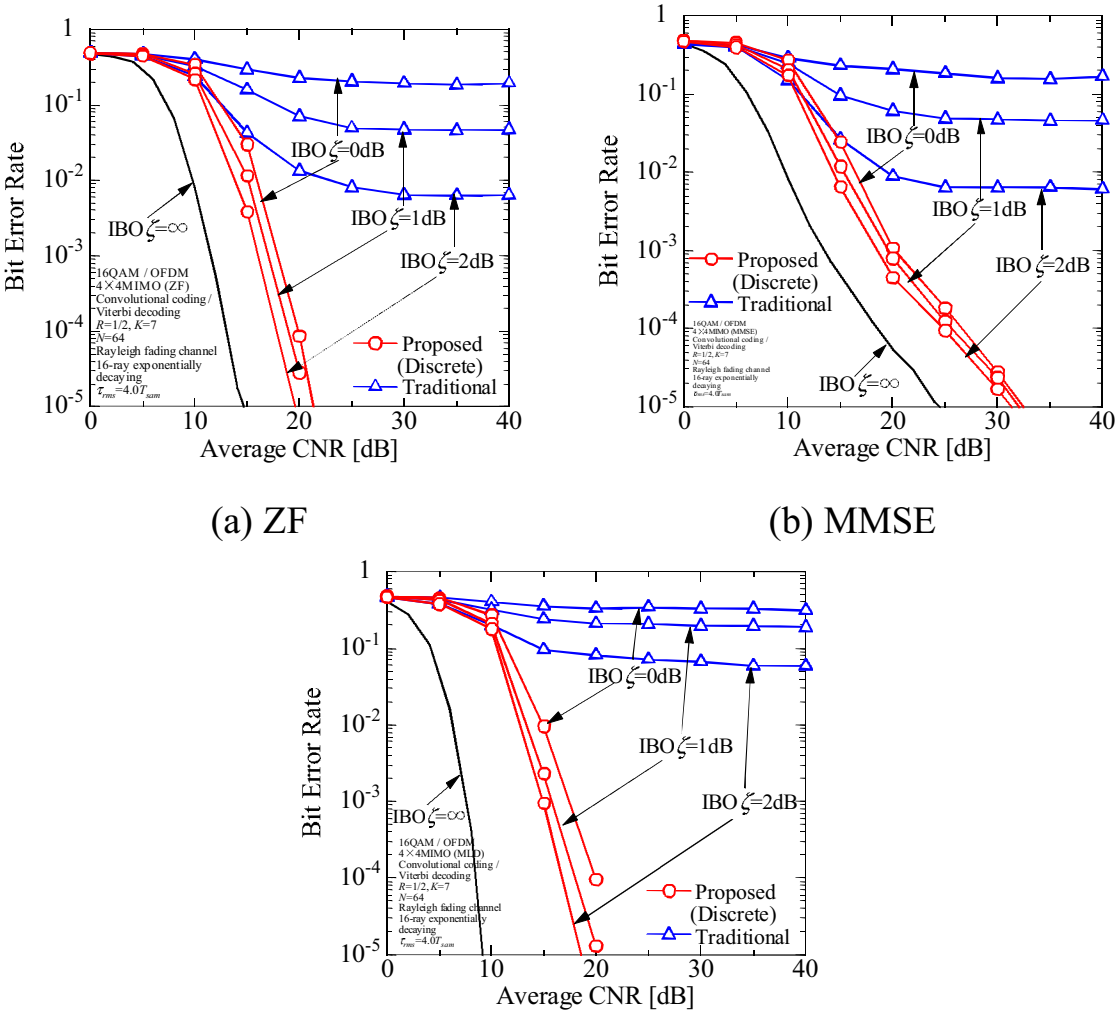

(a) ZF (b) MMSE

(c) MLD

Figure 4.9: Performance comparison, in terms of BER performance versus average CNR, between proposed method and traditional method, where 4×4 SU-MIMO-OFDM is assumed and channel coding is adopted.

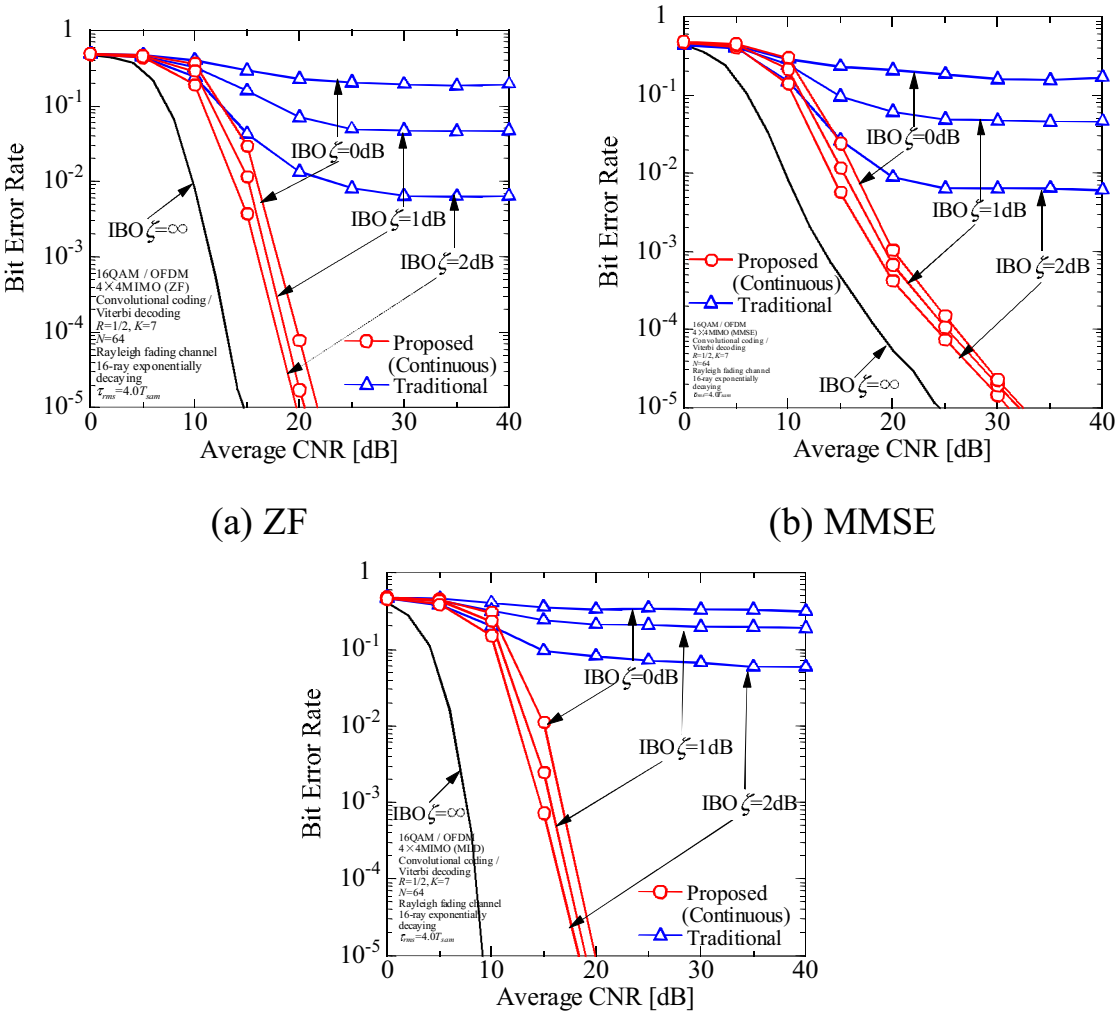

(a) ZF (b) MMSE

(c) MLD

Figure 4.10: Performance comparison, in terms of BER performance versus average CNR, between proposed method and traditional method, where 4×4 SU-MIMO-OFDM is assumed and channel coding is adopted.

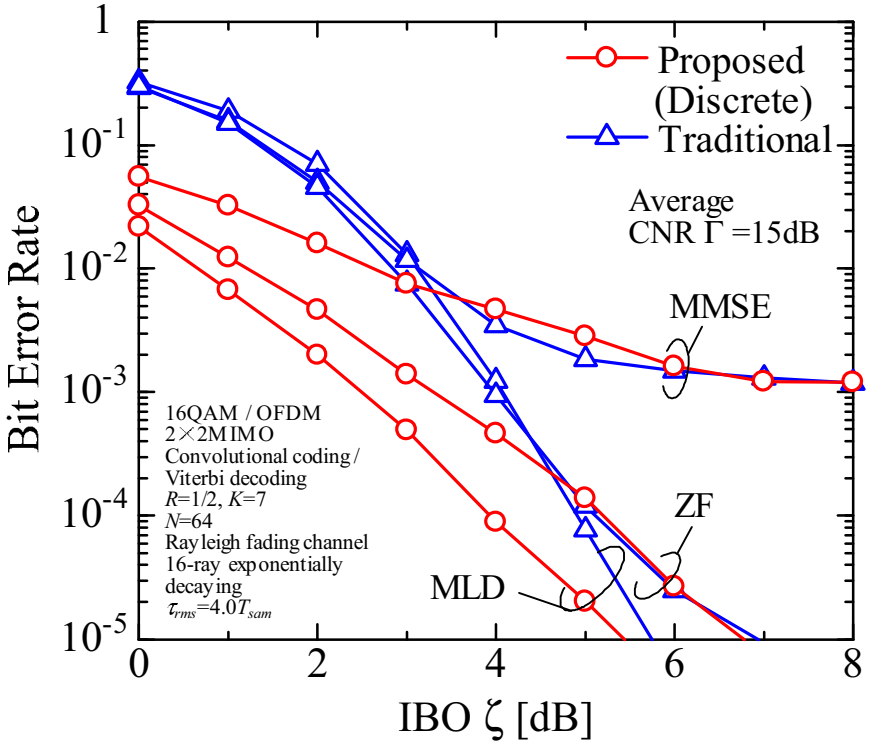

(a) 2×2

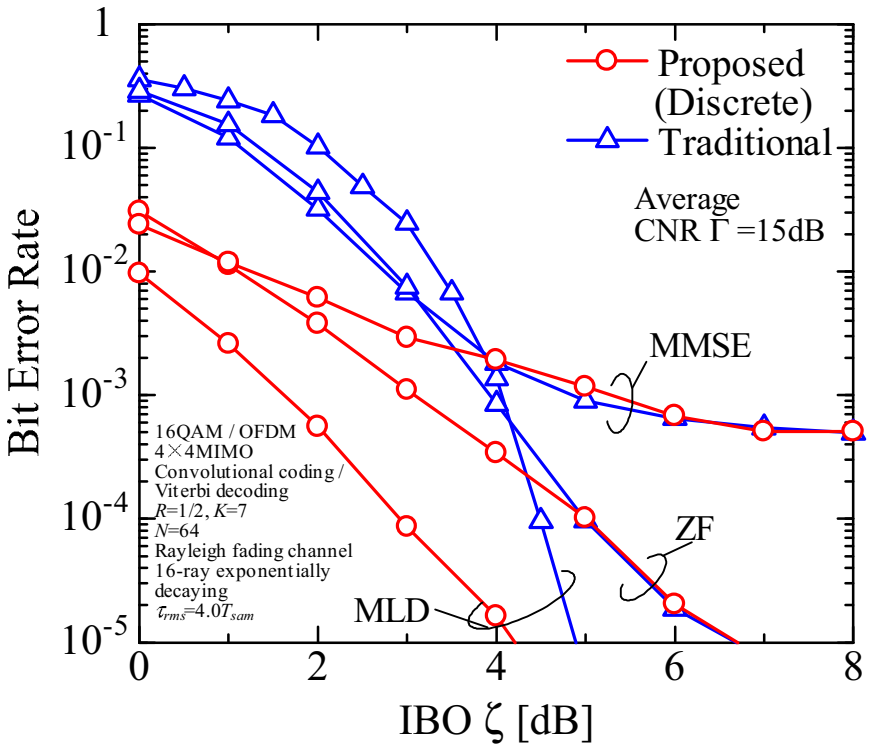

(b) 4×4

Figure 4.11: Performance comparison, in terms of BER performance versus IBO, between proposed method and traditional method, where channel coding is adopted.

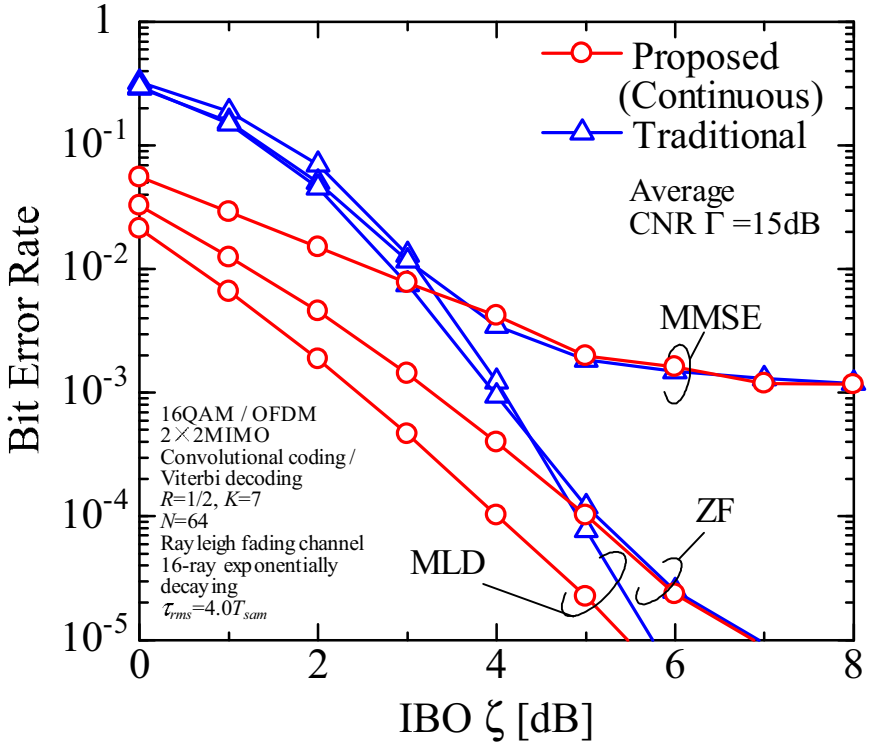

(a) 2×2

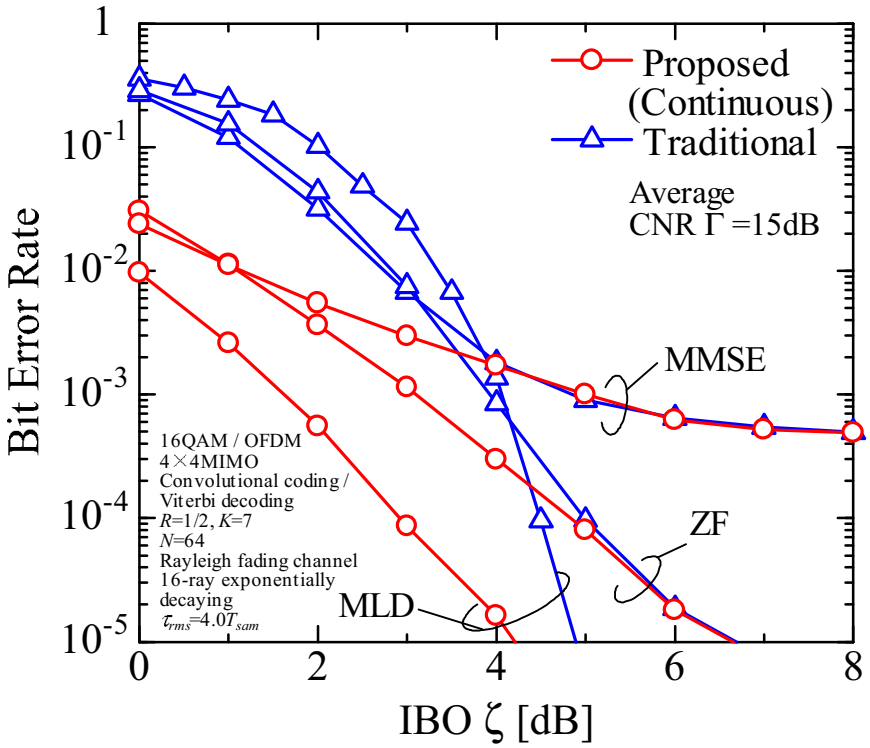

(b) 4×4

Figure 4.12: Performance comparison, in terms of BER performance versus IBO, between proposed method and traditional method, where channel coding is adopted.

4.4 Summary

In this chapter, the proposed clipping and filtering method is adopted for SU-MIMO and its effectiveness of the proposed method on SU-MIMO has been investigated by comparing with the traditional clipping and filtering method. In detail, the problem of SU-MIMO-OFDM under the nonlinear distortion is firstly addressed and then the overall configuration and the BER performance are shown with a parameter of the IBO and the number of transmit and receive antennas. From these results, the following things can be found.

- The proposed method provides the far better BER than the traditional method regardless of the form of the transmit power control and the use of channel coding. This is because the proposed method effectively alleviates the effect of the nonlinear distortion by reducing the transmit power level while the traditional method distorts the transmit OFDM signals in the clipping process.

- In the case of ZF, MMSE, and V-BLAST, the discrete control provides slightly better BER than the continuous control especially in the low IBO. This is because the discrete control can realize the symbol-by-symbol transmit power control while the continuous control is obliged to be performed in a relatively long term.

- In the case of MLD, the continuous control eliminates the error floor while the error floor remains in the discrete method. This is because MLD is much sensitive to the nonlinear distortion than ZF and MMSE and the continuous control can find out more appropriate transmit power level thanks to being no dynamic range of the transmit power control.

- In the case of 4×4 MIMO with V-BLAST and MLD, the proposed method exploits much more diversity benefit than 2×2 MIMO, while the BER of the traditional method is slightly worse than that of 2×2 MIMO case. Therefore, the proposed method contributes to retaining the reasonable

space diversity benefit originally coming from MIMO.

- In a relatively low IBO, the effectiveness of the proposed method becomes remarkable because the proposed method alleviates the distortion caused by clipping and filtering and effectively retains the reasonable space diversity benefit.

5 OFDM Clipping and Filtering Employing Transmit Power Control for MU-MIMO Systems

Multi user multiple input multiple output (MU-MIMO) has become a promising technique for achieving high system capacity over wireless communications systems [42]-[44]. Especially in cellular systems and wireless LAN systems, since the number of antennas of a mobile station (MS) is limited to a few while a lot of antennas can be installed into the base station (BS), MU-MIMO can be seen as an effective technique to meet this requirement. Considering this background, MU-MIMO has already been adopted in LTE system [62] and IEEE802.11ac [63]. Furthermore, MU-MIMO-OFDM which is just a combination of OFDM with MU-MIMO can be seen as an attractive approach to simultaneously achieve high-capacity and reliable wireless network [53]-[55]. In this chapter, the proposed clipping and filtering method is adopted for MU-MIMO and its effectiveness is investigated by means of computer simulations [51], [52].

5.1 Problems in MU-MIMO-OFDM Systems

As described above, MU-MIMO has become an attractive technique for achieving high-speed transmission in multi user systems and the combination of MU-MIMO with OFDM is quite effective to meet the requirement to simultaneously realize high capacity and inter-symbol interference suppression due to multipath fading channels. However, since MU-MIMO-OFDM succeeds the basic properties of OFDM, the nonlinear distortion due to a high PAPR is caused after passing through the HPA, which introduces both the out-of-band radiation and the BER degradation [51], [52]. Moreover, especially in MU-MIMO-OFDM, the effect of the nonlinear distortion becomes severe with increase in the number of transmit antennas because each MS is obliged to receive the nonlinear distortion sent from all transmit antennas. Figure 5.1 shows the concept of MU-MIMO-OFDM systems in the presence of nonlinear distortion. As

shown in Fig. 5.1, the nonlinear distortion of all transmit antennas at the BS is superimposed on each MS in MU-MIMO-OFDM systems, which degrades the BER performance in comparison with SISO-OFDM systems. Therefore, it is important to overcome the nonlinear distortion in MU-MIMO-OFDM systems.

Considering the background described above, we adopt the proposed clipping and filtering method for MU-MIMO-OFDM and clarify the effectiveness of the proposed approach in comparison with the traditional clipping and filtering method [51], [52]. In particular, the proposed method sets the transmit power level to be constant among all transmit antennas considering that the different transmit power levels among the transmit antennas destroy the space orthogonality. Moreover, in order to keep the constant transmit power level, the SNDR averaged over all transmit antennas is obtained by the simple mathematical formula [36] makes use of the CNR averaged over all transmit antennas and is used for transmit power control. The effectiveness of the proposed scheme is demonstrated in comparison with the traditional clipping and filtering method over the nonlinear fading channels.

Figure 5.2 shows the overall configuration of traditional MU-MIMO-OFDM

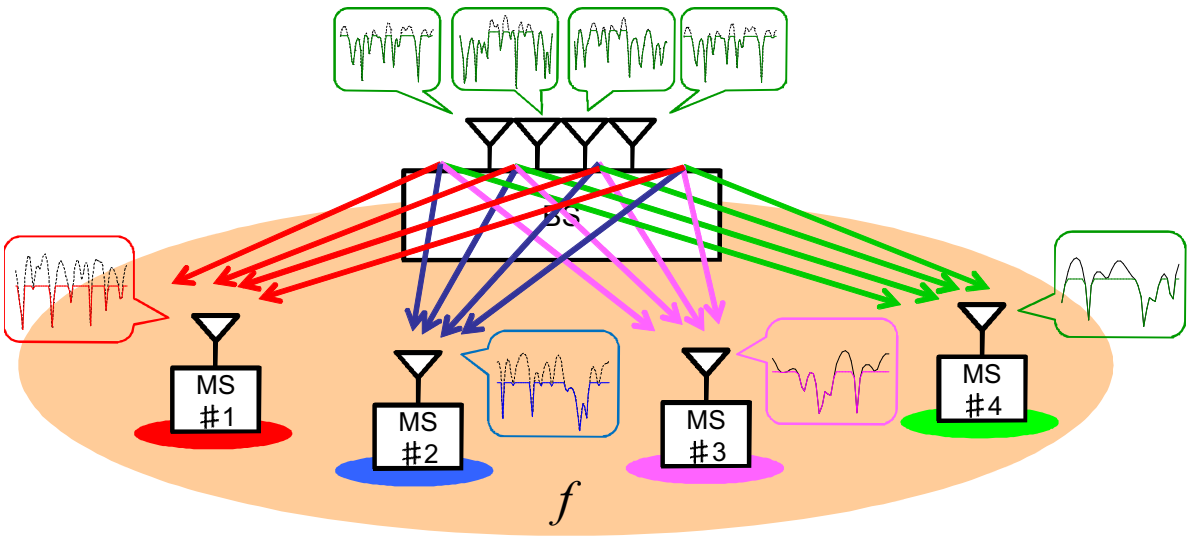

Figure 5.1: Concept of MU-MIMO-OFDM Systems in the Presence of Nonlinear Distortion.

systems, where N and M are the number of transmit antennas and the number of MSs, respectively. As shown in Fig. 5.2, the sub-carrier signals of all users are properly precoded by using the precoding weight $\boldsymbol{W}$ so as to retain the space orthogonality. In the case that Zero-Forcing (ZF) is adopted for the precoding criterion, the precoding weight $\boldsymbol{W}$ is expressed by using the channel matrix $\boldsymbol{H}$ as

$$\boldsymbol{W} = \boldsymbol{H}^{\boldsymbol{H}} \left(\boldsymbol{H}\boldsymbol{H}^{\boldsymbol{H}} \right)^{-1}. \tag{5.1}$$

The precoded sub-carrier signals at each transmit antenna are converted into the time domain OFDM signals by IFFT processing and are input to the HPA. After passing through the HPA, the nonlinear distortion is caused due to very high PAPR as is the same with OFDM. Moreover, it should be noted that MU-MIMO-OFDM is more severe than SISO-OFDM in terms of the risk of the nonlinear distortion. Figure 5.3 shows the signal constellation with a parameter of the number of transmit antennas without the effect of AWGN. For our simplicity, the number of the MSs is set to be the same as N. It can be observed from Fig. 5.3 that the influence of the nonlinear distortion on the signal constellation becomes severe as N increases. The reason is that each MS is unfortunately interfered by the nonlinear distortion of all transmit antennas. Here, in order to clearly understand the effect of the nonlinear distortion in the MU-MIMO-OFDM systems, we represent the effect of the nonlinear distortion by using the mathematical formula.

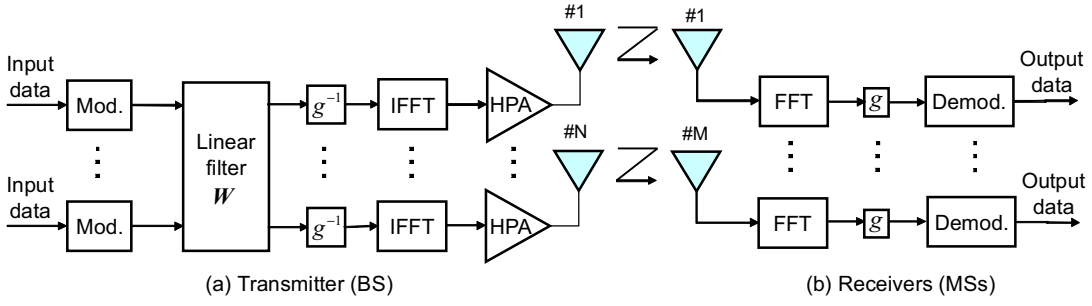

Figure 5.2: Overall configuration of MU-MIMO-OFDM.

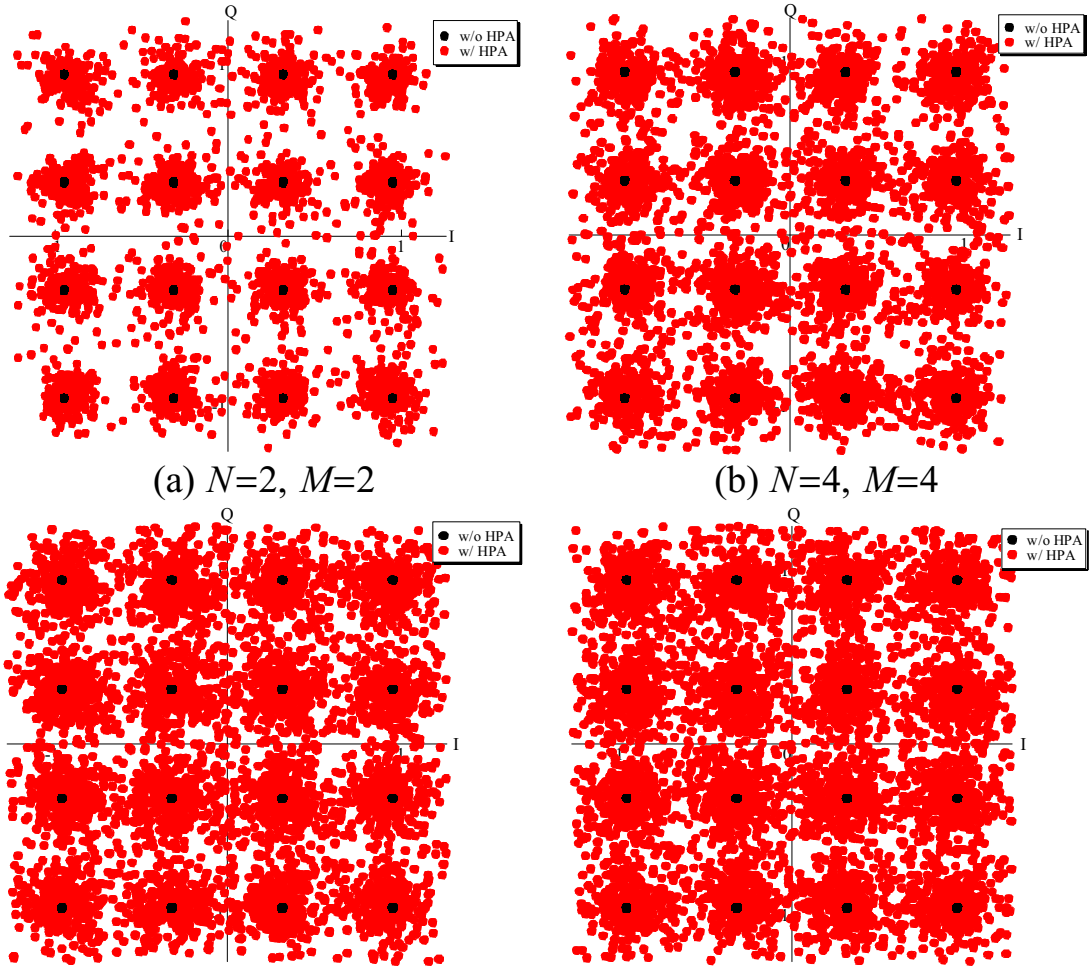

(a) N=2, M=2 (b) N=4, M=4

(c) N=6, M=6 (d) N=8, M=8

Figure 5.3: Signal constellation with a parameter of the number of transmit antennas.

At the BS, the precoded signal vector at the transmit antenna $\boldsymbol{S}$ is represented

by using the weight matrix $\boldsymbol{W}$ and the transmit signal vector $\boldsymbol{X}$ as

$$\begin{aligned}\boldsymbol{S} &= g^{-1}\boldsymbol{W}\boldsymbol{X} \\ &= g^{-1}\begin{bmatrix} w_{11} & \cdots & w_{1N} \\ \vdots & \ddots & \vdots \\ w_{M1} & \cdots & w_{MN} \end{bmatrix}\begin{bmatrix} x_1 \\ \vdots \\ x_N \end{bmatrix} \\ &= g^{-1}\begin{bmatrix} w_{11}x_1 + \cdots + w_{1N}x_N \\ \vdots \\ w_{M1}x_1 + \cdots + w_{MN}x_N \end{bmatrix},\end{aligned} \tag{5.2}$$

where g^{-1} is the power normalization factor.

The nonlinear distorted signal vector at each transmit antenna $\boldsymbol{S_D}$ is expressed as

$$\begin{aligned}\boldsymbol{S_D} &= \alpha\boldsymbol{S} + \boldsymbol{N_D} \\ &= \begin{bmatrix} \alpha_1 g^{-1}\sum_{m=1}^{N} w_{1m}x_m + n_{d1} \\ \vdots \\ \alpha_M g^{-1}\sum_{m=1}^{N} w_{Mm}x_m + n_{dM} \end{bmatrix},\end{aligned} \tag{5.3}$$

where $\boldsymbol{\alpha}^T=[\alpha_1, \cdots, \alpha_M]$ is the attenuation coefficient due to the nonlinear distortion vector, and $\boldsymbol{N_D}^T=[n_{d1}, \cdots, n_{dM}]$ is an uncorrelated nonlinear distortion vector.

As shown in Eq. (5.3), the transmit signal originally includes the nonlinear distortion. In radio propagation, the distorted transmit signals are directly affected by the channel coefficients and therefore, the received signal vector $\boldsymbol{Y}$ at

each MS is represented as $\boldsymbol{H}$ and

$$
\begin{aligned}
\boldsymbol{Y} &= g\boldsymbol{H}\boldsymbol{S_D} + g\boldsymbol{N} \\
&= g\begin{bmatrix} h_{11} & \cdots & h_{1M} \\ \vdots & \ddots & \vdots \\ h_{N1} & \cdots & h_{NM} \end{bmatrix}\begin{bmatrix} \alpha_1 g^{-1}\sum_{m=1}^{N} w_{1m}x_m + n_{d1} \\ \vdots \\ \alpha_M g^{-1}\sum_{m=1}^{N} w_{Mm}x_m + n_{dM} \end{bmatrix} + g\begin{bmatrix} n_1 \\ \vdots \\ n_N \end{bmatrix} \\
&= \begin{bmatrix} \sum_{l=1}^{M}\left\{h_{1l}\alpha_l\sum_{m=1}^{N} w_{1m}x_m\right\} + g\sum_{l=1}^{M} h_{1l}n_{dl} + gn_1 \\ \vdots \\ \sum_{l=1}^{M}\left\{h_{Nl}\alpha_l\sum_{m=1}^{N} w_{Mm}x_m\right\} + g\sum_{l=1}^{M} h_{Nl}n_{dl} + gn_N \end{bmatrix},
\end{aligned}
\tag{5.4}
$$

where $\boldsymbol{N}^T=[n_1, \cdots, n_N]$ is the noise vector.

It can be seen from Eq. (5.4) that the effect of the nonlinear distortion becomes severe as the number of transmit antennas increases. This is because each MS is obliged to receive the nonlinear distortion of all transmit antennas.

From these results, it can be said that the nonlinear distortion suppression is essential in MU-MIMO-OFDM systems.

5.2 System Concept

Figure 5.4 shows the amplitude distribution of the precoded OFDM time domain signal in MU-MIMO-OFDM systems, where the number of transmit antennas is assumed to be 4. It is found from Fig. 5.4 that the amplitude distribution of the OFDM time domain signal at each transmit antenna converges to Rayleigh distribution regardless of the transmit antenna. Figure 5.5 shows the amplitude distribution of the OFDM time domain signal with a parameter of the number of sub-carriers N in both SISO and MU-MIMO cases. It can be observed from Fig. 5.5 that the amplitude distribution in MU-MIMO case easily approaches to Rayleigh distribution compared with the SISO case. This

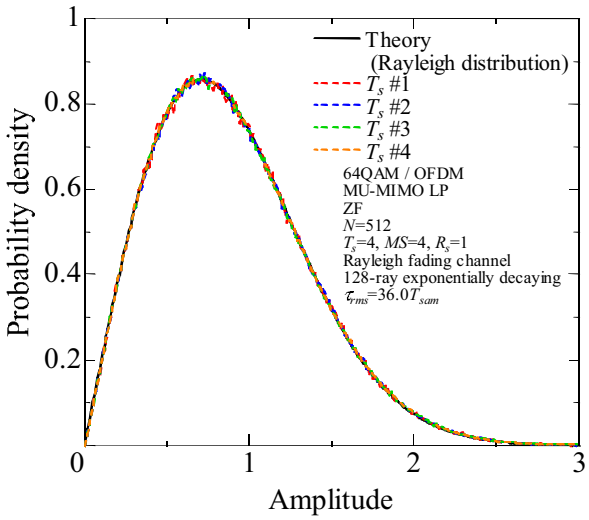

Figure 5.4: Amplitude distribution of time domain precoded signal in MU-MIMO-OFDM.

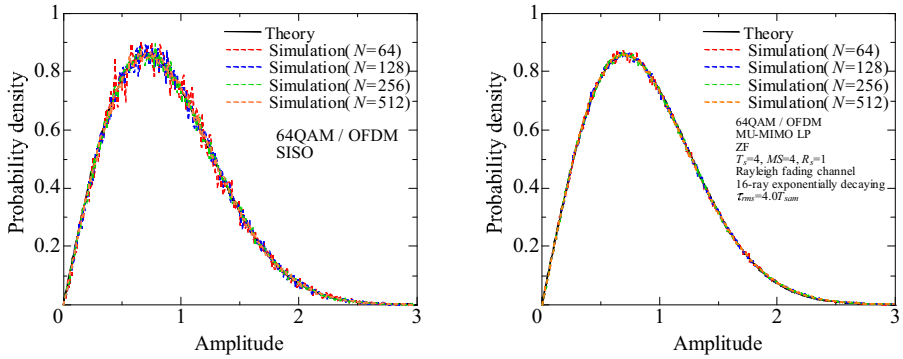

(a) SISO (b) MU-MIMO

Figure 5.5: Amplitude distribution of time domain precoded signal with a parameter of the number of sub-carriers.

is because MU-MIMO mixes the multiple transmit signals with the precoding matrix and consequently the central limit theorem can easily hold true. Hence, the adoption of proposed method for MU-MIMO is considered to be effective to overcome the nonlinear distortion in MU-MIMO-OFDM.

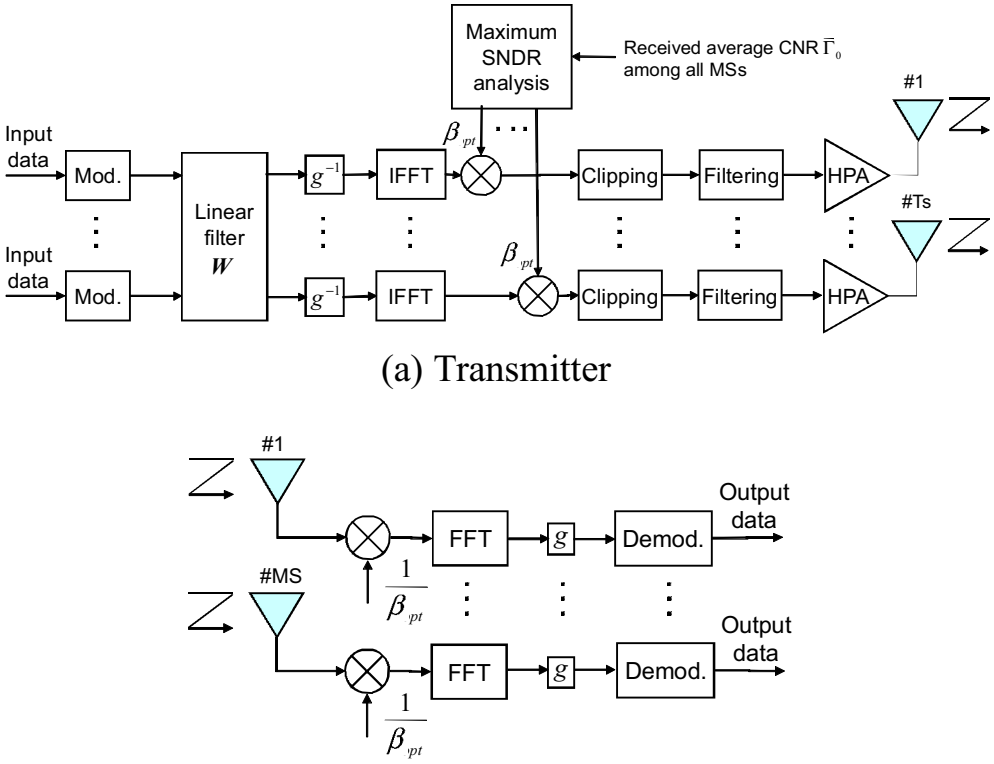

Figure 5.6: Overall configuration of proposed method deployed on MU-MIMO-OFDM systems.

5.3 System Configuration

Figure 5.6 shows the overall configuration of the proposed method for MU-MIMO-OFDM. Here, it should be noted that, since the precoded transmit signals are different among the transmit antennas, the different SNDRs can be naturally generated. If different transmit power levels are allowed after precoding, the space orthogonality is to be completely destroyed because the precoded transmit signal with different power control are not proportional to the original precoded signals any longer, which can be seen as a specific property of MU-MIMO. Thus we set the transmit power levels of all transmit antennas to be the same so as to retain the space orthogonality and determine the best power level

by using the average SNDR. Thus the average SNDR $\overline{\gamma_{nd}}$ is expressed as

$$\overline{\gamma_{nd}} = \frac{1}{MS}\sum_{j=1}^{MS}\gamma_{nd_j} = \frac{1}{MS}\sum_{j=1}^{MS}\frac{|\alpha|^2\beta^2}{\frac{|\alpha|^2\beta^2}{\Lambda}+\frac{1}{\Gamma_{0_j}}} \tag{5.5}$$

$$\because \quad \Lambda = \frac{|\alpha|^2}{\left(1-e^{-\zeta'/\beta^2}\right)-|\alpha|^2},$$

where j is the transmit antenna identifier.

In consequence, the transmit power level determines the SNDR which is calculated by using the precoded time domain signals and the transmit power level with the maximal average SNDR β_{opt} is utilized for actual MU-MIMO-OFDM transmission.

5.4 Numerical Results

In this section, the output power reduction ratio of the proposed method for MU-MIMO is firstly investigated and then the BER performance of the proposed method is compared with the traditional clipping and filtering with the constant transmit power level in order to clarify the effectiveness of the proposed approach.

(a) Output power reduction ratio of HPA

Figure 5.7 shows the performance comparison, in terms of output power reduction ratio versus IBO, between $N = 64$ and $N = 512$. It can be observed from Fig. 5.7 that the performances of $N = 64$ and $N = 512$ are almost the same. This is because the proposed method makes use of the statistical property of the transmit signals which does not depend on the number of sub-carriers.

(b) BER performance

Figure 5.8 shows the performance comparison, in terms of the average CNR versus BER, between the proposed method and the traditional method, where

channel coding is not adopted. Table 5.1 shows the simulation parameters. It is found from Fig. 5.8 that the proposed method provides better BER than the traditional method regardless of the number of transmit antennas and the modulation scheme. This performance improvement comes from the fact that the proposed method alleviates effectively the nonlinear distortion at each transmit antenna while the traditional method destroys the transmit OFDM signals due to the clipping process.

Figure 5.9 shows the performance comparison, in terms of the average CNR versus BER, between the proposed method and the traditional method, where channel coding is adopted. From Fig. 5.9, it is confirmed that the effect of the proposed method is still retained in adoption of channel coding.

Finally, Figure 5.10 shows the performance comparison, in terms of the IBO versus BER, between the proposed method and the traditional method, where channel coding is adopted. It is observed from Fig. 5.10 that the proposed method provides better BER performance than the traditional method regardless of the number of transmit and received antennas.

Table 5.1: Simulation parameters.

Modulation	16QAM, 64QAM / OFDM
FEC	None, Convolutional coding/ Viterbi decoding $R = 1/2, K = 7$
Number of subcarriers N	512
Precoding scheme	Linear precoding
Oversampling rate M	4
Guard interval length T_G	128 T_{sam},
Channel model	128-ray exponentially decaying Rayleigh fading
Delay spread τ_{rms}	36.0 T_{sam},
CR	IBO-2 [dB]
Number of transmit antennas T_s	1, 2, 4
Number of MSs MS	1, 2, 4
Number of MS antenna elements R_s	1

From these results, it is concluded that the proposed clipping and filtering method dramatically improves the BER performance compared with the traditional clipping and filtering method thanks to the use of transmit power control at each transmit antenna while keeping the space orthogonality. Therefore, it can be said that the proposed method contributes to enhancing the channel capacity of MU-MIMO-OFDM.

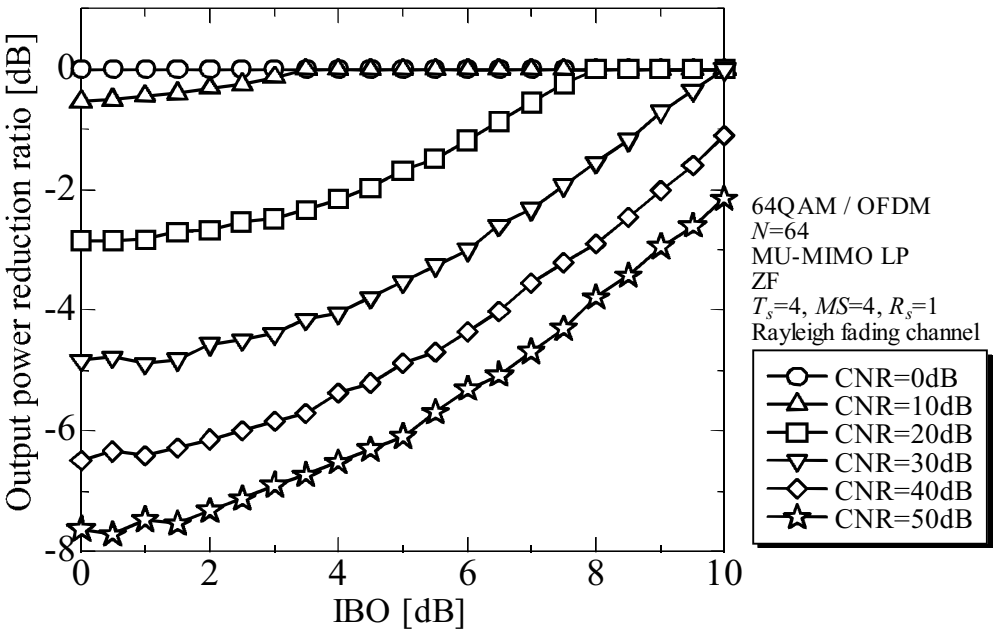

(a) N=64

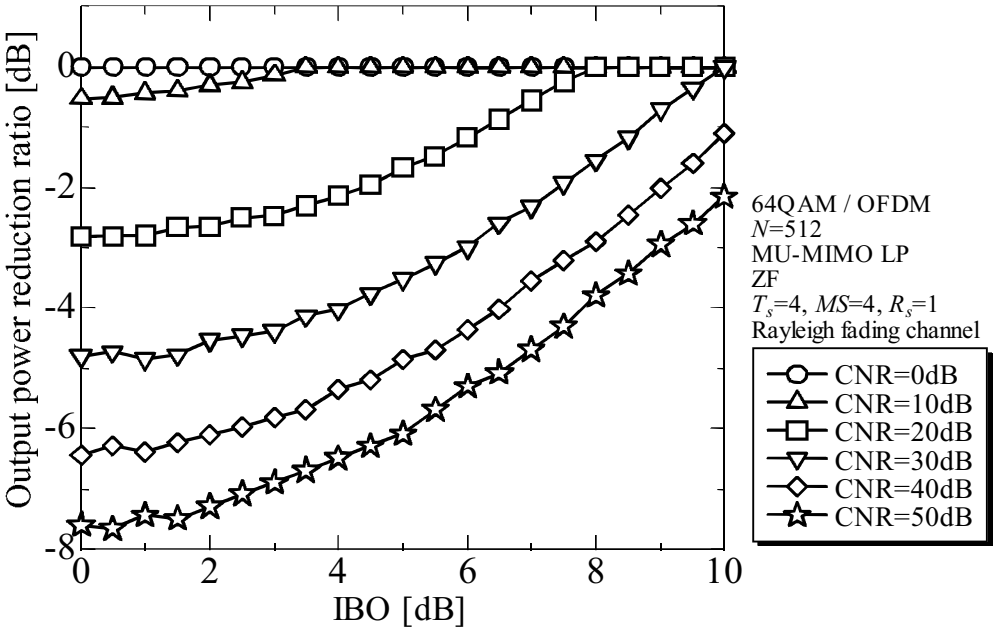

(b) N=512

Figure 5.7: Performance comparison, in terms of output power reduction ratio with proposed method versus IBO, between N = 64 and N = 512, where the MU-MIMO is assumed.

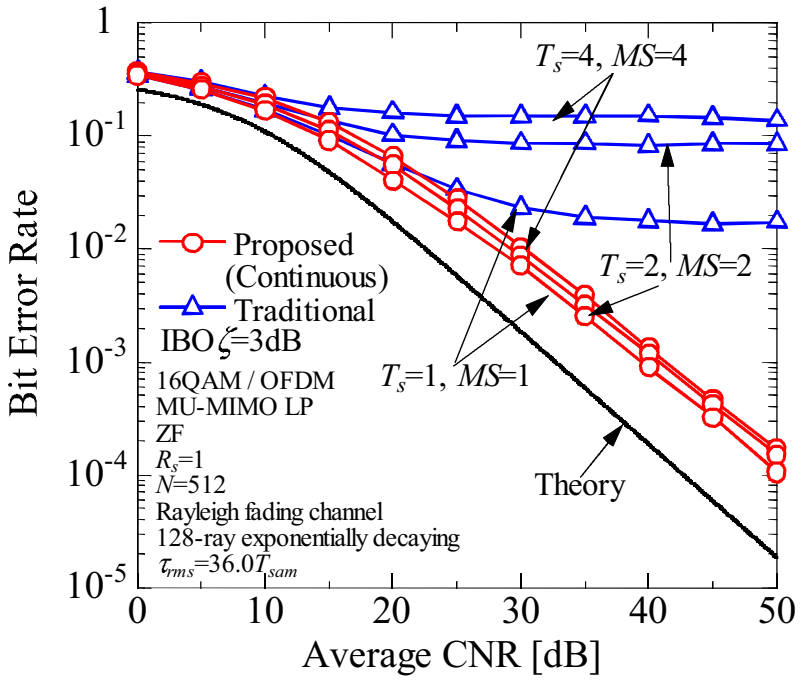

(a) 16QAM

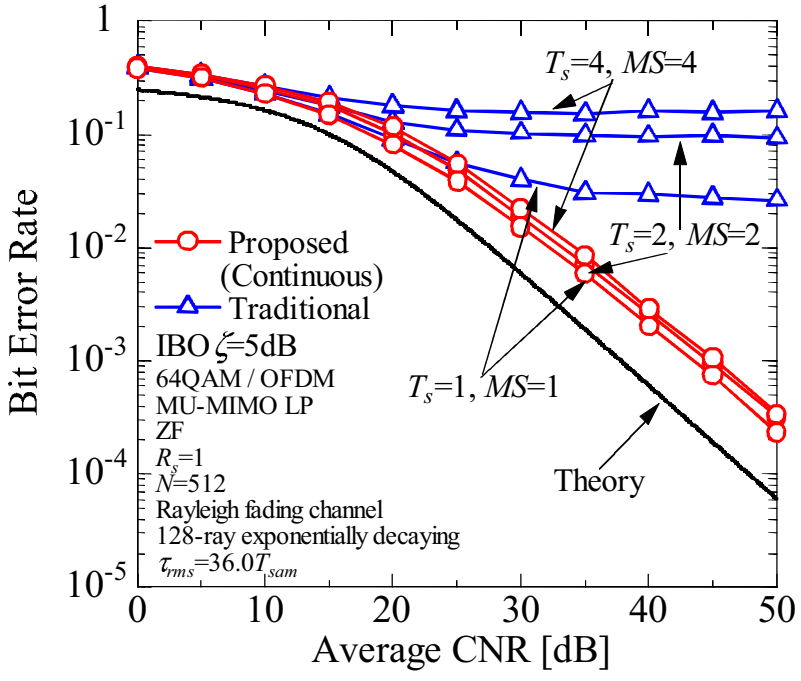

(b) 64QAM

Figure 5.8: Performance comparison, in terms of BER performance versus average CNR, between proposed method and traditional method, where channel coding is not adopted.

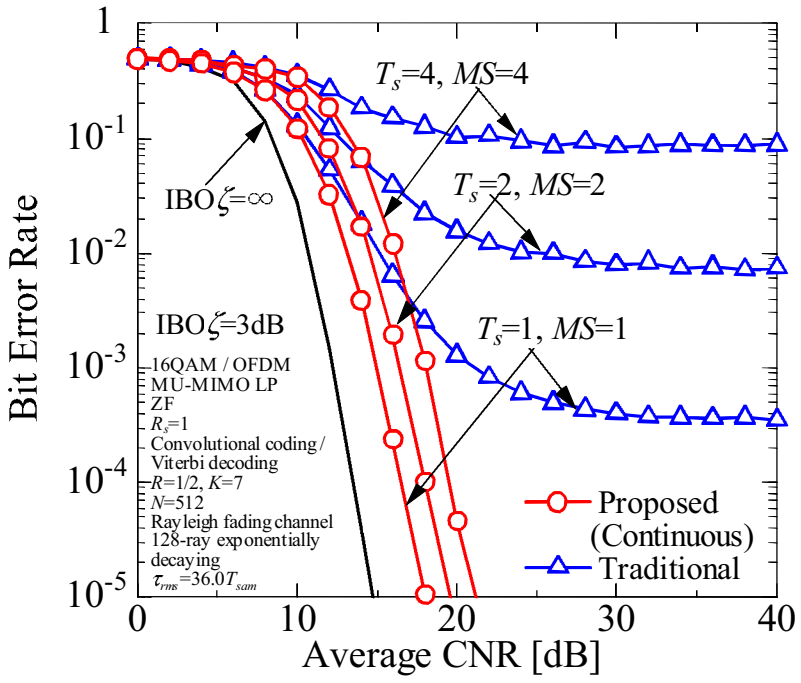

(a) 16QAM

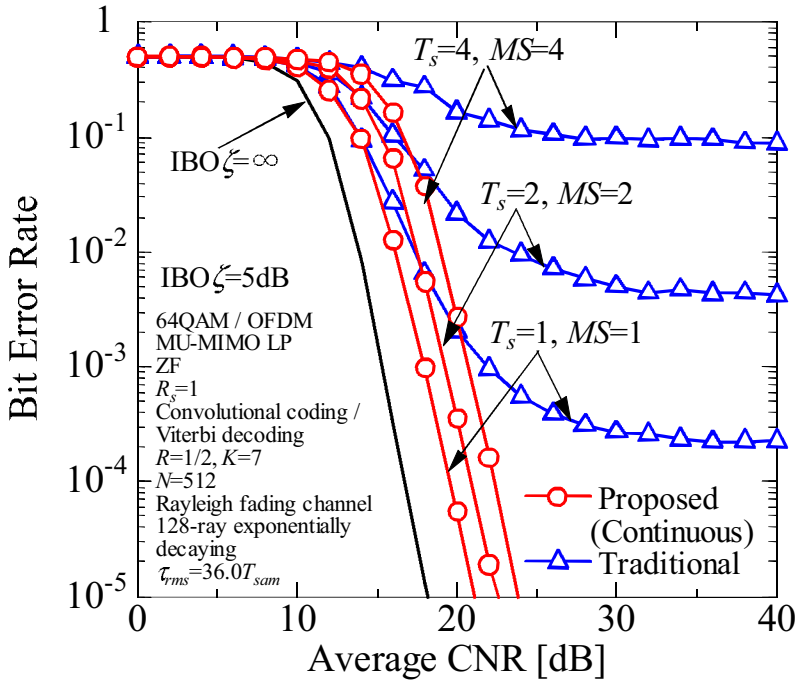

(b) 64QAM

Figure 5.9: Performance comparison, in terms of BER performance versus average CNR, between proposed method and traditional method, where channel coding is adopted.

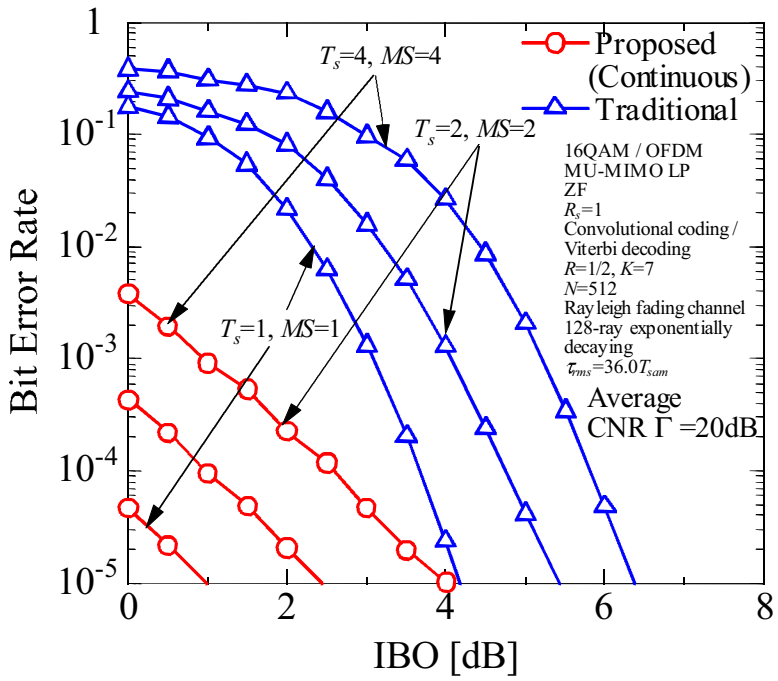

(a) 16QAM

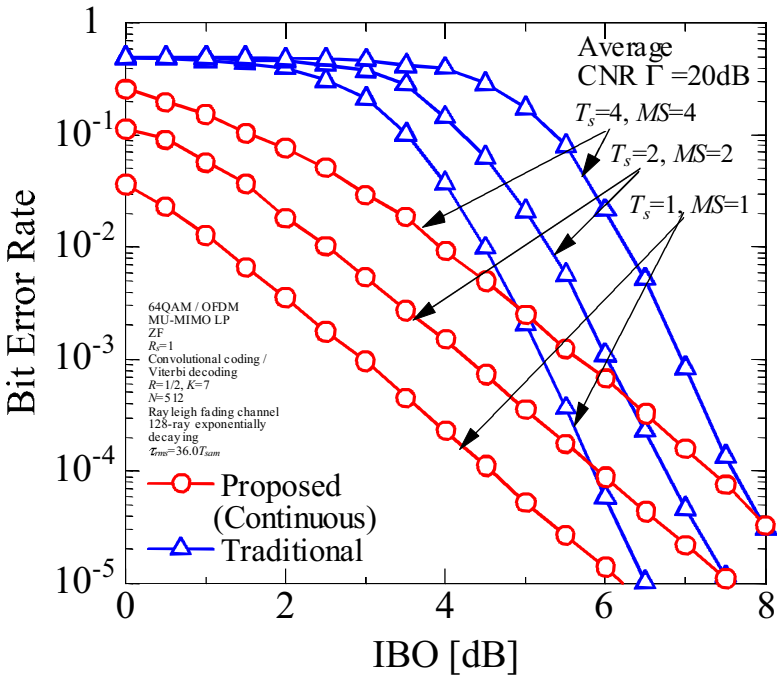

(b) 64QAM

Figure 5.10: Performance comparison, in terms of BER performance versus IBO, between proposed method and traditional method, where channel coding is adopted.

5.5 Summary

In this chapter, the proposed clipping and filtering method is adopted for MU-MIMO and its effectiveness of the proposed method on MU-MIMO has been investigated by comparing with the traditional clipping and filtering method. In detail, the problem of MU-MIMO-OFDM under the nonlinear distortion is firstly addressed and then both the overall configuration and the transmission performance in terms of the output power reduction ratio and the BER are shown with a parameter of the IBO, the number of sub-carriers, and the number of transmit and received antennas. From these results, the following things can be found.

- In application to MU-MIMO, the BER degradation due to the nonlinear distortion becomes severe as the number of transmit antennas increases. This is because the each MS is obliged to receive the distortion component sent from all transmit antennas.
- In adoption of transmit power control for precoded signals, the transmit power level has to be kept constant among all transmit antennas in order to retain space orthogonality which is essential for MU-MIMO.
- The output power reduction ratio is almost not dependent on the number of sub-carriers because the proposed method makes use of the statistical property of the transmit signals which does not depend on the number of sub-carriers.
- The proposed method dramatically improves the BER performance compared with the traditional method thanks to the use of transmit power control to satisfy the maximum SNDR while keeping the space orthogonality.

6 Conclusion

In this dissertation, we have proposed the nonlinear distortion suppression scheme employing transmit power control in OFDM transmission. Contributions are given in the proposed method and its application to SU-MIMO and MU-MIMO systems which are listed as follows.

- The nonlinear distortion suppression scheme employing transmit power control is proposed to overcome the BER degradation which is an inherent problem of the traditional clipping and filtering. The feature of the proposed method is to deterministically control the transmit power level by means of the simple theoretical formula which represents the relationship between the SNDR and the input signal level. Computer simulations showed that the proposed method can determine the transmit power level to satisfy the maximum SNDR and dramatically improve the BER performance because the input signal level is controlled in order to achieve the optimal SNDR.

- The proposed nonlinear distortion suppression scheme is adopted for SU-MIMO systems and its effectiveness is confirmed by means of the computer simulations. Numerical results showed that the proposed scheme is effective to improve the BER performance while the traditional clipping and filtering degrades the BER performance with increase in the number of streams. Moreover, the effectiveness of the proposed method can be seen especially in use of MLD as the signal detection technique for MIMO systems.

- The proposed nonlinear distortion suppression scheme is adopted for MU-MIMO systems and its effectiveness is confirmed by means of the computer simulations. Firstly, it is pointed out that the BER degradation becomes significant in the traditional clipping and filtering with increase in the number of transmit antennas. This is because the effect of the nonlinear distortion caused at each transmit antenna is accumulated at a mobile

station. In application of the proposed scheme to MU-MIMO, it is essential to set the same transmit power level among the transmit antennas because the different transmit power levels destroy the space orthogonality. Numerical results showed that the proposed method can improve the BER performance in comparison with the traditional clipping and filtering regardless of the number of transmit antennas.

For the future work, researches will be deeply continued especially on the following topics.

- The influence of the quantization error which is caused in the notification of the received CNR is to be considered. Moreover, the influence of the imperfect notification of the transmit power level on the BER performance is also meaningful to be investigated.
- In the derivation of theoretical SNDR, the influence of the peak regrowth due to the filtering process is to be taken into account.
- The theoretical SNDR for MU-MIMO is to be derived and its validity is to be confirmed by comparing with the computer simulation results.
- The effectiveness of the proposed scheme in application to MU-MIMO is to be evaluated in different CNRs among multiple users.

References

[1] F. Adachi, " Wireless past and future -evolving mobile communications systems-," *IEICE Trans. Commun.*, vol.E84-A, no.1, pp.55-60, Jan. 2001.

[2] T. S. Rappaport, A. Annamalai, R.M. Buehrer, and W.H. Tranter, " Wireless communications: past events and a future perspective," *IEEE Commun. Mag.*, vol.40, no.5, pp.148-161, May 2002.

[3] *Cisco Visual Networking Index: Forecast and Methodology, 2013-2018* available at http://www.cisco.com/c/en/us/solutions/collateral/service-provider/ip-ngn-ip-next-generation-network/white_paper_c11-481360.pdf.

[4] S. Sampei, Applications of digital wireless technologies to global wireless communications, Prentice Hall, 1997.

[5] John G. Proakis, Digital communications, McGraw-Hill, 2000.

[6] T. S. Rappaport, Wireless communications : Principles and practice, Prentice Hall, 2002.

[7] F. Takahata, F. Maehara, and F. Sasamori, Introduction to digital wireless communications (in Japanese), Baifukan, 2002.

[8] S. B. Weinstein and P. M. Ebert, "Data transmission by frequency-division multiplexing using the discrete fourier transform," *IEEE Trans. Commun. Tech.*, vol.COM-19, no.45, pp.628-634, Oct. 1971.

[9] H. Sari and I. Jeanclaude, " Transmission techniques for digital terrestrial TV broadcasting," *IEEE Commun. Mag.*, vol.33, no.2, pp.100-109, Feb. 1995.

[10] V. Nee and R. Prasad, OFDM for wireless multimedia communications, Artech House, 2000.

[11] K. Fazel and S. kaiser, Multi-Carrier and Spread Spectrum Systems," John Wiley & Sons Inc, 2003.

[12] S. Hara and R. Prasad, Multicarrier techniques for 4G mobile communications, Artech House, 2003.

[13] Operational guidelines for digital terrestrial television broadcasting, ARIB Tech. Rep. TR-B14 Ver.2.4, May 2005.

[14] Wireless LAN medium access control (MAC) and physical layer (PHY) specification, IEEE Std. 802.11a, 1999.

[15] T. Hwang, C. Yang, G. Wu, S. Li, and G. Y. Li, " OFDM and its wireless applications: A survey," *IEEE Trans. on Veh. Tech.*, vol.58, no.4, pp.1673-1694 May 2009.

[16] G. Wunder, R. F. H. Fischer, H. Boche, S. Litsyn, and J. No, " The PAPR problem in OFDM transmission: New directions for a long-lasting problem," *IEEE Signal Process. Mag.*, vol.30, no.6, pp.130-144, Nov. 2013.

[17] Y. Rahmatallah and S. Mohan, " Peak-to-average power ratio reduction in OFDM systems: A survey and taxonomy," *IEEE Commun. Surv. & Tut.*, vol.15, no.4, pp.1567-1592 , 2013.

[18] S. H. Han and J. H. Lee, " An overview of peak to average power ration reduction techniques for multicarrier transmission," *IEEE Wireless Commun.*, vol.12, no.2, pp.56-65, Apr. 2005.

[19] X. Li and L. J. Cimini, " Effects of clipping and filtering on the performance of OFDM," *IEEE Commun. Lett.*, vol.2 no.5 pp.131-133, May 1998.

[20] H. Ochiai and H. Imai, " Performance analysis of deliberately clipped OFDM signals," *IEEE. Trans. Commun.*, vol.50, no.1 pp.89-101, Jan. 2002.

[21] J. Armstrong, " Peak-to-average power ratio reduction for OFDM by repeated clipping and frequency domain filtering," *Elect. Lett.*, vol.38, pp.246-247, Feb. 2002.

[22] H. A. Suraweera, K. R. Panta, M. Feramez, and J. Armstrong, " OFDM peak-to-average power reduction scheme with spectral masking," *Proc. CSNDSP 2004*, pp. 160-163, July 2004.

[23] S. H. Muller and J. B. Huber, "OFDM with reduced peak-to-average power ratio by optimum combination of partial transmit sequences," *Elect. Lett.*, vol.33, no.5, pp.368-369, Feb. 1997.

[24] L. J. Cimini and N. R. Sollenberger, " Peak-to-average power ratio reduction of an OFDM signal using partial transmit sequences," *Proc. IEEE ICC '99*, vol.1, pp.511-515, Jun. 1999.

[25] S. K. Yusof, N. Fisal, and T. S. Yin, " Reducing PAPR of OFDM signals using partial transmit sequences," *Proc. APCC 2003*, vol.1, pp.411-414, Sept. 2003.

[26] A. E. Jones, T. A. Wilkinson, and S. K. Barton, "Block coding scheme for reduction of peak to mean envelope power ratio of multicarrier transmission scheme," *Elect. Lett.*, vol.30 no.22 pp.2098-2099, Dec. 1994.

[27] V. Tarokh and H. Jafarkhani, " On the computation and reduction of the peak-to-average power ratio in multicarrier communications," *IEEE Trans. Commun.*, vol.48 no.1 pp.37-44, Jan. 2000.

[28] M.G.Di Benedetto and P.Mandarini, " An application of MMSE predistortion to OFDM systems," *IEEE Trans. Commun.*, vol.44, no.11, pp.1417-1420, Nov. 1996.

[29] S. Uwano, Y. Matsumoto, M. Mizoguchi, and M. Umehara, " Linearized constant peak-power coded OFDM transmission for broadband wireless

access systems," *IEICE Trans. Commun.*, vol. E82-B no.12 pp.1932-1938, Dec. 1999.

[30] K.Wesolowski and J. Pochmara, " Efficient algorithm for adjustment of adaptive predistorter in OFDM transmitter," *Proc. IEEE VTC2000-Fall*, pp.2491-2496, Sept. 2000.

[31] O. Muta, T. Takata, and Y. Akaiwa, " A peak power reduction scheme with parity carrier for multi-carrier modulation," *IEICE Trans. Commun.*, vol.J84-B, no.5, pp.849-860, May 2001.

[32] R. Toba, S. Tomisato, M. Hata, and H. Fujii, " A multi-stage generating method for peak power reduction signals with adaptive filtering in OFDM transmission," *IEICE Trans. Commun.*, vol.J93-B, no.5, pp.769-780, May 2010.

[33] T. Fujii and M. Nakagawa, " Adaptive clipping level control for OFDM peak power reduction using clipping and filtering," *IEICE Trans. Fundamentals*, vol.E85-A, no.7 pp.1647-1655, July 2002.

[34] H. Chen and A. Haimovich, " An iterative method to restore the performance of clipped and filtered OFDM signals," *IEEE Commun. Letters*, vol.7, pp.305-307, July 2003.

[35] T. Uchino and H. Ochiai, "On the performance of clipping noise cancellation for OFDM systems with high-order coded modulation," *Proc. ISITA 2008*, Dec. 2008.

[36] F. Maehara, " Series expression of BER performance for DQPSK/OFDM signals employing selection combining diversity reception over nononlinear fading channels," *Proc. IEEE VTC2005-Spring*, vol. 2, pp. 1007-1011, May 2005.

[37] S. Takebuchi, T. Arai, and F. Maehara, " Performance evaluation of OFDM clipping and filtering method using transmit power control," *Proc. WTC2012*, PS-25, Mar. 2012.

[38] S. Takebuchi, G. Osada, and F. Maehara, "A deterministic transmit power control for OFDM clipping and filtering," *Proc. IEEE VTC2013-Fall*, pp.1-5, Sept. 2013.

[39] S. Takebuchi, G. Osada, T. Arai, N. Kamiya, and F. Maehara, " OFDM clipping and filtering method employing theoretical SNDR-based transmit power control," *IEICE Trans. Commun.*, vol.J97-B, no.2, pp.216-228, Feb. 2014.

[40] G. Bauch and A. Alexiou, " MIMO technologies for the wireless future," *Proc. IEEE PIMRC 2008*, pp. 1-6, Sep. 2008.

[41] A. Sibille, C. Oestges, and A. Zanella, MIMO: From theory to implementation, Academic Press, 2010.

[42] Q. H. Spencer, C. B. Peel, A. L. Swindlehurst, and M. Haardt, "An introduction to the multi-user MIMO downlink," *IEEE Commun. Mag.*, vol.42, no.10, pp.60-67, Oct. 2004.

[43] G. Bauch and G. Dietl, " Multi-user MIMO for achieving IMT-Advanced requirements," *Proc. 2008 Int. Conf. on Telecom.*, pp.1-7, June, 2008.

[44] G. Bauch and A. Alexiou, " MIMO technologies for the wireless future," *Proc. IEEE PIMRC 2008*, pp.1-6, Sep. 2008.

[45] S. Takebuchi, T. Arai, and F. Maehara, " A novel clipping and filtering method employing transmit power control for OFDM systems," *Proc. IEEE WCNC2012*, pp. 221-225, Apr. 2012.

[46] H. Sampath, S. Talwar, J. Tellado, V. Erceg, and A. Paulraj, " A fourth-generation MIMO-OFDM broadband wireless system: Design, perfor-

mance, and field trial results," *IEEE Commun. Mag.*, vol. 40, no. 9, pp. 143-149, Sept. 2002.

[47] Y. Li, J. H. Winters, and N. R. Sollenberger, " MIMO-OFDM for wireless communications: Signal detection with enhanced channel estimation," *IEEE Trans. Commun.*, vol. 50, no. 9, pp. 1471-1477, Sept. 2002.

[48] C. Dubuc, D. Starks, T. Creasy, and Y. Hou, "A MIMO-OFDM prototype for next-generation wireless WANs," *IEEE Commun. Mag.*, vol. 42, pp. 82-87, Dec. 2004.

[49] S. Nanda, R. Walton, J. Ketchum, M. Wallace, and S. Howard, " A high-performance MIMO OFDM wireless LAN," *IEEE Commun. Mag.*, vol. 43, pp. 101-109, Feb. 2005.

[50] H. Yang, " A road to future broadband wireless access: MIMO-OFDM-based air interface," *IEEE Commun. Mag.*, vol. 43, pp. 53-60, Jan. 2005.

[51] G. Osada, S. Takebuchi, and F. Maehara, " Nonlinear distortion suppression scheme employing transmit power control for MU-MIMO-OFDM systems," *Proc. IEEE RWW2014*, vol.48 no.1 pp.46-48, Jan. 2014.

[52] T. Maruko, S. Takebuchi, G. Osada, and F. Maehara, " Clipping and filtering employing deterministic transmit power control in MU-MIMO-OFDM systems," *Proc. International OFDM Workshop 2014 (InOWo'14)*, pp.106-111, Aug. 2014.

[53] Q. H. Spencer, C. B. Peel, A. L. Swindlehurst, and M. Haardt, "An introduction to the multi-user MIMO downlink," *IEEE Commun. Mag.*, vol. 42, no. 10, pp. 60-67, Oct. 2004.

[54] Q. H. Spencer, A. L. Swindlehurst, and M. Haardt, "Zero-forcing methods for downlink spatial multiplexing in multiuser MIMO channels," *IEEE Trans. Signal Process.*, vol. 52, pp. 461-471, Feb. 2004.

[55] M. Jiang and L. Hanzo, " Multiuser MIMO-OFDM for next-generation wireless systems," *Proceedings of the IEEE*, vol. 95, no. 7, pp. 1430-1469, July. 2007.

[56] N. Kamiya and F. Maehara, " Nonlinear distortion avoidance employing symbol-wise transmit power control for OFDM transmission," *Proc. International OFDM Workshop 2009 (InOWo'09)*, pp.223-227, Sept. 2009.

[57] H. E. Rowe, "Memoryless nonlinearities with gaussian inputs : elementary results," *Bell Syst. Tech. J.*, vol.61, no.7, pp.1519-1525, Sept. 1982.

[58] P. Banelli and S. Cacopardi, " Theoretical analysis and performance of OFDM signals in nonlinear AWGN channels," *IEEE Trans. Commun.*, vol.48 , no.3, pp.430-441, Mar. 2000.

[59] D. Dardari, V. Tralli, and A. Vaccari, " A theoretical characterization of nonlinear distortion effects in OFDM systems," *IEEE Trans. Commun.*, vol.48, no.10, pp.1755-1764, Oct. 2000.

[60] H. Ochiai and H. Imai, "Performance of the deliberate clipping with adaptive symbol selection for strictly band-limited OFDM systems," *IEEE J. Select. Areas Commun.,* vol. 18, no. 11, pp. 2270-2277, Nov. 2000.

[61] H. Ochiai and H. Imai, " Performance analysis of deliberately clipped OFDM signals," *IEEE Trans. Commun.,* vol. 50, no. 1, pp. 89-101, Jan. 2002.

[62] ETSI, TS 136.306, v10.2.0, "User Equipment (UE) radio access capabilities," June 2011.

[63] Wireless LAN Medium Access Control (MAC) and Physical Layer (PHY) specifications: Enhancements for very high throughput for operation in bands below 6GHz, IEEE P802.11ac/D1.0 Std., Jan. 2011.

Publication

Journal Paper:

[1] S. Takebuchi, T. Maruko, H. Tomeba, T. Onodera, M. Kubota, F. Maehara, and F. Takahata, "Hybrid ARQ to mitigate effect of modulo loss in multi-user MIMO THP systems," *IEICE Trans. Commun.*, vol.J98-B, no.1, pp.65-76, Jan. 2015.

[2] S. Takebuchi, G. Osada, T. Arai, N. Kamiya, and F. Maehara, "OFDM clipping and filtering method employing theoretical SNDR-based transmit power control," *IEICE Trans. Commun.*, vol.J97-B, no.2, pp.216-228, Feb. 2014.

[3] S. Takebuchi, R. Kaneko, and F. Maehara, "Theoretical derivation method of bit error rate in MB-OFDM UWB," *IEICE Trans. Fund.*, vol.J96-A, no.5, pp.273-277, May 2013.

[4] T. Shirai, S. Takebuchi, and F. Maehara, "Multi-user MIMO transmission scheme employing redundant degrees of freedom," *IEICE Trans. Commun.*, vol.J96-B, no.5, pp.551-554, May 2013.

Publication

International Conference Paper:

[1] T. Maruko, S. Takebuchi, G. Osada, and F. Maehara, "Clipping and filtering employing deterministic transmit power control in MU-MIMO-OFDM systems," *Proc. International OFDM Workshop 2014 (InOWo'14)*, pp.106-111, Aug. 2014.

[2] K. Nishimura, S. Takebuchi, and F. Maehara, "Theoretical derivation of bit error rate for uplink OFDMA employing space diversity reception over nonlinear fading channels," *Proc. 20th European Wireless (EW) Conference*, pp.366-371, May 2014.

[3] G. Osada, S. Takebuchi, and F. Maehara, "Nonlinear distortion suppression scheme employing transmit power control for MU-MIMO-OFDM systems," *Proc. 2014 IEEE Radio and Wireless Symposium (RWW2014)*, pp. 46-48, Jan. 2014.

[4] S. Takebuchi, H. Tomeba, T. Onodera, M. Kubota, F. Maehara, and F. Tkahata, "Hybrid ARQ for modulo loss reduction in Multi-User MIMO THP systems," *Proc. 2013 International Symposium on Intelligent Signal Processing and Communication Systems (ISPACS 2013)*, WA2-E-4, pp. 375-380, Nov. 2013.

[5] K. Nishimura, S. Takebuchi, and F. Maehara, "Theoretical derivation of bit error rate for uplink OFDMA over nonlinear fading channels," *Proc. 24th annual IEEE international symposium on Personal, Indoor and Moble Radio Communications (PIMRC2013)*, pp. 761-765, Sept. 2013.

[6] S. Takebuchi, G. Osada, and F. Maehara, "A deterministic transmit power control for OFDM clipping and filtering," *Proc. 2013 IEEE 78th Vehicular Technology Conference (VTC2013-Fall)*, pp. 1-5, Sept. 2013.

[7] S. Nagakubo, S. Takebuchi, K. Ogawa, and F. Maehara, “Experimental results of seamless localization employing GPS and wireless LAN,” *Proc. the 10th IEEE Vehicular Technology Society Asia Pacific Wireless Communications Symposium (APWCS2013)*, pp. 251-255, Aug. 2013.

[8] S. Takebuchi, T. Arai and F. Maehara, “A novel clipping and filtering method employing transmit power control for OFDM systems,” *Proc. IEEE Wireless Communications and Networking Conference 2012 (WCNC2012)*, pp. 221-225, Apr. 2012.

[9] S. Takebuchi, T. Arai, and F. Maehara, “Performance evaluation of OFDM clipping and filtering method using transmit power control,” *Proc. World Telecommunications Congress 2012 (WTC2012)*, PS-25, Mar. 2012.